ELSEVIER

Progress in Nuclear Magnetic Resonance Spectroscopy 34 (1999) 93–158

PROGRESS IN NUCLEAR MAGNETIC RESONANCE SPECTROSCOPY

Heteronuclear multidimensional NMR experiments for the structure determination of proteins in solution employing pulsed field gradients

Michael Sattler[a], Jürgen Schleucher[b], Christian Griesinger[c,*]

[a]*Structural Biology, EMBL, Meyerhofstr. 1, D-69117 Heidelberg, Germany*
[b]*Department of Medical Biochemistry and Biophysics, Umeå University, S-90187 Umeå, Sweden*
[c]*Institute for Organic Chemistry, University Frankfurt, Marie-Curie-Str. 11, D-60439 Frankfurt, Germany*

Received 1 August 1998

Contents

* Corresponding author. Tel.: + 49-697982-9130; fax: + 49-697982-9128.
E-mail address: cigr@krypton.org.chemie.uni-frankfurt.de (C. Griesinger)

0079-6565/99/$ - see front matter
PII: S0079-6565(98)00025-9

Keywords: Multidimensional NMR; Protein NMR; Gradient enhanced triple resonance spectroscopy; Transfer amplitudes; Resonance assignment

1. Introduction

During the last decade a variety of triple resonance pulse sequences that are used for the structure determination of proteins by heteronuclear multidimensional NMR spectroscopy have been introduced and optimized. Here, we would like to give a critical review of experiments that have been proposed for chemical shift assignment and for the extraction of distance restraints based on NOE experiments. Detailed descriptions of useful implementations of pulse sequences will be given with respect to improvements in signal-to-noise ratio and artifact reduction, especially by the use of pulsed field gradients in combination with sensitivity enhancement and water-flip-back schemes.

The introduction of three- and four-dimensional NMR experiments [1–5] and the availability of ^{13}C-, ^{15}N-labelled proteins [6–16] allow one to assign the proton, nitrogen and carbon chemical shifts of proteins and protein complexes with molecular weights well above 25 kD [17,18] and to determine their structures in solution [19–22]. The resonance assignment of singly (^{15}N or ^{13}C) labellled proteins using 3D experiments [23] is basically an extension of Wüthrich's strategy which exclusively relies on homonuclear ^{1}H NMR experiments [24]. The conventional assignment strategies for unlabellled or singly labelled molecules make combined use of experiments with coherent (COSY, TOCSY) and incoherent (NOESY, ROESY) magnetization transfer. However, incoherent magnetization transfer using the dipolar interaction is dependent on the secondary structure, which can cause misassignments, especially in crowded spectra. The introduction of heteronuclear triple resonance experiments relying exclusively on $^{1}J/^{2}J$ couplings, which are to first order independent of conformation [9,25] triggered a development that to date has yielded a large number of experiments for ^{13}C-, ^{15}N-labelled proteins and new assignment strategies. As $^{1}J/^{2}J$ couplings are relatively large, they yield fast coherence transfers that can compete with the loss of magnetization as a result of relaxation during the pulse sequence. This becomes more and more important with increasing molecular weight. Recently, the use of deuterium labelling has been shown to increase the relaxation times dramatically, thereby allowing the study of proteins with molecular weights well above 30 kD [26,27].

The intention of this review is to summarize triple resonance pulse sequences that have been introduced and to evaluate their performance and applicability with respect to the molecular weight of the protein to be studied. Useful implementations of these experiments based on the practical experience of the authors are presented in greater detail. Further, experimental aspects and optimizations of the pulse sequences are discussed. We will especially focus on the use of pulsed field gradients in combination with sensitivity-enhanced magnetization transfers and water-flip-back schemes to improve the quality of the NMR spectra.

In Section 2, the various assignment strategies that depend on the respective isotope labelling scheme are introduced. In Section 3, basic building blocks and experimental aspects of the implementation of multidimensional triple resonance experiments are discussed. Pulse sequences for the assignment of backbone (Section 4) and side-chain resonances (Section 5) in ^{13}C-,^{15}N-labelled proteins are described, thereafter including modified pulse sequences for deuterated samples. 3D and 4D NOESY experiments used to derive internuclear distance restraints for structure calculations are

discussed in Section 6. For applications on complexes (e.g. between an unlabellled peptide and a ^{13}C-, ^{15}N-labellled protein) these experiments can be modified by the use of spectral editing and filter elements in order to separate inter- and intramolecular NOEs (Section 6.2).

We would also like to direct the reader's attention to some recent developments which are not discussed in this review but are expected to have a great impact in the field of biomolecular NMR spectroscopy in the near future. In the context of studying protein/ligand interactions we would like to refer to a very elegant and efficient technique that is used for identifying and designing high-affinity binding ligands for proteins in pharmaceutical research. The method called ''SAR by NMR'' (Structure Activity Relationship by NMR) is based on monitoring chemical shift changes of amide protons and nitrogens which accompany the titration of potential ligands to a solution of ^{15}N-labelled protein [28,29].

More recently, some promising new methodological developments have been introduced. These refer to novel types of structural restraints that have been investigated for use in high-resolution NMR studies of biomolecules. One type of restraints is based on residual dipolar couplings that are observed if a small alignment of the biomolecule can be achieved in solution [30–32]. The angle- and distance dependence of these residual dipolar couplings provide true long range structural restraints. Thus, if used in combination with NOE-based distance restraints these should significantly increase the precision and accuracy of NMR-derived structures. Another type of experiment exploits the angular dependence of cross-correlated relaxation, i.e. dipole/dipole or dipole/CSA [33]. In these experiments direct projections of bond vectors onto each other are obtained without the need for calibration, as is required for angular restraints derived from *J*-couplings. These projection restraints should therefore improve structure determination in a similar way as the orientational restraints derived from residual dipolar couplings. Moreover, since the novel long range restraints not only supplement but may also partially replace NOE based distance restraints, it is conceivable that – in combination with ^{2}H-labelling schemes – this will allow the determination of three-dimensional structures for proteins with molecular weights well above 50 kD.

In addition, NMR techniques, called Transverse Relaxation-Optimized Spectroscopy (TROSY) [34], have recently been introduced that largely attenuate T_2-relaxation at high magnetic fields by mutual cancellation of dipole/dipole and CSA relaxation mechanisms. Similar effects have been observed by removing the heteronuclear dipolar relaxation through multiple quantum line narrowing (see Section 3.6). Combination of these principles with other strategies, i.e. deuteration and the aforementioned novel structural restraints, should provide an avenue to successful NMR structure determination for very large biological macromolecules with molecular weights well above 50 kD.

2. Strategies and experiments for the resonance assignment of uniformly ^{13}C-, ^{15}N-labelled proteins

The assignment strategy for proteins that are not isotopically enriched [24] makes use of a combination of COSY/TOCSY and NOESY or ROESY spectra. The spin systems attached to each H^N are identified in the COSY and TOCSY spectra. NOESY or ROESY are used for the sequential assignment of the individual spin systems. The establishing of the sequential connectivity relies on the occurrence of the resonance frequency of the $H_\alpha(i)$ proton of amino acid (i), which is observed in the $H^N(i)$, $H_\alpha(i)$ cross peak in the COSY (TOCSY) spectrum and in the $H^N(i+1)$, $H_\alpha(i)$ cross peak in the NOESY spectrum (Fig. 1a). (Especially in α-helical proteins the sequential connectivity is also supported from $H^N(i)$, $H^N(i+1)$ cross peaks in the NOESY spectrum). Resonance overlap becomes so severe in the 2D spectra of proteins with more than 80 amino acids, that it is often impossible to identify adjacent spin systems by utilizing only a single common resonance frequency of the connecting cross peaks. In 3D assignment experiments, each cross peak is labelled by three frequencies rather than by two frequencies as in 2D experiments. Using ^{15}N labelling it is then possible to resolve the resonance frequencies of the amide protons according to the ^{15}N chemical shift of the attached amide nitrogens. This is done in 3D $^{15}N,^{1}H$-HSQC-TOCSY [35–38] and 3D $^{15}N,^{1}H$-HSQC-NOESY [23,39–43] experiments (Fig. 1b). While this facilitates the identification as well as the sequential assignment of the

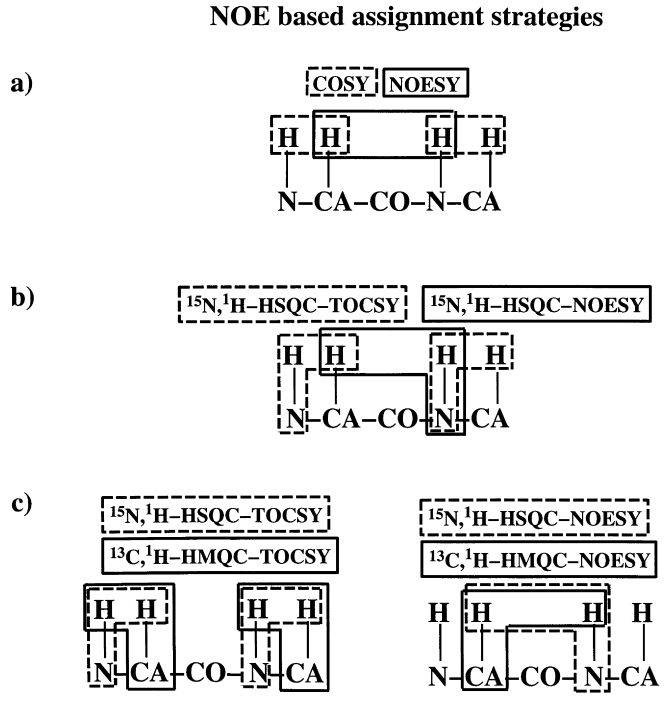

Fig. 1. Assignment strategies for unlabelled or singly (^{13}C- or ^{15}N-labelled) proteins. The sequential assignment relies on NOE cross peaks between protons of adjacent amino acids. (a) Classical assignment strategy based on COSY (TOCSY) and NOESY spectra. The sequential assignment is based on the chemical shift of the H_α(i) protons in the COSY and NOESY cross peaks. (b) Overlap among proton resonances can be resolved by dispersing the proton resonances in a third dimension of the chemical shift of the directly-bound heteronucleus. For ^{15}N-labelled proteins, the resolution of the H^N resonances is improved in ^{15}N edited TOCSY or NOESY spectra. (c) In the case of ^{13}C-labelled compounds, ^{13}C edited spectra can be used (in a similar way).

spin systems, the sequential connectivity still relies mainly on the common chemical shift of the $H_\alpha(i)$ proton (Fig. 1b), which can introduce ambiguities. In order to resolve overlapping H_α chemical shifts, 3D ^{13}C,^{1}H-HMQC-TOCSY and 3D ^{13}C,^{1}H-HMQC-NOESY spectra can be recorded on a ^{13}C-labelled sample (Fig. 1c). However, the use of the conformationally dependent NOE effect for the sequential assignment is a principal drawback of these strategies. As the secondary structure is not known at this stage of the resonance assignment, an assignment based on interactions that rely on the conformation may be erroneous. The dependence of the ^3J coupling constants used in COSY and TOCSY experiments on the conformation can also hinder the assignment process since cross peaks between spins that share a small coupling (i.e. the H^N and H_α protons in an α-helix) may be missing.

The problems of limited resolution among the H_α resonances and the conformation dependence of the NOE and ^3J coupling constants are overcome in the assignment strategies for ^{13}C-, ^{15}N-labelled proteins since they employ coherence transfer via ^1J (and in part ^2J) couplings only, which are largely independent of conformation. Also, since the ^1J (^2J) couplings are generally larger than the linewidth ($J > \Delta\nu_{1/2}$) of nuclei under consideration, the transfer via these couplings remains efficient for relatively large molecules with short transverse relaxation times T_2*. Fig. 2 shows the spin system of the peptide backbone and indicates the size of the coupling constants used for magnetization transfer in doubly ^{13}C-, ^{15}N-labelled proteins.

The nomenclature for these triple resonance experiments reflects the magnetization transfer pathway of the experiments. Nuclei that are involved in

Table 1
Pulse sequences typically used for protein structure determination as described in this review. The relative sensitivity of backbone assignment experiments compared to the HNCO experiment based on Figs. 21, 24 and 26 is given. Bruker pulse programs for these experiments can be obtained from http://www.nmr.EMBL-Heidelberg.de/

Experiment	Nuclei observed	Evaluation	Relative S/N [%]	Section
HNCO	H(i), N(i), C′($i-1$)	< 20 kD, above use ^{2}H labelling	100	4.1
HNCA	H(i), N(i), $C_\alpha(i)$,$C_\alpha(i-1)$	< 20 kD, above use ^{2}H labelling	50/15	4.1
HN(CO)CA	H(i), N(i), $C_\alpha(i-1)$	< 20 kD, above use ^{2}H labelling	71	4.2
HN(CA)CO	H(i), N(i), C′(i)	< 20 kD, above use ^{2}H labelling	13/4	4.3
CBCA(CO)NH	H(i), N(i), $C_\alpha(i-1)$, $C_\beta(i-1)$	< 20 kD, above use ^{2}H labelling	13/9 α/β	5.1
HBHA(CO)NH	H(i), N(i), $H_\alpha(i-1)$, $H_\beta(i-1)$	< 20 kD, above use ^{2}H labelling	13/9 α/β	5.1
CBCANH, HNCACB	H(i), N(i), $C_\alpha(i)$, $C_\beta(i)$,$C_\alpha(i-1)$,$C_\beta(i-1)$	< 15 kD, above use ^{2}H labelling	4/1.7 α/β (i) 1.3/0.5 α/β(i-1)	5.2
(H)CC(CO)NH-TOCSY	H(i), N(i), $C^{aliph.}$($i-1$)	< 15–20 kD, above use ^{2}H labelling		5.3
H(CC)(CO)NH-TOCSY	H(i), N(i), $H^{aliph.}$($i-1$)	< 15–20 kD, above use ^{2}H labelling		5.4
HCCH-TOCSY	$H^{aliph.}$, $C^{aliph.}$	< 25 kD, – sensitive, but tedious to analyze, combine with HCCONH type experiments		5.5
Aromatic side-chain experiments		< 15 kD, for aromatic resonance assignments		5.6
CT-HNCA with ^{2}H-decoupling	H(i), N(i), $C_\alpha(i)$,$C_\alpha(i-1)$	with ^{2}H-labelling excellent S/N up to 64 kD has been shown		5.8
NOESY-^{1}H, ^{15}N- HSQC	$H(i) \overset{NOE}{\rightarrow} H(j), N(j)$	NOEs of amide protons		6.1
NOESY-^{1}H, ^{13}C- HMQC	$H(i) \overset{NOE}{\rightarrow} H(j), C(j)$	NOEs to ^{13}C bound protons; record preferably in D_2O; yields the majority of NOE derived distance restraints		6.1
ω_2-filtered NOESY	$^1H \overset{NOE}{\rightarrow} {}^1H - (^{12}C/^{14}N)$	for unlabelled ligand: intra- and intermolecular NOEs		6.2
^{1}H, ^{13}C-HMQC-ω_3-filtered NOESY	$^1H(-^{13}C) \overset{NOE}{\rightarrow} {}^1H\text{-}(^{12}C/^{14}N)$	unambiguous identification of intermolecular NOEs, S/N problems for complexes > 25 kD		6.2

magnetization transfers form the name of an experiment. Spins, whose chemical shifts are not evolved are put in parentheses. For an out-and-back type experiment [44], where magnetization of a spin is transfered to a remote spin and then brought back

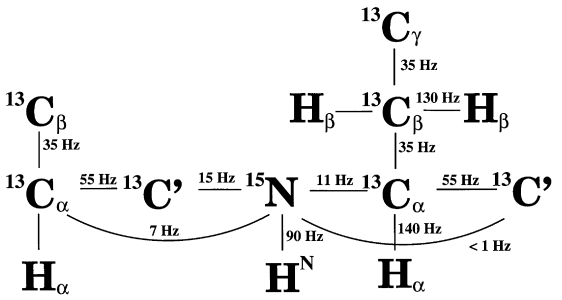

Fig. 2. Spin system of the peptide backbone and the size of the ^1J and ^2J coupling constants that are used for magnetization transfer in ^{13}C-, ^{15}N-labelled proteins.

the same way, only the first half of the magnetization transfer is used for its name. For example, the out-and-back experiment that transfers magnetization from the amide proton (H^N) via the amide nitrogen (N) to the carbonyl C′ (CO) of the previous residue is called HNCO. If another magnetization transfer step to the C_α (CA) of the previous residue is included and the corresponding C_α chemical shift is recorded, the experiment is referred to as H(N)COCA. The parentheses indicate that magnetization is only transferred via the nitrogen spin, without chemical shift evolution taking place. In the following section, NMR experiments for the assignment of ^{13}C-,^{15}N-labelled proteins are summarized and the corresponding assignment strategies are discussed. Table 1 provides a summary of sections in this review where the pulse sequences of important experiments are discussed. Also, comments are given regarding sensitivity and

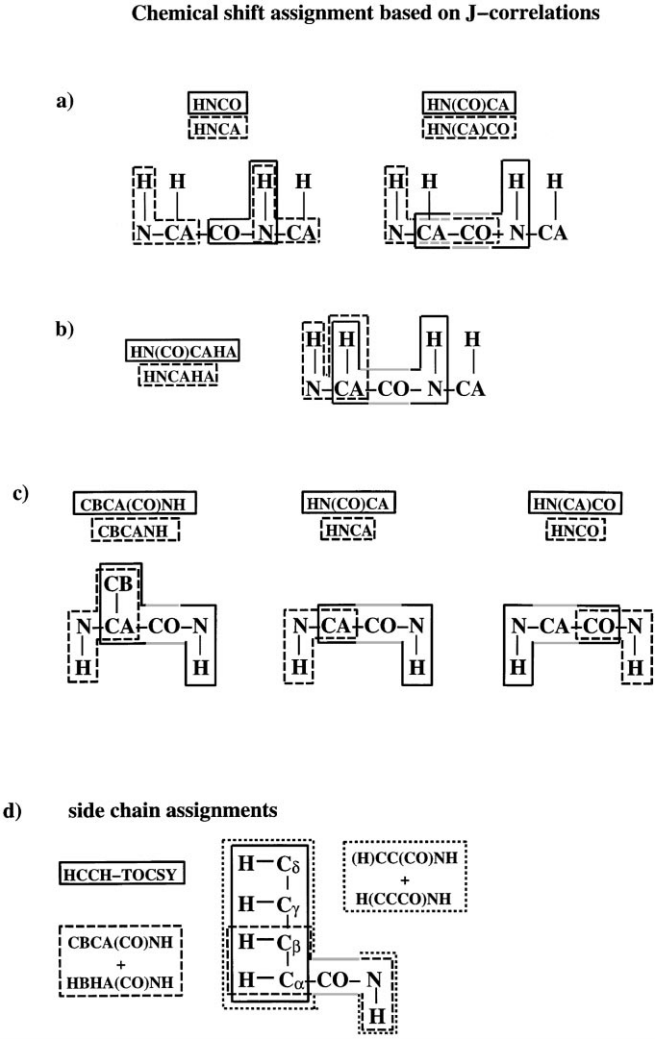

Fig. 3. Assignment strategies for ^{13}C-,^{15}N-labelled proteins using coherent magnetization transfer only. (The boxes drawn around the spin system indicate the connectivity established in the respective experiment. Grey parts of the boxes indicate that a spin is used as a relay spin, without chemical shift evolution. Sequential assignment of the backbone resonances is obtained either from a combination of four 3D experiments (a), or in two 4D experiments (b). These experiments use only correlations among the backbone resonances of H^N, N, C_α, H_α, and C'. (c) The sequential assignment is improved if combinations of C_β and C_α chemical shifts are available. (d) Assignment of the spin systems of the aliphatic proton and carbon-resonances: The H,C spin systems identified in an HCCH-TOCSY experiment are connected with the backbone resonances H^N and N using the chemical shifts of $H_{\alpha,\beta}$and $C_{\alpha,\beta}$ nuclei from the HCCH-TOCSY spectrum and the CBCA(CO)NH or HBHA(CO)NH spectra. Alternatively, the aliphatic proton and carbon chemical shifts can be correlated directly with the chemical shifts of the amide moiety in (H)CC(CO)NH-TOCSY and H(CC)(CO)NH-TOCSY experiments. A combination of both strategies, however, is more likely to yield complete side-chain assignments.

applicability of these experiments with respect to molecular weight.

The strategies that have been developed for resonance assignment using triple resonance experiments are summarized in Fig. 3.

The strategy originally proposed by Bax's group employs the 3D experiments HNCO, HNCA, HN(CO)CA, HCACO and HCA(CO)N [25,45–48] to exclusively correlate the resonances of the peptide backbone ($H^N(i)$, $N(i)$, $C_\alpha(i)$, $H_\alpha(i)$,

$C_\alpha(i-1)$ $H_\alpha(i-1)$, $C'(i)$ and $C'(i-1)$) (Fig. 3a). Equivalent information can be obtained from the 4D experiments HN(CO)CAHA and HNCAHA [49] or HCANNH and HCA(CO)NNH [50,51] (Fig. 3b). For smaller proteins with more favorable T_2 relaxation times of the C_α spins (see Section 4.1.1), the assignment of the resonances of $H^N(i)$, $N(i)$, $C_\alpha(i)$, $H_\alpha(i)$, $C_\alpha(i-1)$ and $H_\alpha(i-1)$ can be accomplished using the 3D experiment H(CA)NNH [52] or HN(CA)HA [53], or using a combination of HN(CA)NNH and H(NCA)NNH [54]. The HN(CA)CO [55,56] or H(N)CACO experiments [57] support the assignments using the C' chemical shifts but are usually less sensitive unless applied to a deuterated protein sample (see Section 5.8).

Further developments involved including the chemical shifts of side-chain carbon and proton spins to achieve the sequential assignment (Fig. 3c and d). In these experiments chemical shifts of side-chain resonances are correlated to the amide proton by combinations of the 3D experiments CBCA(CO)NH [58] and CBCANH [59] or HNCACB [60], HBHA-(CO)NH [61], HCC(CO)NH-TOCSY [62–65] and HCCNH-TOCSY [64,66] or with a 4D HCC(CO)NH-TOCSY experiment [67]. Information about the chemical shifts of the C_α and C_β carbons is especially valuable for the assignment process, since they are characteristic of the different types of amino acids and can therefore help to position a sequentially connected stretch of amino acids within the known primary sequence of the protein [61].

The recommended set of experiments to achieve sequential chemical shift assignments is summarized in Fig. 3c (see Section 5). From the combination of CBCA(CO)NH and CBCANH experiments the backbone resonance assignments and the sequential connectivities can be obtained. These experiments will be sensitive enough for proteins < 130 residues and provide the C_α and C_β chemical shifts to establish the sequential link between neighboring residues. Further, the C_α and C_β chemical shifts provide important information about the amino acid type and the secondary structure. In addition to sequential assignments, these two experiments can, in principle, provide the secondary structure of the protein. However, for proteins >15 kD the CBCANH or HNCACB experiment become less sensitive. Then the more sensitive experiments HNCA and HN(CO)CA can be used in addition to establish the sequential connectivities. If the C_α and C_β chemical shifts obtained from these four experiments still leave some ambiguities, the pair of HNCO and HN(CA)CO can be used to resolve the overlap. However, since the HN(CA)CO experiment is quite insensitive, this approach will be useful only in combination with a deuterated protein. Then the set of six backbone experiments shown in Fig. 3c should allow the unambiguous assignment even for larger proteins (30 kD).

Assignment of the side chain proton resonances is a prerequisite for analyzing NOE interactions (Section 6) which yield distance restraints that are used for structure calculations. Experiments that use C,C-TOCSY transfer to establish side chain assignments via correlation of side chain protons with backbone resonances (Fig. 3d) become insensitive with increasing molecular weight. In these cases, the side chain spin systems are identified in 3D HCCH-COSY [68,69] or preferably 3D/4D HCCH-TOCSY [70–73] experiments. The $H_{\alpha/\beta}$ and $C_{\alpha/\beta}$ chemical shifts of the side chains are then used to link the side chain spin systems to the backbone assignments (Fig. 3d).

For proteins with molecular weights above 30 kD, the sensitivity of all heteronuclear triple resonance experiments declines as a result of increasing T_2 relaxation rates. Owing to the strong dipolar coupling in C–H fragments, this problem is especially severe for aliphatic carbons, especially the C_α spins. Partial (75%) or complete (100%) deuteration was proposed as a remedy [74,75], since the dipolar coupling in a C–D fragment compared to a C–H fragment is scaled down because of the lower gyromagnetic ratio, $\gamma(^2H) \approx 1/6.5\ \gamma(^1H)$. Dilution of protons by deuterons thus leads to longer relaxation times for the ^{13}C spins. Modified pulse sequences for backbone [26,27] and sidechain [76,77] assignments of partially deuterated proteins with deuterium decoupling have been published in the meantime, and the expected increase in sensitivity and higher resolution in the carbon dimensions have been observed (Section 5.8).

In all 3D and 4D experiments described so far, chemical shift evolves for one spin per dimension only. The dimensionality of a 3D (*n*D) experiment can be reduced to 2D((n − 1)D), if chemical shifts of two nuclei are recorded simultaneously. The application of this principle on triple resonance

experiments was first demonstrated by Wüthrich and coworkers [78–80] and has been extended by Marion and coworkers [81,82]. These experiments are discussed further in Section 4.4.

A number of experiments especially designed for the assignment of the aromatic proton and carbon chemical shifts in ^{13}C-labelled proteins have been proposed. Assignment of these resonances is particularly important, since aromatic side chains are usually involved in NOE contacts that define the tertiary structure. These experiments are discussed in some detail in Section 5.7.

Several experiments have been proposed to identify certain amino acid residue types, e.g. prolines [83] or glycines [84,85]. Other pulse sequences were designed for the assignment of side chain resonances of Met [86], His, Trp [87], Glu, Asp, Gln and Asn residues [88–92]. Experiments have been introduced to obtain assignments for arginine side chain resonances [93–96]. The guanidinium group of the arginine side chain is often involved in intermolecular contacts e.g. to phosphorylated proteins or nucleic acids. In order to define these important interactions it is necessary to assign the arginine side chain resonances. These experiments are discussed in Section 5.7.

The availability of complete sets of chemical shifts for all ^{1}H, ^{13}C and ^{15}N resonances in proteins enabled correlations between chemical shifts and secondary structure elements to be established [97–102]. The secondary chemical shift for a nucleus in an amino acid in a given secondary structure element is defined as the difference between the average chemical shift found for the nucleus in this secondary structure element and the average chemical shift of the nucleus in all proteins assigned to date. So far, it has been found that the secondary chemical shifts of H_α, C_α, C_β and C' nuclei correlate well with the secondary structure (characterized by the backbone dihedral angles ϕ and ψ). Using this information the secondary structure of a protein can be established at an early stage of the structure determination process. The secondary chemical shift has also been used during the refinement of NMR-derived structures. It has been shown that the root-mean-square deviation of the ensemble of structures can be slightly improved using this ''chemical shift refinement'' [103–105].

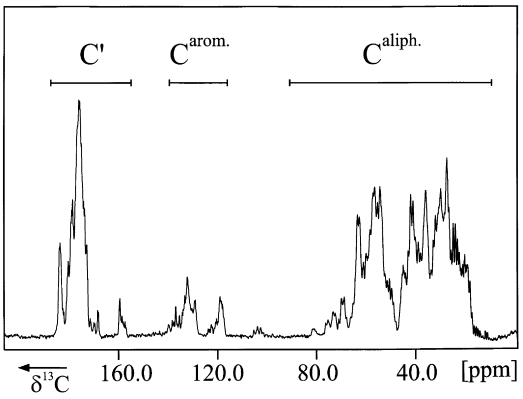

Fig. 4. 150.9 MHz proton-coupled 1D ^{13}C spectrum of the protein Rhodniin (103 amino acids). The three separate spectral regions contain the carbonyl (C') resonances (around 175 ppm), the aromatic resonances (around 130 ppm) and the aliphatic ^{13}C resonances between 10 and 85 ppm.

3. Basic tools and experimental aspects of triple resonance pulse sequences

The NMR pulse sequences for the assignment of uniformly ^{13}C-, ^{15}N-labelled proteins are composed of a large number of pulses that have to be applied at three or four different frequencies in order to excite ^{1}H, ^{15}N, aliphatic ^{13}C and $^{13}C'$ resonances. As signal losses as a result of miscalibration or pulse imperfections accumulate, accurate calibration of pulses and good RF homogeneity of the probe on all frequency channels is essential. The aliphatic and carbonyl pulses can either be generated in separate spectrometer channels, or a single channel can be used, as explained in the following.

In addition, special techniques and the use of pulsed field gradients in the design of pulse sequences have led to improved signal-to-noise and better artifact suppression in NMR experiments. Some basic principles will be discussed later.

3.1. Selective pulses

A ^{13}C spectrum of the protein Rhodniin (103 amino acids) is displayed in Fig. 4. Three separate regions are visible, corresponding to the carbonyl (C'), aromatic and aliphatic resonances. It is therefore possible to selectively manipulate the C' and aliphatic carbon resonances, using either rectangular pulses

adapted for this purpose [106] or shaped pulses. If the pulses on either side of the spectral regions do not disturb populations or coherences of spins belonging to the other region, the aliphatic and C′ carbons can be regarded as a heteronuclear spin system. In our experience G4 (bandselective 90° pulse) and G3 (bandselective 180° pulse) pulses introduced by Emsley and Bodenhausen [107] are useful for these purposes. The excitation profiles of these pulses will be discussed later. In addition, a number of different pulse shapes (e.g. BURP [108]) with comparable performance have been introduced for selective excitation, inversion and refocusing [109].

As an alternative to treating the different carbon nuclei as a heteronuclear spin system by the application of selective pulses, extremely broadband pulses can be implemented as frequency-swept adiabatic pulse shapes. These pulses can be used for extremely broadband decoupling (e.g. to cover the full ^{13}C chemical shift range at high magnetic field strengths at an acceptable RF power). However, adiabatic decoupling introduces artifacts in the form of cycling side bands which have to be taken care of when applied in heteronuclear decoupled proton/proton correlation spectra, e.g. heteronuclear NOESY experiments [110–112]. A very elegant application of frequency swept adiabatic pulses has been introduced for ^{12}C-filtered experiments (see Section 6.2) [113,114].

If pulses for carbonyl and aliphatic carbons are to be delivered by a single RF channel, the frequency of this channel is centered in one of these regions, while pulses on the remote carbon frequencies are generated by phase- or amplitude-modulated shaped pulses. Compared to switching the carrier frequency, this has the advantage that phase coherence is retained throughout the pulse sequence. Phase modulation of a shaped pulse leads to a shift in the excitation region of the shaped pulse, while amplitude modulation generates two excitation side bands, each having to a first approximation the same excitation profile as the unmodulated shape. Shaped pulses are executed by the spectrometer hardware as a series of pulse steps, which each have a defined amplitude and phase. Consider a shaped pulse of duration τ_P and consisting of $0 < j <$ NP steps. If a frequency offset $\Delta\Omega$ [Hz] of this pulse is achieved by superimposing a phase gradient on the shape, the phase $\phi_{mod}(j)$ of pulse step j is

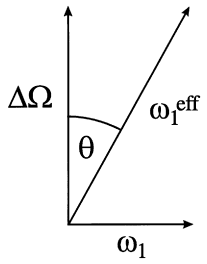

Fig. 5. Definition of the effective field $\omega_1^{eff} = -\gamma B_1^{eff}$ as a function of the offset $\Delta\Omega$ and the RF field strength $\omega_1 = -\gamma B_1$. The orientation of ω_1^{eff} defines the axis about which magnetization precesses during the RF pulse. θ is defined by $\sin\theta = \omega_1/\omega_1^{eff}$.

given by Eq. (1a). Symmetrical excitation at $\pm\Delta\Omega$ can be achieved by a cosine modulation of the amplitude of a shaped pulse. If the amplitude of step j of the unmodulated shaped pulse is denoted by A(j), the amplitude $A_{mod}(j)$ of the amplitude-modulated pulse is given by Eq. (1b).

Phase modulation:

$$\phi_{mod}(j) = \phi(j) - (2\pi^*\Delta\Omega^*\tau_p^*j/NP) \quad (1a)$$

Amplitude modulation:

$$A_{mod}(j) = A(j)\ 2\cos(2\pi^*\Delta\Omega^*\tau_p^*j/NP) \quad (1b)$$

As amplitude-modulation according to Eq. (1b) leads to two excitation side bands, an amplitude-modulated shaped pulse has a peak field strength twice as high as the unmodulated shape. Thus, the RF power required is up to four-fold higher compared to using the unmodulated shape.

Rectangular pulses can replace shaped pulses for the selective excitation of the two carbon frequency ranges to some degree. The selectivity of a rectangular pulse is achieved by adjusting their field strength [106]. To see how this can be achieved, the effective field ω_1^{eff} at a frequency offset $\Delta\Omega$ for a pulse with applied with a field strength ω_1 is shown in Fig. 5.

For a spin with offset $\Delta\Omega$, the effective field ω_1^{eff} is defined by Eq. (2):

$$(\omega_1^{eff})^2 = (\Delta\Omega)^2 + \omega_1^2 \quad (2)$$

To achieve selectivity for one group of spins, ω_1^{eff} is chosen such that the spins to be excited (inverted) experience a flip angle of $\pi/2$ (π), while the flip angle at offset $\Delta\Omega$ is 2π. This condition is met if

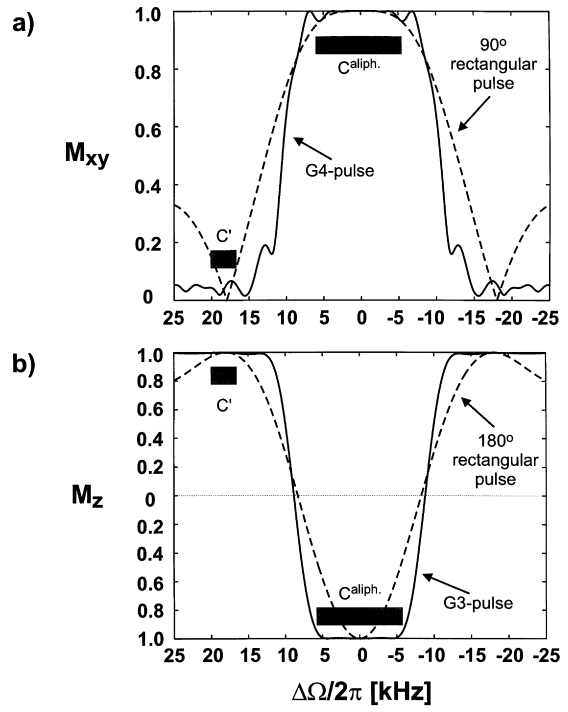

Fig. 6. (a) Excitation of transverse magnetization ($M_{xy} = (M_x^2 + M_y^2)^{1/2}$) from z magnetization by a 90°$_x$ pulse and by a G4 pulse as a function of the offset $\Delta\Omega$. In order to avoid excitation of frequencies with an offset ± 18 kHz (corresponding C′ in proteins at 150 MHz with the ^{13}C carrier in the C_α region) the pulse duration for the 90° pulse is $\tau_P = 53.8$ μs (corresponding to $\omega_1/2\pi = \Delta\Omega/(2\pi\sqrt{15}) =$ 4.65 kHz). The excitation profile of the rectangular pulse is compared to that of a G4 pulse with $\tau_p = 400$ μs ($\gamma B_1^{max}/2\pi =$ 11.48 kHz). (b) Inversion of z magnetization by a rectangular pulse and by a G3 pulse. The pulse width of the 180° rectangular pulse is $\tau_p = 48$ μs ($\omega_1/2\pi = \Delta\Omega/(2\pi\sqrt{3}) = 10.3$ kHz), to avoid excitation of resonances at ± 18 kHz. In contrast to the rectangular pulse, the selective G3 pulse ($\tau_p = 250$ μs, $\gamma B_1^{max}/2\pi =$ 14.37 kHz) shows almost ideal inversion for the desired bandwidth (± 5 kHz), while off-resonance magnetization remains unperturbed.

$\omega_1 = -\gamma B_1 = \Delta\Omega/\sqrt{15}$ for a 90° pulse and $-\gamma B_1 = \Delta\Omega/\sqrt{3}$ for a 180° pulse. Fig. 6a shows the excitation profile of a rectangular pulse and a G4 pulse, both adjusted to excite $^{13}C_\alpha$ magnetization while leaving the carbonyl resonances untouched. The inversion profiles of a rectangular pulse and of a G3 pulse adjusted to selectively invert z magnetization of C_α are shown in Fig. 6b. In contrast to the rectangular pulses, the shaped pulses achieve nearly homogenous excitation or inversion, while leaving the whole carbonyl region undisturbed.

3.2. Bloch–Siegert phase shifts

A common fragment of multinuclear pulse sequences is evolution of chemical shift of one group of carbon spins with the coupling to another group of off-resonance carbon spins being refocused by a selective pulse. Application of the selective refocusing pulse leads to a phase shift for the on-resonance coherence, known as Bloch–Siegert phase (BSP) [115,116]. This phase shift is introduced even if the condition $|\Delta\Omega| > |\omega_1|$ holds, i.e. if the on-resonance spin is not excited by the selective pulse. Bloch–Siegert effects are also introduced when selective decoupling sequences [117–120] are applied [121]. In this case small frequency shifts are produced for the off-resonant spins.

The Bloch–Siegert phase shift has the same origin as the Bloch–Siegert frequency shift, which introduces a shift of resonance frequencies in the vicinity of an irradiation RF frequency [115,122,123]. It results from interference of the selective pulse with the evolution of off-resonance transverse magnetization. An example is shown in Fig. 7 for a rectangular π pulse applied at an offset $-\Delta\Omega = -\sqrt{3}\omega_1$: The on-resonance (zero order) Bloch–Siegert phase for this pulse can be derived as follows: Viewed in a coordinate system rotating on-resonance with the frequency of the applied pulse of duration τ_π, magnetization at an offset $\Delta\Omega$ experiences an effective rotation of 2π due to $\omega_1^{eff} = 2\omega_1$. Thus, the orientation of the magnetization after the pulse is unchanged, its phase is $\phi_{pulse} = 0$. However, in absence of the pulse, the magnetization would have evolved a phase $\phi_{nopulse} = \Delta\Omega * \tau_\pi$ since it has an offset $\Delta\Omega$ (Fig. 7b). Thus, the zero order Bloch–Siegert phase, which is the phase difference with and without application of an off-resonance pulse, $\phi_{pulse} - \phi_{nopulse}$, equals:

$$\mathrm{BSP}(0) = -\Delta\Omega * \tau_\pi = -\sqrt{3}\omega_1 * \pi/\omega_1$$
$$= -\sqrt{3}\pi \sim 48.2^\circ \quad (3)$$

In Eq. (3) the fact that BSP(0) is determined only *modulo* 2π has been used. An alternative description in a coordinate system that is on-resonance with the

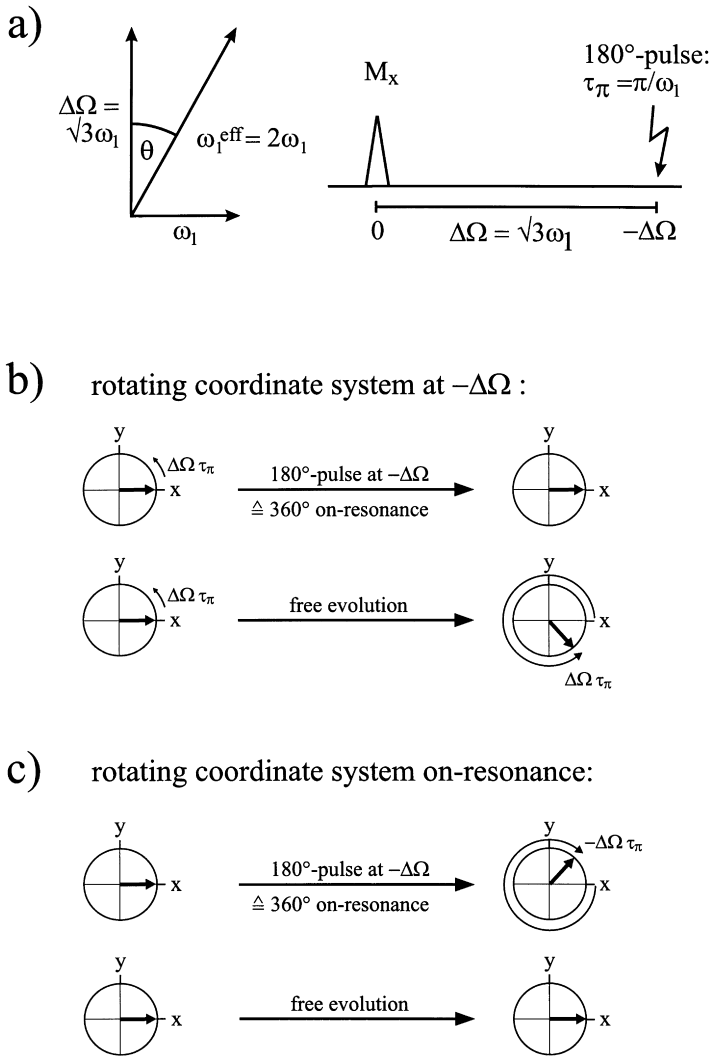

Fig. 7. (a) Effective field ω_1^{eff} of transverse magnetization during application of an off-resonance π pulse of field strength $B_1 = -\omega_1/\gamma$ and duration τ_π at an offset $-\Delta\Omega = \sqrt{3}\omega_1$. The off-resonance π pulse acts as a 2π pulse for the magnetization under consideration. (b) Viewed in a coordinate system rotating at angular frequency $-\Delta\Omega$, the off-resonance pulse π aligns the magnetization at the same position as before. However, in the absence of the pulse, it would have developed a phase $\Delta\Omega^*\tau\pi$ because of chemical shift evolution. (c) In the coordinate system on-resonance with the magnetization, the phase of the magnetization with application of the pulse is shifted by $-\Delta\Omega^*\tau_\pi$, because this coordinate system rotates $\Delta\Omega$ faster than the one in (b). However, without the off-resonance pulse, the magnetization would not have developed a phase. Both descriptions lead to the same value of the zero order Bloch–Siegert Phase BSP(0) $= \phi_{pulse} - \phi_{nopulse} = -\Delta\Omega^*\tau_\pi = -\sqrt{3}\pi$ (cf. Eq. (3)).

magnetization yields the same result (Fig. 7c): since this coordinate system rotates with $\Delta\Omega$ compared to Fig. 7b, the magnetization with application of the off-resonance π-pulse has a phase $\phi_{\text{pulse}} = -\Delta\Omega^*\tau_\pi$. However, without an off-resonance pulse it will not evolve chemical shift, because this coordinate frame is rotating on-resonance with the magnetization ($\phi_{\text{pulse}} = 0$). Again, BSP(0) $= \phi_{\text{pulse}} - \phi_{\text{nopulse}} = -\sqrt{3}\pi$. Note, that the sign of the Bloch–Siegert phase shift will be reversed if the off-resonance pulse is applied at $\Delta\Omega$ rather than $-\Delta\Omega$. Therefore, amplitude modulated pulses do not introduce a

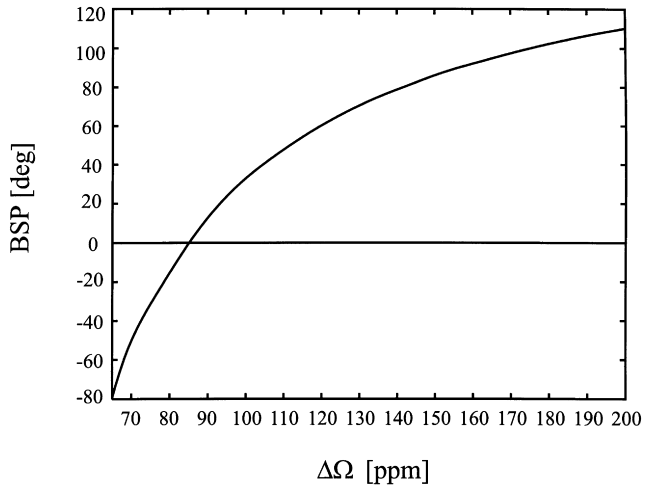

Fig. 8. Bloch–Siegert Phase (BSP) of a G3 pulse with an inversion bandwidth of 70 ppm as a function of the offset [ppm].

zero order Bloch–Siegert phase on-resonance (vide infra).

The Bloch–Siegert phase introduced by a shaped pulse depends primarily on the total rotation angle of the pulse and is therefore usually larger than the Bloch–Siegert phase induced by a rectangular pulse applied with the maximum RF field of the shaped pulse. The Bloch–Siegert phase for a G3 pulse with an inversion bandwidth of 70 ppm ($\tau_P = 250$ μs, $\gamma B_1^{max}/(2\pi) = 14.37$ kHz for ^{13}C at 150 MHz) is shown in Fig. 8 as a function of the offset in [ppm]. For offsets in the range 130 ± 10 ppm, which corresponds to the separation of the C_α and C' resonances, the BSP is nearly linear as a function of $\Delta\Omega$ and can therefore be compensated approximately by a phase shift of RF pulses (equal to the frequency-independent ''zero order'' BSP(0)) and the introduction of a delay (reversing the linearly frequency-dependent ''first order'' BSP(1)).

This method and two alternative methods used to compensate BSP shifts are depicted in Fig. 9. In this example, the off-resonance inversion pulse on C' introduces BSP shifts for the transverse C_α magnetization during the evolution time $2T$.

The second possibility for compensating Bloch–Siegert phase shifts makes use of amplitude modulation instead of phase-modulation (Fig. 9b). An amplitude-modulated pulse has two excitation bands

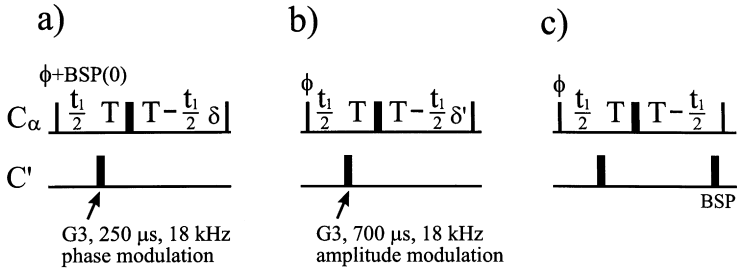

Fig. 9. A phase-modulated G3 pulse, applied during the evolution time of C_α nuclei to refocus the C',C_α coupling, induces a Bloch–Siegert phase shift on the C_α nuclei, which can be compensated in different ways: (a) The zero and first order BSP shifts can be determined and can be compensated for by a adjusting the phase of a 90° pulse and introducing a delay δ, respectively. For the G3 pulse applied to C' in this example (duration 250 μs, offset 18 kHz), a phase change of BSP(0) = 55° and a delay of $\delta = -25$ μs are needed. (b) Replacing the phase-modulated C' pulse by an amplitude-modulated shape of 700 μs duration leads to cancellation of the zero order BSP, a delay $\delta' = -15$ μs is still needed to eliminate the first order BSP. (c) A second off-resonance shaped pulse, (denoted ''BSP'') separated from the first one by an on-resonance (C_α) 180° pulse, leads to compensation of BSP shifts of all orders.

at $\pm \Delta\Omega$. The Bloch–Siegert phase shifts of the two side bands interfere, such that the zero order Bloch–Siegert phase shifts cancel completely while first order shifts cancel at least on-resonance. A drawback of this compensation is that the shaped pulse must have twice the RF amplitude.

In the third method (Fig. 9c) a second shaped pulse is applied, which is separated from the first shaped pulse by a 180° pulse applied to the on-resonance spins. This on-resonance 180° pulse does not further complicate the pulse sequences, since it is needed anyway for refocussing ^{13}C chemical shifts. This method eliminates BSP shifts of all orders. However, the additional off-resonance phase-modulated pulse can still cause some loss in sensitivity.

3.3. Pulsed field gradients

Pulsed field gradients are linear spatial changes ($G_\alpha = dB_0/d\alpha$, $\alpha = x,y,z$) of the static B_0 field applied for relatively short (millisecond) durations. Until 1990, weak B_0 gradients along the z-axis were used as homogeneity spoiling (homospoil) pulses [124] in high resolution NMR spectroscopy. Since then, problems with shielding of eddy currents that prevented gradients from achieving their final value and led to delayed decay after switching off the gradient have been solved. Therefore, gradients of up to 50 G/cm are now available for high resolution NMR experiments. A number of pulse sequences have been introduced that incorporate pulsed field gradients for coherence selection and achieve superior suppression of solvent signals and artifacts [125–132]. In the following, we summarize useful implementations of gradients as tools in NMR pulse sequences. For comprehensive reviews about the use of pulsed field gradients in high resolution NMR see [133,134]. More recently it has been shown, that ''impossible cross-peaks'' e.g. from intermolecular multiple quantum coherences, can be observed in combination with the use of gradients in aqueous solutions [135]. These peaks, that are usually undesired because they lead to poor solvent suppression, can be suppressed by the use of magic angle gradients, that can be obtained in probes with multiple-axis gradients. These probes also allow optimized automated shimming of samples by three-dimensional mapping of the B_0 field [136]. However, in heteronuclear experiments single axis gradients are usually sufficient for the suppression of solvent signals and artifacts [137].

A gradient pulse with amplitude $\mathbf{G} = (G_x, G_y, G_z)$ and a duration τ_G introduces a phase $\phi(\mathbf{r})$ on spin coherence at the position $\mathbf{r}$:

$$\phi(\mathbf{r}) = (\mathbf{G}\tau_G\mathbf{r}) \sum_k (p_k \gamma_k) \tag{4}$$

p_k is the coherence order of spin k with the gyromagnetic ratio γ_k. For a sufficient gradient strength $\mathbf{G}\tau_G$, coherences over the sample volume experience phase shifts between 0° and several hundred 2π rotations. Thus, no macroscopic coherence (which is obtained by integration over the active sample volume) is observable (fanned-out arrows in Fig. 10a). However, the spin systems within the active volume of the probe are in a well-defined state. Application of a second gradient with strength $-\mathbf{G}\tau_G$ reverses the action of the first gradient. The dephased coherence is being refocused and thus becomes macroscopically observable (Fig. 10a). This is called a gradient echo [138]. In an NMR experiment where j gradients $(\mathbf{G}\tau_G)_j$ are applied, a coherence transfer pathway involving the coherence orders p_{kj} is refocused by a gradient echo, if

$$\sum_j \{(\mathbf{G}\tau_G)_j \sum_k (p_{kj}\gamma_k)\} = 0 \tag{5}$$

For example, two gradients with identical strength placed symmetrically around a 180° pulse refocus all coherences for which the sign is inverted but for which the absolute value is kept constant by the 180° pulse (Fig. 10b). In general, only coherence from selected pathways is refocused and observable at the beginning of acquisition.

The suppression of artifacts by pulsed field gradients is achieved within a single scan. This is in contrast to phase cycled experiments, where suppression of artifacts is achieved by subtraction of signals from two or more scans. Imperfect subtraction is the main source of t_1 noise in multidimensional experiments. Another advantage of pulsed field gradients is the suppression of solvent signals that usually constitute the most severe artifacts in NMR spectra. If solvent signal suppression, e.g. for samples dissolved in H_2O, is achieved by presaturation, the maximum receiver gain is still determined by the incompletely suppressed solvent signal and the suppression must be

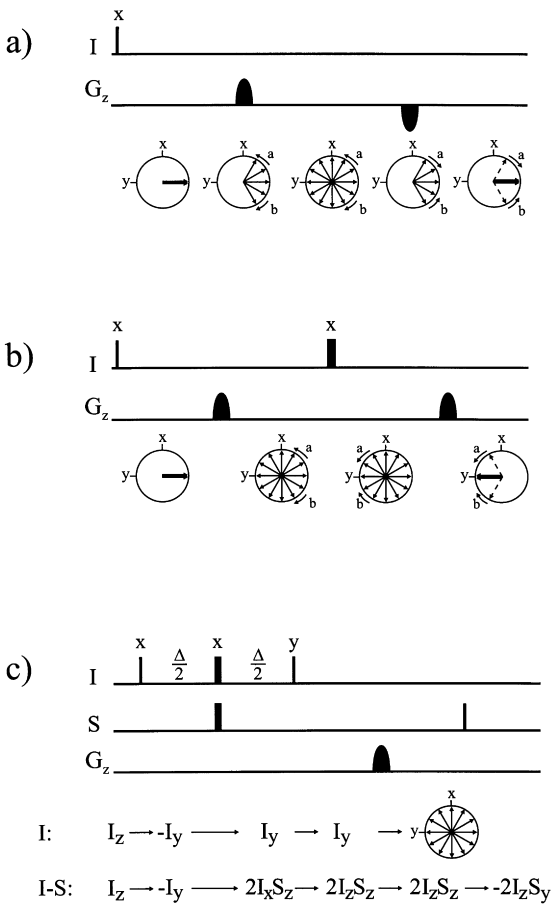

Fig. 10. Effects of gradients. (a) *I*-spin coherence of order *p* is dephased by a gradient with strength $G_z\tau_G$ by $pG_z\tau_G\gamma_I$, where γ_I is the gyromagnetic ratio for the *I* spins. The projections of magnetization vectors into the *xy*-plane are shown. Given a sufficient dephasing power of the first gradient pulse, no magnetization is observable macroscopically because signals from different volume elements of the active volume cancel. Application of a second gradient of opposite sign ($-G_z\ \tau_G$) leads to rephasing of the coherence forming a gradient echo. (b) A 180° pulse inverts the coherence order, thus application of two gradients of the same sign on both sides of a 180°-pulse will produce a gradient echo. Artifacts resulting from imperfect refocusing will be dephased. (c) In the initial part of a HSQC experiment the magnetization of interest exists as longitudinal two-spin order $2I_zS_z$. Therefore, a spoil gradient during this period will dephase transverse magnetization. The residual water magnetization depends solely on the imperfections of the three proton pulses that may produce water magnetization along the *z*-axis at the time of the gradient.

considerably improved by signal averaging. In contrast, solvent suppression by the use of heteronuclear gradient echoes, as described in the following, allows optimum use of the dynamic range of the receiver.

The various implementations of gradients in multidimensional NMR experiments differ with respect to performance. There are two concerns: first, the desired coherences should be fully refocused at the end of the pulse sequence. This cannot always be achieved, because many pulse sequences rely on retaining multiple coherence orders during most of the delays, e.g. normally coherences with opposite sign but equal value of the coherence order have to be selected simultaneously. Application of gradients during such a time of simultaneous existence of several coherence orders can annihilate some of the pathways, leading to a reduction of signal-to-noise. This will be explained in more detail in the next section. The second goal to achieve is the suppression of undesired pathways which is usually perfect except for accidential refocusing because of a less than optimal selection of gradient values. The amount of suppression achievable by a certain selection of gradients can be quantified and the gradients can be selected such that the undesired pathways are maximally suppressed [139]. However, especially for solvent suppression the goal is not only to reject certain coherence order pathways but to completely suppress any signal derived from these molecules.

With respect to solvent signal suppression, two distinct classes of pulse sequences employing gradients can be distinguished. In the first case, the undesired spin system topology is, in principle, able to generate the selected coherence orders. Thus the degree of suppression relies on the performance of the pulse sequences to prevent excitation of the selected coherences for the undesired spin topologies. This is the case when using spoil gradients e.g. for solvent suppression (Fig. 10c). Pulse or phase imperfections can produce undesired spin topologies (e.g. *z*-magnetization of the water resonance after the $(\pi/2)_y(I)$ pulse (Fig. 10c) which can pass the pulse sequence. Therefore, the quality of suppression relies critically on minimal pulse imperfections. In the second class of gradient experiments, the undesired spin topology is physically unable to form the selected coherences (e.g. because a heteronuclear spin with a

certain gyromagnetic ratio is missing). In this case the degree of suppression relies only on the duration and amplitude of the gradients employed and is not limited by pulse or phase imperfections. This is the case for the ^{1}H signal of H_2O in ^{1}H,X correlation experiments with coherence selection by a heteronuclear gradient echo. Coherence selection for the X spins during the evolution period combined with application of a second gradient before detection establishes a heteronuclear gradient echo for ^{1}H, X spin topologies. As the ^{1}H spins of H_2O can never lead to X spin coherence they are efficiently suppressed by the application of a heteronuclear gradient echo, independent of pulse imperfections. In a 2 mM aqueous solution suppression factors of $\approx 10^6$ are required to observe resonances of the solute under the solvent signal. This is achievable by the use of heteronuclear gradient echoes in contrast to the use of spoil gradients. Therefore the implementation of a heteronuclear gradient echo is recommended if efficient solvent suppression is required. Optimum implementations of heteronuclear gradient echoes with respect to sensitivity and artifact suppression will be discussed in the following section.

3.4. Sensitivity enhancement

An ingenious idea to improve the sensitivity of two-dimensional NMR experiments has been introduced by Rance et al. in 1991 [140–142], reviewed in [143]. In conventional 2D NMR experiments a cosine and a sine *amplitude*-modulated signal has to be recorded in different scans in order to achieve quadrature detection in the indirect dimension. This corresponds to selecting S_x and S_y during the t_1 evolution period, e.g. in a heteronuclear experiment with a coherence transfer step (CTS).

$$S_x \xrightarrow{t_1} S_x \cos(\Omega_S t_1) \xrightarrow{\text{CTS},t_2} I^- \cos(\Omega_S t_1) e^{i\Omega_I t_2}$$

$$S_x \xrightarrow{t_1} S_y \sin(\Omega_S t_1) \xrightarrow{\text{CTS},t_2} I^- \sin(\Omega_S t_1) e^{i\Omega_I t_2}$$

Only one of the two magnetization components is selected in each case, the other part does not contribute to the observed signal. However, by using a *phase-modulating* pulse sequence, both signals are retained and the signal-to-noise ratio (S/N) of the

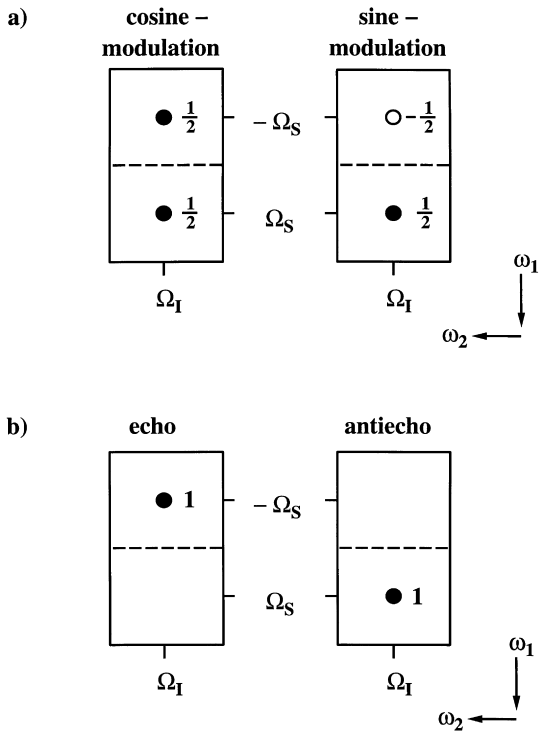

Fig. 11. (a) Fourier transform of the two amplitude-modulated signals, that are required for quadrature detection in the indirect evolution time in a two-dimensional experiment. Combination of the cosine- and sine-modulated 2D spectra yields a spectrum with pure phases and sign discrimination in ω_1. (b) Fourier transform of the echo- and anti echo signals in a phase-modulating pulse sequence. The numbers indicate the relative signal-to-noise.

experiment can be improved by $\sqrt{2}$, as is derived in the following [144,145]. The cosine- and sine- modulated signals in a conventional NMR experiment represent two signals with intensity $IN = (1/2)$ at positions $\pm\ \Omega_S$ in the spectrum (Fig. 11a). These four signals are added and folded during processing and Fourier transformation and yield a single cross peak in the final spectrum with a signal intensity of $4 * (1/2) = 2$. Assuming that the standard deviation of the statistical noise σ at each of the four signals is $\sigma = 1$, the noise at the peak position in the final spectrum is $\sqrt{4}$, yielding a signal-to-noise of S/N $= 2/2 = 1$. More generally:

$$\text{S/N} = (IN*\sqrt{n})/\sigma \quad (7)$$

In contrast to this amplitude-modulating coherence transfer, the use of a phase-modulating pulse sequence

achieves coherence order selective transfers corresponding to the echo- ($S^+ \rightarrow I^-$) and antiecho signal ($S^- \rightarrow I^-$):
Antiecho:

$$S_x \xrightarrow{t_1} S^- e^{i\Omega_S t_1} \xrightarrow{\text{COS-CTS},t_2} I^- e^{i\Omega_S t_1} e^{i\Omega_I t_2}$$

Echo:

$$S_x \xrightarrow{t_1} S^+ e^{-i\Omega_S t_1} \xrightarrow{\pi(S),\text{COS-CTS},t_2} I^- e^{-i\Omega_S t_1} e^{i\Omega_I t_2}$$

Complex Fourier transformation yields two signals with intensity 1, since both S_x and S_y components are transfered simultaneously (Fig. 11b). Folding with respect to $\omega_1 = 0$ yields a cross peak with intensity 2, that can be phased to absorption. However, the noise is only increased by $\sqrt{2}$, thus S/N = $\sqrt{2}$ (cf. Eq. (7)).

Echo- and antiecho spectra can either be processed separately and combined to a single data set with pure phases, or prior to Fourier transformation they can be transformed to an amplitude-modulated time domain signal, which can be processed in the conventional manner [141]. Combination of the two time domain signals follows Eq. (9):

$$\begin{aligned} &e^{i\Omega_S t_1} e^{i\Omega_I t_2} \\ &\qquad \xrightarrow{\text{addition}} \cos(\Omega_S t_2) e^{i\Omega_I t_2} \\ &e^{-i\Omega_S t_1} e^{i\Omega_I t_2} \end{aligned}$$

$$\begin{aligned} &e^{i\Omega_S t_1} e^{i\Omega_I t_2} \\ &\qquad \xrightarrow[90^\circ \text{ zero order phase in } \omega_2]{\text{subtraction,}} \sin(\Omega_S t_2) e^{i\Omega_I t_2} \\ &e^{-i\Omega_S t_1} e^{i\Omega_I t_2} \end{aligned} \tag{9}$$

The combination of a gradient echo with amplitude- or phase-modulating pulse sequences has very different effects on the signal-to-noise ratio. The implementation of a gradient echo during the evolution time of an amplitude-modulating pulse sequence reduces the S/N to $\frac{1}{\sqrt{2}}$ compared to the experiment without gradients (S/N = 1). This is explained in Fig. 12.

Gradient echoes cause phase modulation of the NMR signal, even if the pulse sequence is amplitude modulating. Thus, only the echo- or the antiecho signal that contribute to the cosine- or sine-modulated magnetization components (Fig. 12a, compare Fig. 11a) is selected (Fig. 12b). With Eq. (7) we obtain S/N = (1/2) $*$ $\sqrt{2} = 1/\sqrt{2}$. However, the application of a gradient echo is fully compatible with a phase-modulating pulse sequence. Therefore, the sensitivity improvement of $\sqrt{2}$ compared to a conventional NMR experiment is retained (Fig. 12c, compare Fig. 11b). As phase-modulating pulse sequences select only a single coherence order even without application of a gradient echo, they are called **C**oherence **O**rder **S**elective (COS) [144–146]. An alternative name reflecting the fact that both cartesian operators are transfered is PEP for **P**reservation of **E**quivalent **P**athways [147].

Pulse sequences have been introduced that achieve coherence order selective coherence transfer (COS-CT) in homonuclear TOCSY experiments [140], and for heteronuclear coherence transfer via a double INEPT transfer [141] (Fig. 13b) and heteronuclear, planar TOCSY sequences [146] (Fig. 13c). The latter two are compared to a conventional HSQC experiment in Fig. 13a. The combination of sensitivity enhancement with a heteronuclear gradient echo was first demonstrated on a sensitivity-enhanced HSQC experiment by Kay and coworkers [148] and later on a three-dimensional HNCO experiment [144,149]. Modification of the coherence transfer steps for application to I_nS versus IS spin systems are discussed in [146]. Upper bounds for such coherence transfers have been derived from a systematic optimization procedure [150].

In addition, experiments have been developed that achieve in-phase COS-CT ($S^- \rightarrow I^-$) [151], and a pulse sequence element for simultaneous COS-CT ($^{13}C \rightarrow {}^1H$ and $^{15}N \rightarrow {}^1H$) has been introduced [152]. An extension of sensitivity enhancement to *n*-dimensional NMR experiments is discussed in [153]. There it is derived, that in an *n*-dimensional NMR experiment, the signal-to-noise can be improved by $2^{(n-1)/2}$, if COS-CT is used starting from the first evolution period until acquisition. Applications are shown for HNCO and HCCH-TOCSY. Applications

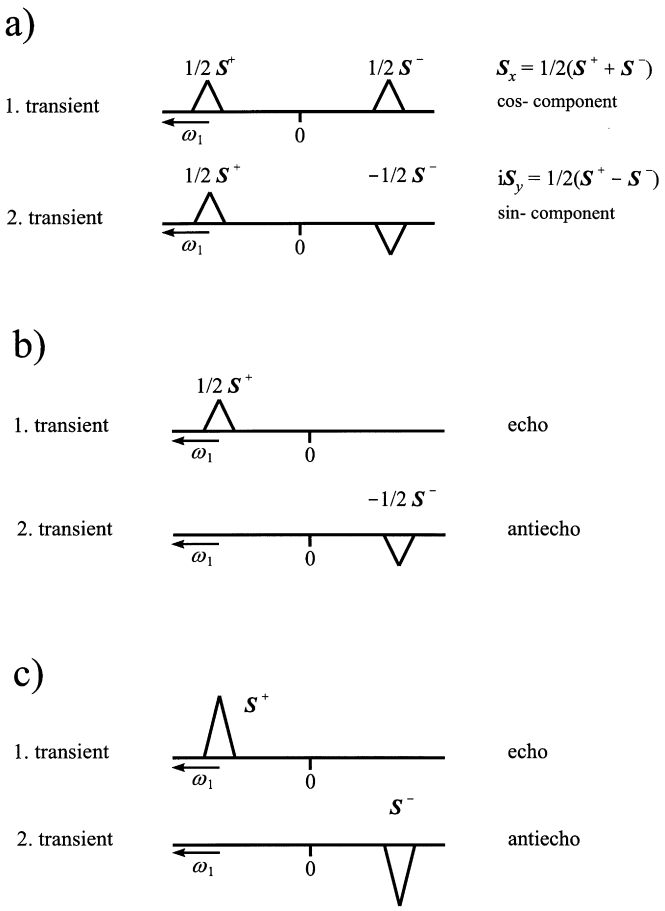

Fig. 12. Fourier transform of signals in the ω_1 dimension of two-dimensional experiments. (a) amplitude modulated signals, (b) phase-modulated signals obtained by implementing a gradient echo in an amplitude-modulating pulse sequence and (c) phase-modulated signals in a phase-modulating pulse sequence combined with a gradient echo.

to HSQC-TOCSY and TOCSY-HSQC experiments have also been published [154,155]. The mixing time required for homonuclear COS-CT equals the mixing time for a conventional in-phase transfer. In contrast, the mixing time for heteronuclear COS-CT from antiphase to in-phase coherence is twice as long as a conventional coherence transfer. This reduces the sensitivity of heteronuclear COS-CT steps, depending on the relaxation times of the nuclei involved in the coherence transfer [153]. This becomes more critical with increasing molecular weight of the molecule studied. However, in combination with deuterium labelling, relaxation rates are significantly reduced. Therefore, the sensitivity-enhanced methods are recommended to be used for proteins with molecular weights $<15-20$ kD or for larger molecules in combination with ^{2}labelling (see Section 5.8). In any case, the excellent solvent and artifact suppression achieved by the application of heteronuclear gradient echoes makes this a recommended accessory for heteronuclear NMR experiments, especially for use with samples that are dissolved in H_2O.

3.5. Water-flip-back

While dephasing of the H_2O magnetization by applying a heteronuclear gradient echo (e.g. in the pulse sequences of Fig. 13b,c) achieves dramatically improved solvent suppression compared to presaturation, the dephasing may still reduce the sensitivity for

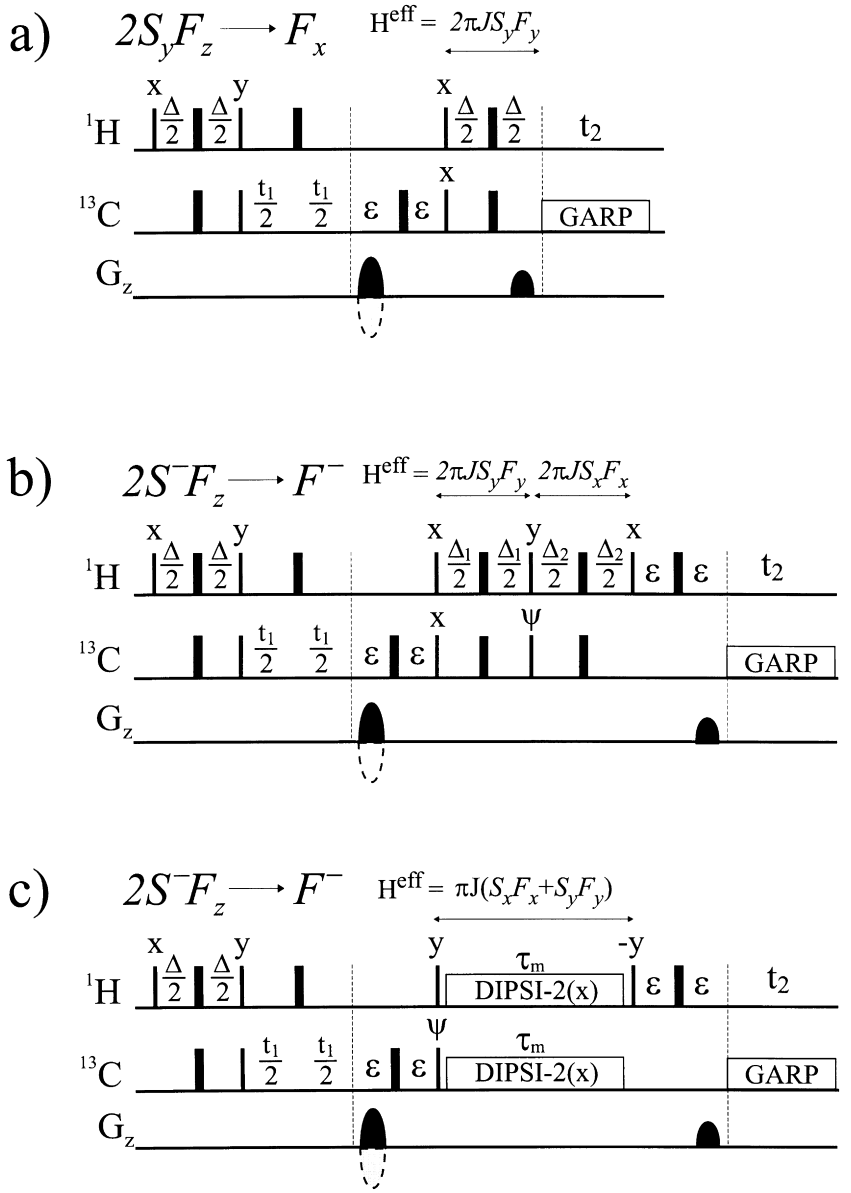

Fig. 13. Heteronuclear correlation experiments employing a heteronuclear gradient echo. Note that the gradient for dephasing the ^{13}C coherence during t_1 is applied before the 180°(^{13}C) refocusing pulse in order to suppress artifacts from imperfect refocusing by this pulse. The coherence transfer between t_1 and t_2 is indicated for each pulse sequence. Also the effective Hamiltonian imposed by the mixing sequence is given on top of each figure. (a) Conventional ^1H,^{13}C-HSQC experiment with heteronuclear gradient echo. For optimum coherence transfer, $\Delta = 1/2J(H,C)$. (b) and (c) Sensitivity-enhanced HSQC with COS-CT for the $^{13}C \rightarrow {}^1H$ transfer. Echo- and antiecho selection is achieved by inversion of the gradient following t_1 in combination with inversion of the phase ψ and storing the resulting two FIDs in separate memory locations (see Section 3.4). The transfer amplitude depends on the ^{13}C multiplicity. In (b) for *IS* spin systems both delays should be set to $1/2J(H,C)$, for I_nS spin systems ($n = 1, 2, 3$) recommended settings are $\Delta_1 = 1/4J(H,C)$ and $\Delta_2 = 1/2J(H,C)$. In (c) τ_m should be $1/J$ or $0.7/J$ for the observation of *IS* or I_nS spin systems.

the observation of solvent exchangeable spins, e.g. amide protons. The much longer T_1 relaxation time of H_2O compared to the protein resonances prevents the solvent magnetization from complete relaxation and thus leaves the solvent signal in a partially saturated state at the end of the NMR pulse sequence. Thus, chemical exchange and spin diffusion between protein protons (mainly the H^N and H_α spins) and partially saturated water lead to partial saturation of the H^N spins (''saturation transfer'') and therefore reduce the magnetization available for the next scan. This can be avoided by turning the water magnetization back along the *z*-axis (''water-flip-back'') before or after the acquisition time, and dephasing only the residual water magnetization during acquisition. In some sequences, e.g. where proton frequencies near the water resonance should be observed, water-flip-back has to be accomplished without the use of a water-selective pulse. For example, radiation damping automatically flips the water magnetization back along the *z*-axis within a short delay of few milliseconds [156], e.g. during the mixing time in a NOESY experiment, provided the water magnetization is transverse and not dephased by gradients. The time needed for this process is determined by the quality factor (*Q*) of the probe. However, in pulse sequences that explicitely employ water-flip-back pulses (see the following) radiation damping of the water magnetization should be avoided because it may interfere with the water-flip-back scheme. In these pulse sequences, it is therefore important to keep all transverse components of the water dephased throughout the whole pulse sequence by the application of suitable dephasing and rephasing gradients during delays and to only rephase the water magnetization before it is turned along the *z*-axis prior to acquisition.

For example, the standard HSQC experiment inherently contains water-flip-back if the phases of the 90°(H) proton pulse are set accordingly [157]. Radiation damping of the water magnetization can be prevented by employing two gradients just before and after the 90°(N) pulses that flank the t_1-evolution period as indicated in Fig. 14a. In order to combine this pulse sequence with an efficient water suppression scheme, the experiment in Fig. 14b can be used. In Fig. 14b water-flip-back is combined with a WATERGATE [158,159] pulse sequence by employing water-selective pulses. Without water-flip-back the solvent magnetization is transverse during the reverse INEPT and efficiently dephased by the WATERGATE element, because the element 90°(selective) − 180°(non-selective)-90°(selective) leads to a net rotation of 0° for the solvent magnetization. The application of water-flip-back pulses aligns the solvent magnetization along *z* during the WATERGATE sequence, which therefore will only dephase residual water magnetization that has not been flipped back along the z-axis beforehand. This concept [160] has been demonstrated by Grzesiek and Bax for experiments that detect amide protons, e.g. ^1H,^{15}N-HSQC and ^{15}N-{^1H}-NOE [161]. Sensitivity improvements of 10%–20% have been observed.

In sensitivity-enhanced heteronuclear correlation experiments with a heteronuclear gradient echo, the H_2O magnetization is completely dephased at the beginning of the acquisition period. Thus, through the mechanism described before, dephased H_2O magnetization can be transfered to H^N spins and result in reduced initial H^N magnetization for the following scan. However, by the use of appropriate phases for the ^1H pulses and water selective pulses, the H_2O magnetization is aligned along $+z$ at the beginning of the acquisition time [149,157] (Fig. 14c). Remaining transverse magnetization components of the solvent signal (resulting from pulse imperfections) are efficiently dephased by the heteronuclear gradient echo. The signal-to-noise and water-suppression using a one-dimensional version of the pulse sequence Fig. 14c and different states of the water magnetization before acquisition is illustrated in Fig. 14d. Almost any pulse sequence can be combined with water-flip-back to avoid H_2O saturation and thus improve the signal-to-noise ratio.

3.6. Multiple-quantum line narrowing

Another principle to improve the sensitivity in heteronuclear NMR spectra of isotopically labelled biomacromolecules has been utilized recently. This is based on the fact, that the relaxation of ^1H-spins bound to ^{13}C is largely dominated by the dipolar interaction between the ^{13}C- and the ^1H-spin. However, it has been shown earlier that for molecules in the slow tumbling limit the dipolar coupling between two nuclei (e.g. ^1H–^{13}C) does not contribute, to first

a)

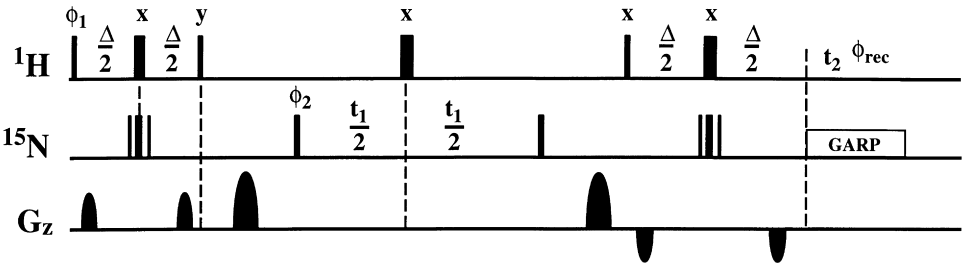

ϕ_1= x; ϕ_2 = x, −x + TPPI (t_1); ϕ_{rec} = x, −x.

b)

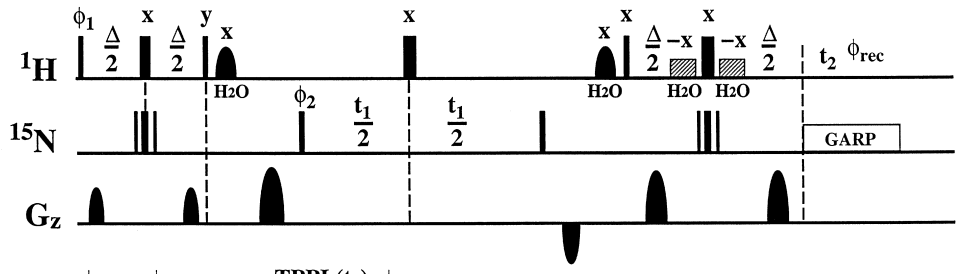

ϕ_1= x; ϕ_2 = x, −x + TPPI (t_1); ϕ_{rec} = x, −x.

c)

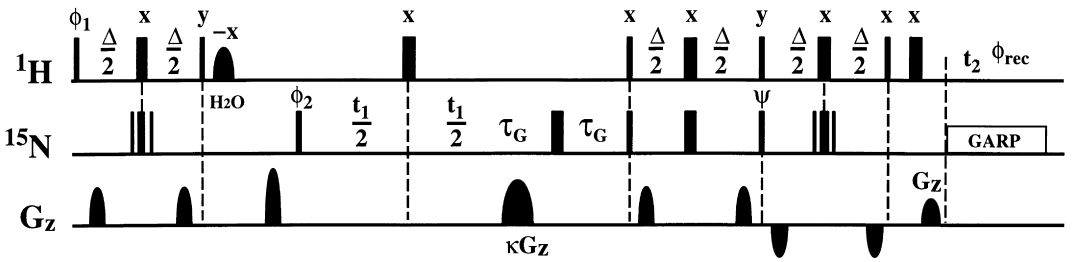

κ = +/−10; ψ = +/−y; ϕ_1= x; ϕ_2 = x, −x; ϕ_{rec} = x, −x.

d)

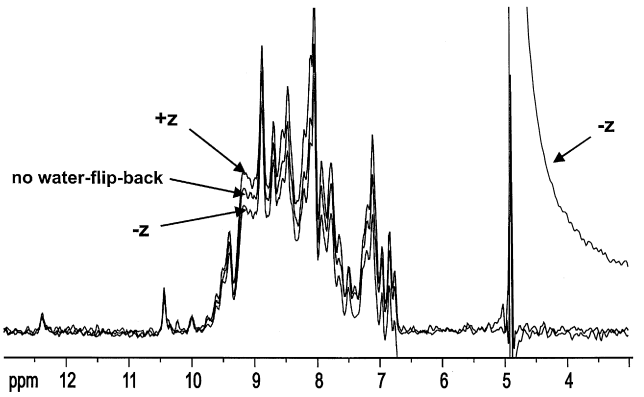

Fig. 14.

order, to the relaxation of multiple quantum coherence between the two spins [162]. Therefore, the main relaxation pathway for protons in ^{13}C-labelled biomacromolecules can be eliminated by utilizing the evolution of heteronuclear ^{1}H,^{13}C multiple quantum rather than ^{1}H or ^{13}C single quantum coherences during an NMR pulse sequence. This so-called multiple-quantum line narrowing has been demonstrated in a number of applications to proteins [163,164], also in combination with fractional deuteration [165]. As a result, ^{13}C constant-time evolution can be used even with molecules $>$ 20 kD molecular weight, if the HMQC-type rather than HSQC-type experiments are implemented.

For carbon multiplicities $>$ 1, the same principle can be exploited. However, for CH_2 groups, the evolution of ^{13}C, ^{1}H, ^{1}H triple-spin, triple- and single-quantum coherences is required. A technique that allows the combined evolution of two-spin and three-spin multiple quantum coherences has been recently introduced and has been shown to yield significantly reduced relaxation rates for an RNA molecule [166]. The signal-to-noise improvement of ≈ 3 observed in the RNA 36mer is larger than what has been demonstrated for proteins. This is because there are fewer additional ^{1}H,^{1}H relaxation pathways in RNA or DNA than in proteins as a result of the smaller proton density in nucleic acids.

4. Experiments for the assignment of backbone resonances

In the following two sections, recommended pulse sequences for the assignment of backbone and side-chain resonances using uniformly ^{13}C,^{15}N-labelled proteins will be discussed. Where appropriate, sensitivity-enhanced back transfer is combined with a heteronuclear gradient echo and water-flip-back. The use of these building blocks yields excellent solvent suppression without saturation of exchangeable proton signals. This is of prime importance since most of the experiments described excite amide proton magnetization which is subject to exchange with the solvent, especially at neutral or basic pH or in partially folded biomolecules.

The transfer amplitudes given for the individual experiments include terms for chemical shift evolution only for real-time implementations, not for constant-time evolution. Relaxation of z operators is ignored considering that, for large molecules, longitudinal relaxation times are much longer than transverse relaxation times. In addition, the gain of up to $\sqrt{2}$ in signal-to-noise as a result of the use of the sensitivity-enhanced back-transfer is not included in the transfer functions. In pulse sequences where sensitivity enhancement is employed the gradient amplitude κ and the pulse phase ψ have to be inverted and the resulting FIDs stored in a different memory location for data processing as described in Section 3.4. $K \approx \gamma H/\gamma x$ is experimentally optimized. In the pulse sequences, 180° C_α or C' pulses that are merely applied to compensate for Bloch-Siegert phase shifts are labelled ''BSP''. If pulse phases have to be adjusted in order to compensate for Bloch–Siegert phase shifts this is indicated in the phase cycle given below the pulse sequences. Pulse phases not stated explicitly in the pulse sequence are along x.

4.1. 3D HNCO and 3D HNCA

The pulse sequences for the 3D HNCO and 3D HNCA experiments (Fig. 15) are identical, except for the interchange of C_α and C' pulses. Two types of cross peaks are observed in the HNCA experiment, namely the correlations $H^N(i)$, $N(i)$, $C_\alpha(i)$ and $H^N(i)$,

Fig. 14. (a) Conventional ^{1}H,^{15}N-HSQC experiment combined with water-flip-back by suppression of radiation damping. (b) Solvent suppression with the WATERGATE technique in a conventional HSQC experiment can be combined with water-flip-back. For the shaped water-selective proton pulses a 1 ms 90° Gaussian or a 2.5 ms 270° Gaussian pulse (then with inverted phase) can be used. As rectangular water-flip-back pulses in the WATERGATE element a 90° pulse of 1 ms duration can be employed. (c) Sensitivity enhanced ^{1}H,^{15}N-HSQC experiment with water-flip-back employing a 2.5 ms 270° Gaussian shaped pulse. Note that the two-step phase cycle on ϕ_2 is optional, because the heteronuclear coherence is already selected by the heteronuclear gradient echo. (d) Comparison of 500 MHz proton 1D experiments using the pulse sequence (c) on a 1 mM sample of a PH domain at pH 7.0. The phase of the water-selective pulse was chosen such that the water-magnetization is aligned along $+z$ or $-z$ prior to acquisition. For the experiment without water-flip-back the water-selective pulse was omitted. The S/N and the water supression are optimal when the water magnetization is aligned along z at the beginning of acquisition. Note that the water suppression is unacceptable if the water magnetization is aligned along -z prior to acquisition.

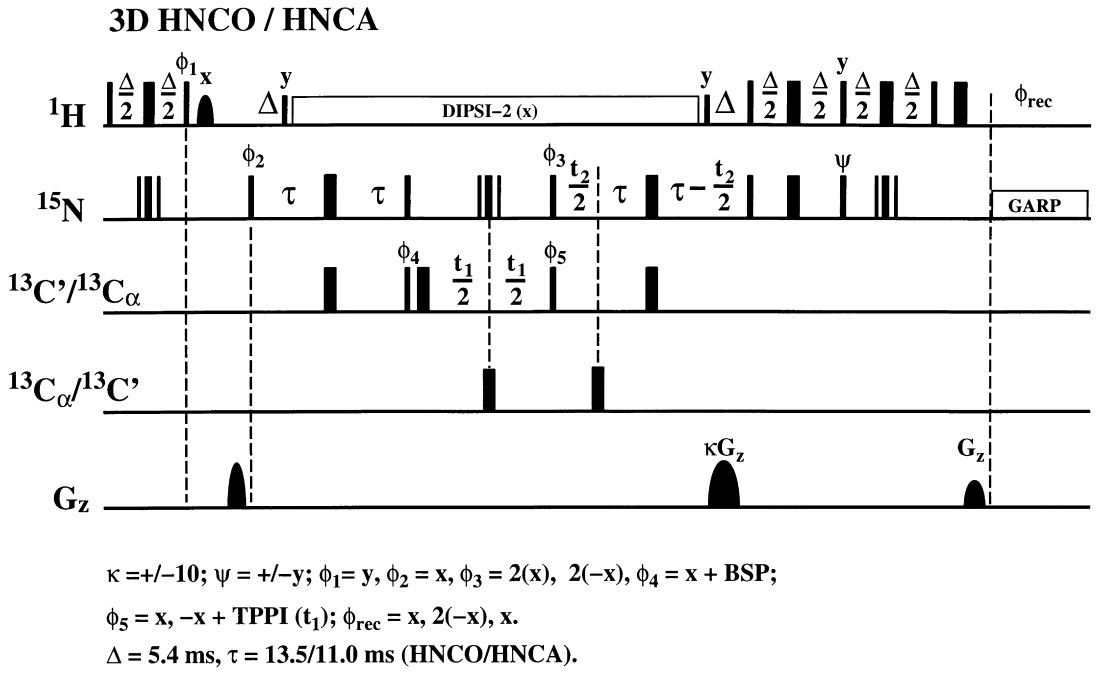

Fig. 15. Pulse sequences for 3D HNCO and HNCA experiments. HNCO and HNCA are identical but for the interchange of pulses acting on C_α and C' nuclei. Note, that for the selection of echo/antiecho pathways, which is required to achieve frequency discrimination for the ^{15}N dimension (ω_2), for every t_2 point a second experiment has to be recorded with the gradient κ and the phase ψ inverted and the resulting FIDs have to be converted as described in Section 3.4.

N(i), $C_\alpha(i-1)$ because both the couplings $^1J_{C\alpha(i),N(i)} = 11$ Hz and $^2J_{C\alpha(i\text{-}1),N(i)} = 7$ Hz are of similar size (cf. Fig. 2). In contrast, only the correlations $H^N(i)$, N(i), $C'(i-1)$ are observed in the HNCO, since $^1J_{C'(i\text{-}1),N(i)} = 15$ Hz, while $^2J_{C'(i),N(i)} \approx 0$.

The pulse sequences shown in Fig. 15 are published pulse sequences [45] and have been improved by the introduction of sensitivity enhancement in the N–H back transfer. This results in a gain in sensitivity of up to $\sqrt{2}$ compared to the corresponding unmodified experiment. Both experiments use constant time evolution of ^{15}N and both are ''out and back'' experiments. Thus, the transfer pathway starts on a nucleus (the H^N in these experiments) and magnetization is detected on the same nucleus, after chemical shifts of other nuclei have been monitored. The ''out and back'' pathway is not the only conceivable way to correlate nuclei, but magnetization can also be transferred from a starting nucleus to another nucleus to be detected (transfer experiment). In the following section, ''out and back'' and transfer experiments will be compared with respect to sensitivity using the HNCA as an example, as will be the implementations of these experiments with constant time or real

Fig. 16. Different implementations of the HNCA experiment. (a) 3D HNCA as transfer experiment. Note that the pulse sequence corresponds to the 3D HCANNH experiment [50–52]. A pulse serving to compensate Bloch–Siegert phase shifts (cf. Fig. 9c) is labelled ''BSP'' (b) Implementation of a 3D HNCA as an ''out-and-back'' experiment. This is the optimal implementation with respect to sensitivity. (c) Out-and-back HNCA experiment with constant-time chemical shift evolution of C_α frequencies during t_1. This experiment provides higher resolution for the C_α dimension but is much less sensitive than the corresponding RT implementation shown in (b). However, in combination with deuterium labelling this is the experiment of choice. (d) Out-and-back HNCA with separate evolution of ^{15}N chemical shifts during t_2 followed by a delay $2\tau_2$ for refocusing of the ^{13}C,^{15}N antiphase coherence. Apart from being less sensitive than the sequence shown in (b), this implementation would also lead to phase-twisted line shapes in ω_2 because two couplings ($^1J_{C,N}$ and $^2J_{C,N}$) evolve during $2\tau_2$.

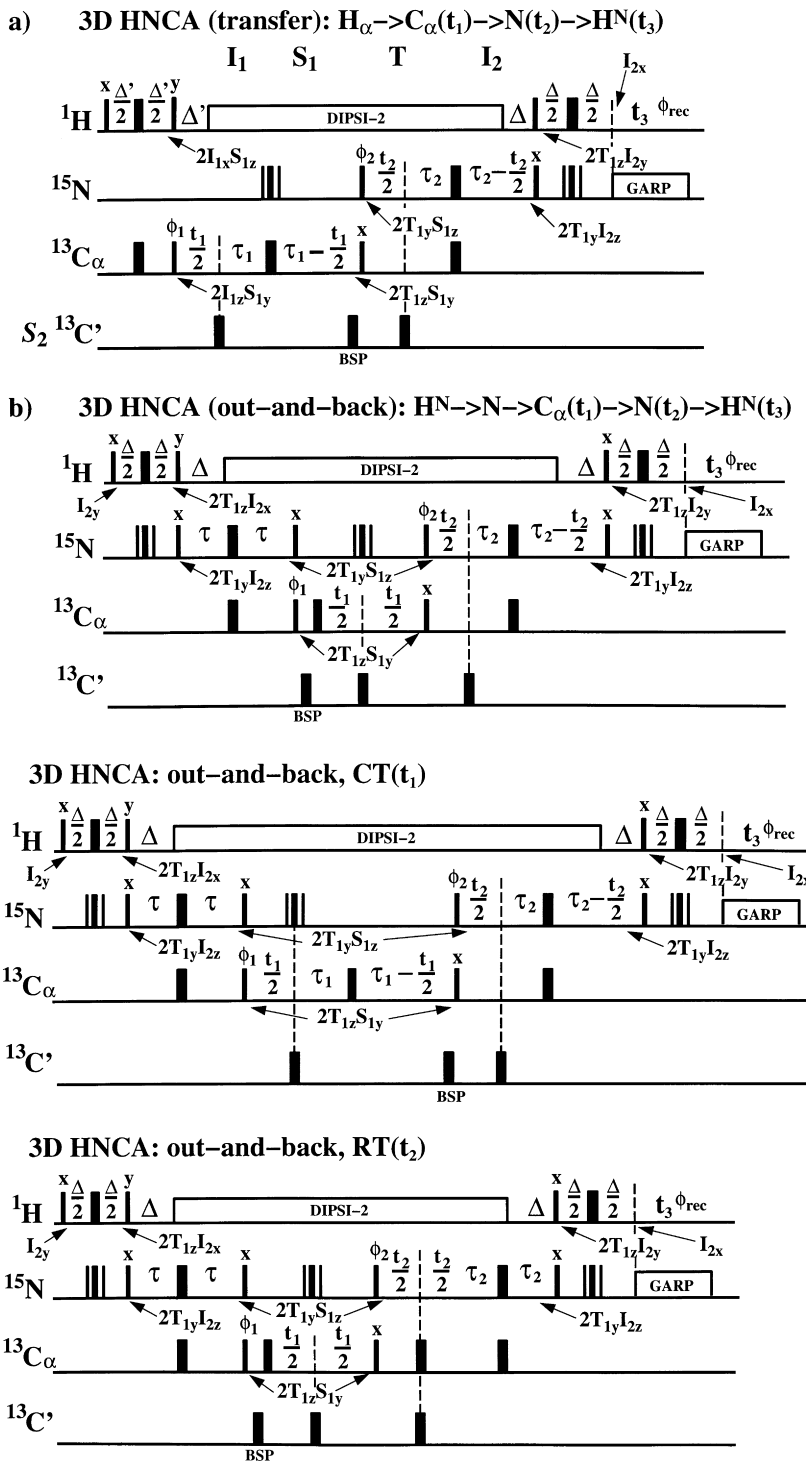
a) 3D HNCA (transfer): Hα–>Cα(t1)–>N(t2)–>HN(t3)
I1 S1 T I2
DIPSI–2
GARP
BSP
b) 3D HNCA (out–and–back): HN–>N–>Cα(t1)–>N(t2)–>HN(t3)
DIPSI–2
GARP
BSP
c) 3D HNCA: out–and–back, CT(t1)
DIPSI–2
GARP
BSP
d) 3D HNCA: out–and–back, RT(t2)
DIPSI–2
GARP
BSP

Fig. 16.

time evolution. The ratio of active to passive couplings as well as the values of the relaxation time T_2* determine which implementation is preferable.

4.1.1. ''Out and back'' versus transfer experiments

Fig. 16 shows the pulse sequences for the implementation of HNCA as transfer experiment (a) and as a ''out and back'' experiment (b). In the transfer experiment, which has been introduced as HCANNH experiment [50–52], the evolution times for C_α (t_1) and ^{15}N (t_2) are implemented as constant time evolution times, and the durations $2\tau_1$, $2\tau_2$ of the constant time delays are chosen such that $\sin(\pi^1 J_{C\alpha,N} 2\tau_1)\cos(\pi^2 J_{C\alpha,N} 2\tau_1)$ $\sin(\pi^1 J_{C\alpha,N} 2\tau_2)C\alpha(\pi^2 J_{C\alpha,N}{}^2 J_2)$ are maximal. For the couplings encountered in proteins, this corresponds to maximum transfer for $2\tau_1, 2\tau_2 \approx 28$ ms. Constant time evolution times of this duration allow for sufficient resolution in the heteronuclear dimension, at the same time the homonuclear C_α, C_β coupling is refocused during t_1. The transfer amplitude for the $H^N(i)$, $N(i)$, $C_\alpha(i)$ cross peak in this experiment is given by:

Transfer experiment:

$$H_\alpha \rightarrow C_\alpha(t_1) \rightarrow N \rightarrow H^N(t_3)$$

$$\sin^2(\pi^1 J_{H\alpha,C\alpha}\Delta')\exp(-\Delta'/T_{2H\alpha})$$

$$\sin(\pi^1 J_{C\alpha,N} 2\tau_1)\cos(\pi^2 J_{C\alpha,N} 2\tau_1)$$

$$\cos(\pi^1 J_{C\alpha,C\beta} 2\tau_1)\exp(-2\tau_1/T_{2C\alpha})$$

$$\sin(\pi^1 J_{C\alpha,N} 2\tau_2)\cos(\pi^2 J_{C\alpha,N} 2\tau_2)$$

$$\exp(-2\tau_2/T_{2N})\sin^2(\pi^1 J_{N,HN}\Delta)\exp(-\Delta/T_{2HN}) \qquad (10)$$

The transfer amplitude for the $H(i)$, $N(i)$, $C_\alpha(i)$ cross peak in the ''out-and-back'' experiment (Fig.16b) is given by:

''Out-and-back''-HNCA:

$$H^N \rightarrow N \rightarrow C_\alpha(t_1) \rightarrow N(t_2) \rightarrow H^N(t_3)$$

$$\sin^4(\pi^1 J_{N,HN}\Delta)\exp(-2\Delta/T_{2H}N)$$

$$\sin^2(\pi^1 J_{C\alpha,N} 2\tau)\cos^2(\pi^2 J_{C\alpha,N} 2\tau)$$

$$\exp(-4\tau/T_{2N})\cos(\pi^1 J_{C\alpha,C\beta} t_1)\exp(-t_1/T_{2C\alpha}) \qquad (11)$$

Neglecting relaxation, both implementations have the same transfer amplitudes of 0.45 and therefore the same sensitivity, assuming typical values for $^1J_{HN,N} =$ 92 Hz, $^1J_{H\alpha,C\alpha} = 140$ Hz, $^1J_{C\alpha,C\beta} = 35$ Hz and $2\tau = 2\tau_1 = 2\tau_2 \approx 28$ ms, $\Delta = 1/(2^1J_{HN,N})$, $\Delta' = 1/(2^1J_{H\alpha,C\alpha})$. However, assuming relaxation times T_2* for $^1H_\alpha$, $^{13}C_\alpha$, $^1H^N$ and ^{15}N spins to be 20, 20, 100 and 100 ms, we obtain a ratio of sensitivities for the first increment ($t_1 = 0$) of 0.23/0.06 for the ''Out-and-back'' variant versus the transfer variant. Although the ''Out-and-back'' pulse sequence looks more complicated, this implementation is more sensitive, because the evolution of fast-decaying transverse magnetization of the C_α- and H_α-spins during extended time periods is avoided. As the overall transfer efficiency of any experiment is a function of both the couplings involved and relaxation times T_2*, the values of the delays have to be optimized for each experiment. Taking the relaxation terms into account, it becomes clear that $2\tau_1$ should be chosen to be shorter than $2\tau_2$ in the HNCA transfer experiment, because relaxation is much faster during $2\tau_1$.

4.1.2. ''Constant time'' versus ''real time'' evolution

Two types of evolution times can be distinguished in multidimensional hetero-nuclear NMR experiments: either only chemical shift evolution is desired to take place, with all couplings being refocused, or one coupling is to evolve for a certain time during the evolution time as well, to prepare a coherence transfer step. In both cases, the evolution time can be implemented in a ''constant time'' (CT) or ''real time'' (RT) fashion. The two implementations will have different sensitivity, depending on the desired resolution, the size of passive couplings and the relaxation time of the evolving nucleus. The sensitivity is given as the time-averaged integral over the FID taken on-resonance at the signal of interest.

We first consider the ''real time'' evolution of the C_α chemical shift in an ''out-and-back''-HNCA experiment (Fig. 16b). In the constant time version of this experiment (Fig. 16c), the t_1 evolution period $[(t_1/2)180°(C',N)(t_1/2)]$ is replaced by $H[(t1/2)180°(C',N)(\tau_1)180°(C\alpha)(\tau_1-t_2/2)]$. Chemical shift evolution for C_α takes place during a delay $2\tau_1 \approx 1/^1J_{C\alpha,C\beta}$ in order to refocus the C_α,C_β coupling. This is to be compared with the ''real time'' implementation (Fig. 16b), in which

t_1^{max} is restricted to $\approx$10 ms ($\approx 1/(3^1J_{C\alpha,C\beta})$), because the $^1J_{C\alpha,C\beta}$ coupling is not removed in ω_1 and therefore the spectral resolution is limited by the size of the $^1J_{C\alpha,C\beta}$ coupling constant. (Note, that the C_α,C_β coupling can also be refocused by application of a C_β- or C_α-selective 180° pulse during t_1, because, with the exception of Gly, Ser and Thr residues, the frequency bands of C_α and C_β chemical shifts are reasonably well separated [167,168]).

To compare the sensitivity S_{CT} of the constant-time version ($t_1^{max} = 2\tau_1 = 1/(^1J_{C\alpha,C\beta})$) with the sensitivity S_{RT} of the real time implementation ($t_1^{max} = 2\tau_1/3 = 1/(3^1J_{C\alpha,C\beta})$, we obtain using $J = ^1J_{C\alpha,C\beta}$ and $\beta = \pi J t_1$:

$$S_{CT} = \frac{1}{t_1^{max}} \int_0^{t_1^{max}} (\cos(\pi J 2\tau_1)\exp(-2\tau_1/T_2))\, dt_1$$

$$= \cos(\pi J 2\tau_1)\exp(-2\tau_1/T_2) \quad (12a)$$

$$S_{RT} = \frac{1}{t_1^{max}} \int_0^{t_1^{max}} (\cos(\pi J t_1)\exp(-t_1/T_2))\, dt_1$$

$$= 3/(\pi J 2\tau_1) \int_0^{\pi/3} (\cos\beta \exp(-\beta/(\pi J T_2))\, d\beta \quad (12b)$$

For $a = -1/(\pi J T_2)$ we obtain:

$$S_{RT} = 3/\pi \left\{ \frac{1}{1+a^2} e^{a\beta} (\sin\beta + a^*\cos\beta)|_0^{\pi/3} \right\} \quad (12c)$$

and with the integration limits:

$$S_{RT} = \frac{3JT_2}{1+(\pi J T_2)^2} \times \left(e^{-1/(3JT_2)} \left(\pi J T_2 \sin\frac{\pi}{3} - \cos\frac{\pi}{3} \right) + 1 \right) \quad (12d)$$

It should be pointed out that it is appropriate to determine the intensity of the real time cross peak on-resonance at the C_α signal, because the evolution time is too short to resolve the $^1J_{C\alpha,C\beta}$ splitting. Under these circumstances, maximum intensity is expected at the center of the cross peak and not at the positions of the two lines of the C_α doublet. With the same argument, the calculation also accounts for the line broadening caused by the evolution of the $^1J_{C\alpha,C\beta}$ coupling during t_1, which reduces the signal intensity.

For $^1J_{C\alpha,C\beta} = 35$ Hz, $2\tau_1 = 1/^1J_{C\alpha,C\beta}$ and for a C_α T_2 of 20 ms, the ratio of sensitivities is:

$$|S_{RT}/S_{CT}| = 0.67/0.24 \approx 2.8 \quad (12e)$$

Thus, the real-time implementation is far superior for the $^{13}C_\alpha$ evolution time. The corresponding integrals are represented graphically in Fig. 17a and b.

Second, we consider the chemical shift evolution of ^{15}N during t_2. In both the HNCA and the HNCO experiment, optimal refocusing of $J_{C,N}$ is needed, in addition to the evolution of ^{15}N chemical shifts. In the constant-time evolution of the ^{15}N chemical shift during t_2 (Fig. 16a,b,c), coupling and shift evolution take place simultaneously during a constant-time delay $2\tau_2 = 1/(2^1J_{C',N})$ for the HNCO and $2\tau_2 \approx 1/(4^1J_{C\alpha,N})$ for the HNCA experiment, respectively. The spectral resolution in ω_2 is limited by $t_2^{max} = 2\tau_2$. During $2\tau_2$, the magnetization decays with T_{2N} of the ^{15}N spins. In the real-time version of an HNCO (Fig. 16d, HNCA not feasible due to mentioned phase twist), ^{15}N chemical shift evolution in t_2 with decoupling of all $J_{C,N}$ couplings is followed by refocusing of the ^{13}C, ^{15}N antiphase coherence during a delay $2\tau_2 = 1/(2^1J_{C',N})$. To obtain the same resolution in both experiments, $t_2^{max} = 1/(2^1J_{C'N})$ must be chosen. (The HNCA is not considered here, since it would be impossible to obtain a purely in phase absorptive line shape in the ^{15}N frequency dimension as a result of the different dephasing of the $^1J_{C\alpha}$,N and $^2J_{C\alpha}$,N couplings during $2\tau_2$). The relative sensitivities of the CT and the RT-HNCO experiments are ($J = {}^1J_{C',N}$, $T_2 = T_{2N}$):

$$S_{CT}^{HNCO} = \sin(\pi J 2\tau_2)\exp(-2\tau_2/T_2) \quad (13a)$$

$$S_{RT}^{HNCO} = 1/(2\tau_2) \int_0^{2\tau_2} \exp(-t_2/T_2))\, dt_2 \sin(\pi J 2\tau_2) \times \exp(-2\tau_2/T_2) \quad (13b)$$

$$S_{RT}^{HNCO} = 2JT_2(\exp(-t_2/T_2)]|_0^{1/(2J)} . S_{CT} \quad (13c)$$

$$S_{RT}^{HNCO} = 2JT_2(1 - \exp(-1/(2JT_2)))S_{CT} \quad (13d)$$

With $J = {}^1J_{C',N} = 15$Hz, $2\tau_2 = 1/(2^1J_{C',N}) = 33.33$ ms, and $T_2 = 100$ ms we obtain:

$$\left| S_{CT}^{HNCO}/S_{RT}^{HNCO} \right| = 0.72/0.61 \approx 1.16 \quad (13e)$$

As can also be expected from comparing Fig. 17c

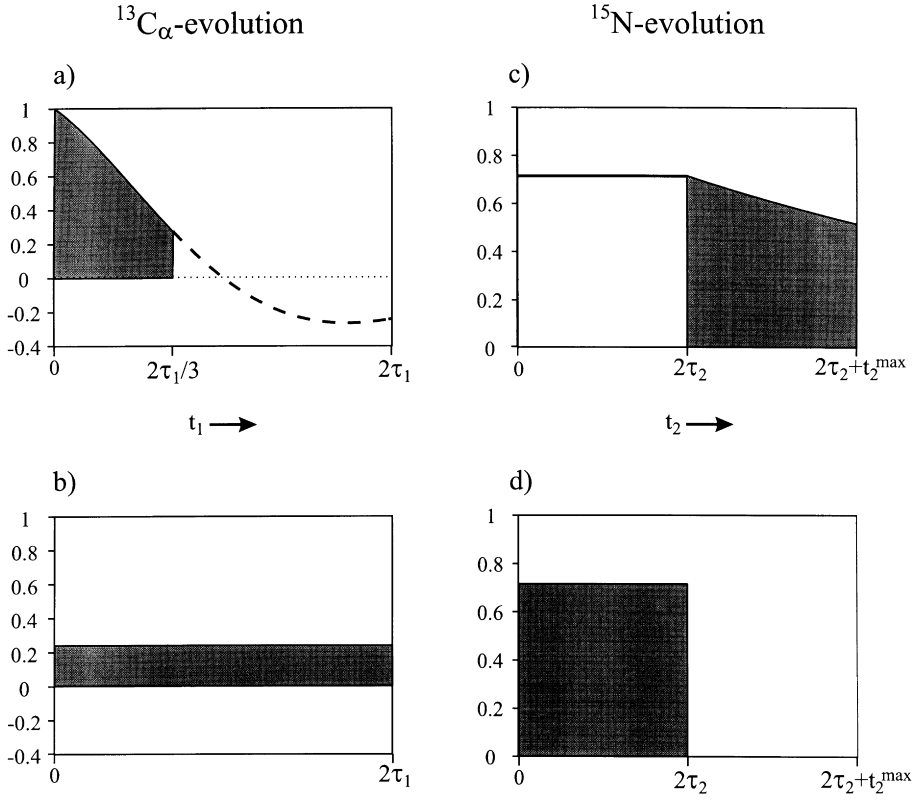

Fig. 17. Relative sensitivities of constant-time (CT) and real-time (RT) evolution times, as calculated as integrals taken over the respective FIDs. The integrals have to be normalized with respect to the maximum evolution time $t_{1,2}^{max}$ (Eqs. (12) and (13)). In (a) and (b), evolution of couplings is not desired during the evolution time. (a) real time evolution ($t_1^{max} = 2\tau_1/3 = 10$ ms) (compare Fig. 16b) (b) constant time evolution ($t_1^{max} \leq 2\tau_1 = 1/J$) (compare Fig. 16c). A relaxation time T_2 of $0.7/J$ was assumed for the spin evolving chemical shift, e.g. for $^{13}C_\alpha$ with $J = {}^1J_{C\alpha,C\beta} = 35$ Hz and $T_2 = 20$ ms. (c), (d) Relative sensitivities for evolution times where evolution of a coupling and chemical shifts is needed. (c) Real time evolution with $2\tau_2 \leq (2\tau_2 + t_2) \leq (t_2^{max} + 2\tau_2)(t_2^{max} = 2\tau_2 = 1/(2J))$ (see Fig. 16d) and (d) constant time evolution ($t_2^{max} \leq 2\tau_2 = 1/(2J)$) (as in Fig. 16a,b,c). A relaxation time of $T_2 \approx 1.5/J$ was assumed for the nucleus evolving chemical shift. (E.g. for ^{15}N with $J = {}^1J_{C',N} = 15$ Hz and $T_2 = 100$ ms.)

and d, the constant-time implementation is about 20% more sensitive.

The use of constant time evolution is always advantageous if a delay for the evolution of a coupling is needed at that point of the pulse sequence, in order to prepare a coherence transfer step. If the delay is not long enough to provide adequate resolution of the chemical shift (as in the case of the large $^1J_{HC}$ or $^1J_{HN}$ couplings), it can be extended in what is called ''shared-time'' or ''semi-constant-time'' [61,65] evolution. This will be explained in Section 5.5 using the example of an HCCH-TOCSY experiment.

In summary, in heteronuclear multidimensional NMR experiments it is necessary to minimize delays during which transverse magnetization is evolving of spins that relax fast or that have many homonuclear couplings. In a protein backbone, these conditions are most critical for the C_α and H_α spins, which relax fast as a result of their dipolar interaction and the large number of homonuclear coupling partners. The H_α is broadened by couplings to the H^N and H_β spins, and the C_α as a result of couplings to the aliphatic side-chain carbons. In contrast, the amide nitrogen does not have any, and the H^N spin has only one homonuclear

coupling partner. Further, the dipolar interaction of the H^N spins with the directly bound nitrogen is smaller by a factor $[\gamma(^{13}C)/\gamma(^{15}N)]^2 \approx 6$, because $\gamma(^{15}N)$ is smaller than $\gamma(^{13}C)$ [169].

We now have the tools at hand to discuss heteronuclear triple resonance experiments in detail. In this discussion, we will especially keep in mind the sensitivity of the experiments and the use of pulsed field gradients for solvent- and artifact suppression.

The pulse sequence for the ''out-and-back'' CT-HNCO (Fig. 15) can be described as a series of INEPT transfers $H^N \rightarrow N$, $N \rightarrow C'$, and back to the H^N for detection. The HNCO experiment yields a single cross peak per amide arising from the $^1J_{C',N}$-coupling (the $^2J_{C',N}$ coupling is ≈ 0). The transfer amplitude for this experiment is given by:

$$\text{3D HNCO } H^N \rightarrow N \rightarrow C'(t_1) \rightarrow N(t_2) \rightarrow H^N(t_3)$$

$$\sin^4(\pi^1 J_{N,HN}\Delta)\exp(-2\Delta/T_{2HN})\sin^2(2\pi^1 J_{C',N}\tau)$$

$$\exp(-4\tau/T_{2N}) \qquad (14)$$

The decoupling of the protons in the middle part of the pulse sequence by a multiple pulse decoupling sequence (e.g. DIPSI-2, or WALTZ-16) yields higher sensitivity compared to the use of refocusing pulses [170,171]. The reason for this lies in the relaxation properties of the operators present during this time: the relaxation for antiphase coherence of the type $2N_{x,y}H_z$ (N and H denote the spin operators for ^{15}N and ^1H spins) is effected by T_{2N} and T_{1H} while in-phase coherence $N_{x,y}$ relaxes only with the T_{2N}. This leads to higher sensitivity of the experiment with decoupling.

The pulse sequence of the HNCA experiment (Fig. 15) is identical to the HNCO, with the exception that pulses on C_α and C' are interchanged. However, the HNCA experiment yields two cross peaks at the frequencies $H^N(i)$, $N(i)$, $C_\alpha(i)$ and $H^N(i)$, $N(i)$, $C_\alpha(i-1)$, because the $^1J_{C\alpha,N}$ (11 Hz) and the $^2J_{C\alpha,N}$ (7 Hz) couplings are both non zero. To enhance the valuable transfer to *both* the intra- and interresidual C_α $2\tau \approx 22$ ms $\approx 1/(4J_{C\alpha,N})$ is chosen. The transfer amplitudes for the two cross peaks are:

$$\text{3D HNCA } H^N \rightarrow N \rightarrow C_\alpha(t_1) \rightarrow N(t_2) \rightarrow H^N(t_3)$$

$$\sin^4(\pi^1 J_{N,HN}\Delta)\exp(-2\Delta/T_{2HN}) * f(\tau)$$

$$* \exp(-4\tau/T_{2N})\cos(\pi^1 J_{C\alpha,C\beta}t_1)\exp(-t_1/T_{2C\alpha}) \qquad (15a)$$

where $f(\tau)$ for the cross peak correlating $C_\alpha(i)$ is given by:

$$f(\tau) = \sin^2(2\pi^1 J_{C\alpha,N}\tau)\cos^2(2\pi^2 J_{C\alpha,N}\tau) \qquad (15b)$$

and for the $C_\alpha(i-1)$ cross peak:

$$f(\tau) = \sin^2(2\pi^2 J_{C\alpha,N}\tau)\cos^2(2\pi^1 J_{C\alpha,N}\tau) \qquad (15c)$$

The transfer efficiencies for the $H^N(i)$, $N(i)$, $C_\alpha(i-1)$ and $H^N(i)$, $N(i)$, $C_\alpha(i-1)$ cross peaks as a function of the delay 2τ are plotted in Fig. 21a at the end of this section.

4.2. 3D HN(CO)CA and 3D H(N)COCA

The 3D HN(CO)CA [45] and 3D H(N)COCA experiments correlate the spins $H^N(i)$, $N(i)$, $C_\alpha(i-1)$ and $H^N(i)$, $C'(i-1)$, $C_\alpha(i-1)$. Thus, they connect the amide proton of amino acid *i* with resonance frequencies of the preceding amino acid. Whether 3D HN(CO)CA or 3D H(N)COCA is preferable depends on the dispersion of the 2D $H^N(i)$, $N(i)$ and 2D $H^N(i)$,$C'(i-1)$ correlation spectra. In Fig. 18, these 2D correlations of the protein rhodniin are displayed. The resolution of the $H^N(i)$, $C'(i-1)$ spectrum is higher than that of the 2D $H^N(i)$, $N(i)$ spectrum, and the H(N)COCA experiment is therefore preferable for the correlation of the C_α $(i-1)$ spins.

The pulse sequence for the 3D HN(CO)CA experiment is shown in Fig. 19a. The experiment is derived from the HNCO experiment: After an HSQC-type magnetization transfer from H^N to N the magnetization is transferred to C' in a second HSQC-type step.

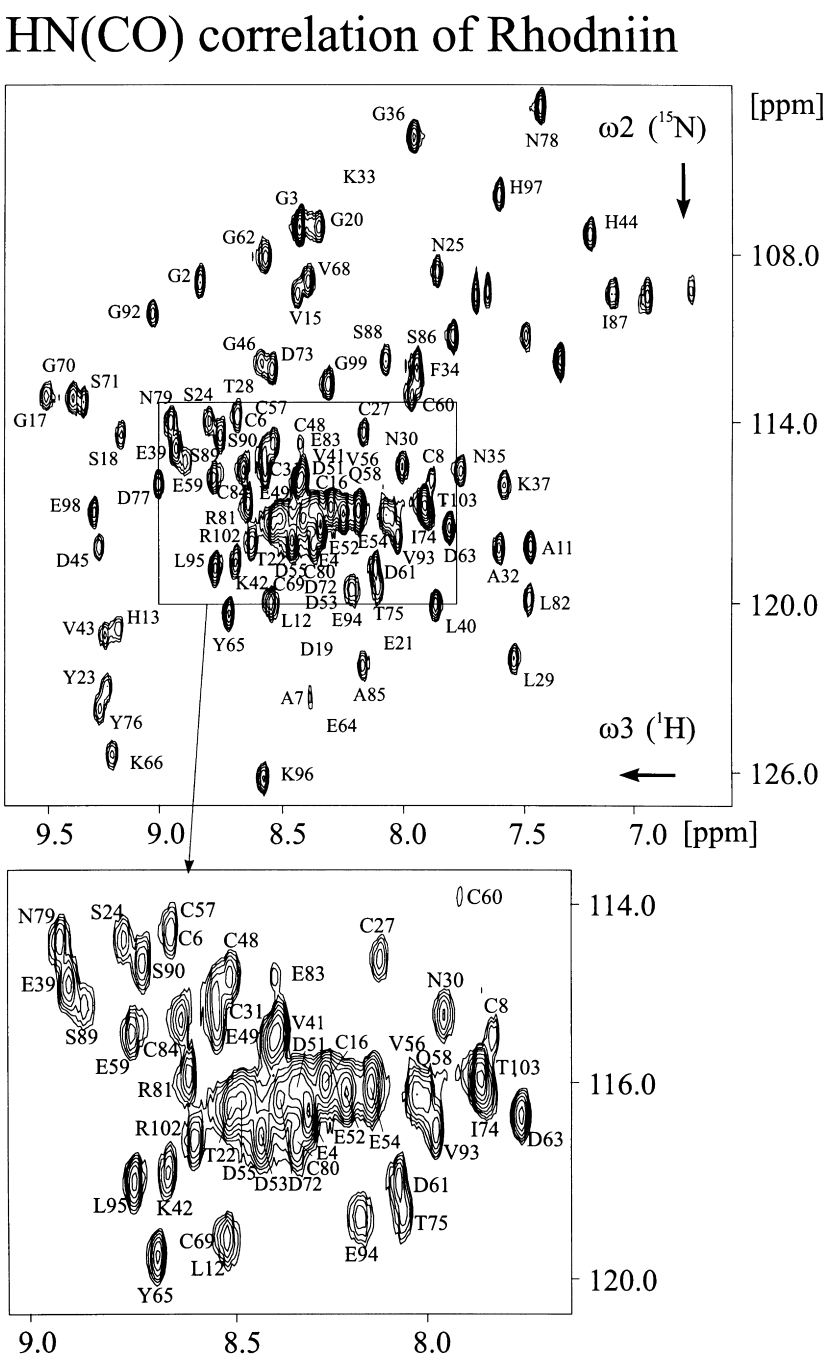

Fig. 18. Comparison of the (a) 2D $H^N(i)$,N(i) and (b) 2D $H^N(i)$,C′($i-1$) projections of a 3D HNCO experiment of ^{13}C-,^{15}N-labelled rhodniin recorded at 600 MHz proton frequency.

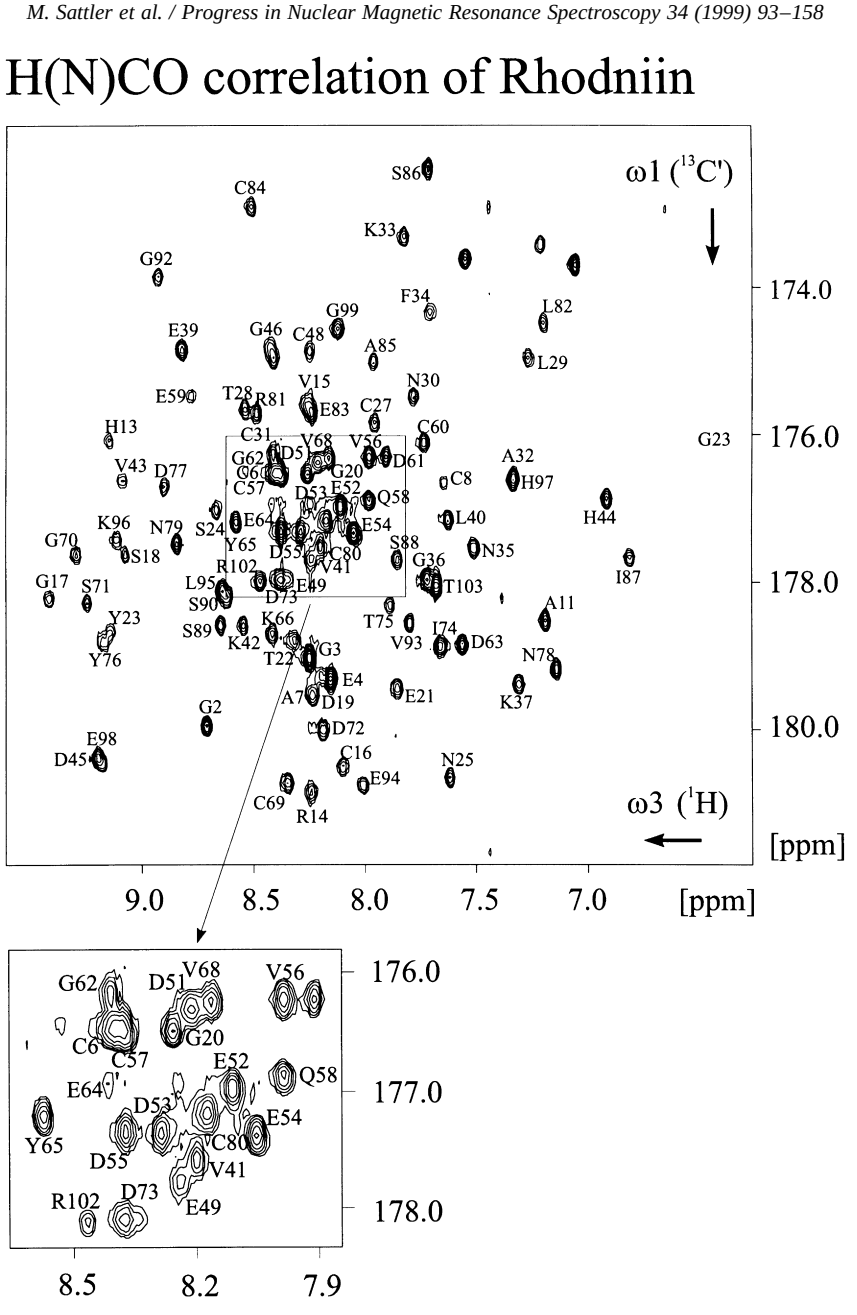

Fig. 18. (*continued*)

For the C',C_α transfer, the HMQC implementation proves to be superior. After chemical shift evolution of the C_α, the magnetization is transferred back along the reversed path, a COS-INEPT building block is used for the final N, H^N transfer to increase the sensitivity. The transfer amplitude for the pulse sequence

a) 3D HN(CO)CA

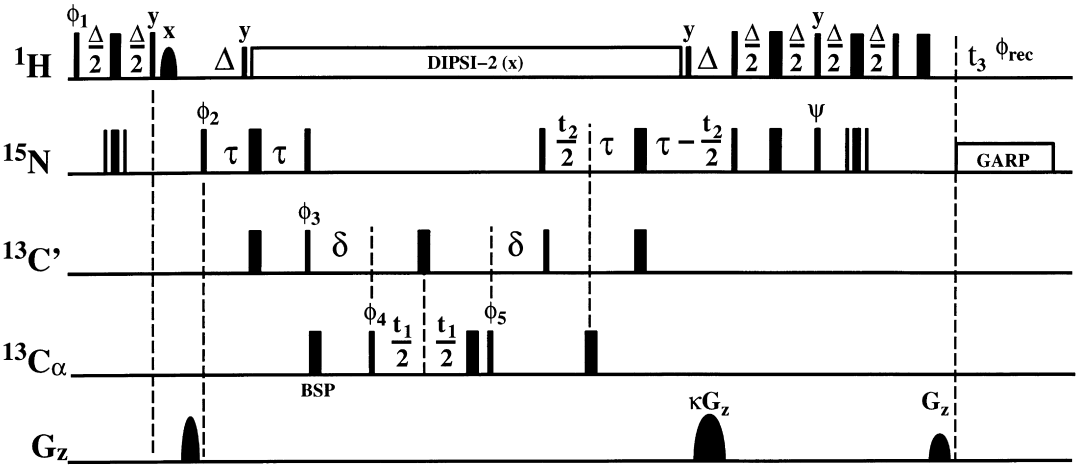

κ = +/−10; ψ = +/−y; ϕ_1= x; ϕ_2 = x; ϕ_3 = 2(x), 2(−x);

ϕ_4 =x, −x + TPPI (t_1); ϕ_5 = x+BSP; ϕ_{rec} = x, 2(−x), x;

Δ = 5.4 ms, τ = 13.5 ms, δ = 7 ms.

b) 3D H(N)COCA

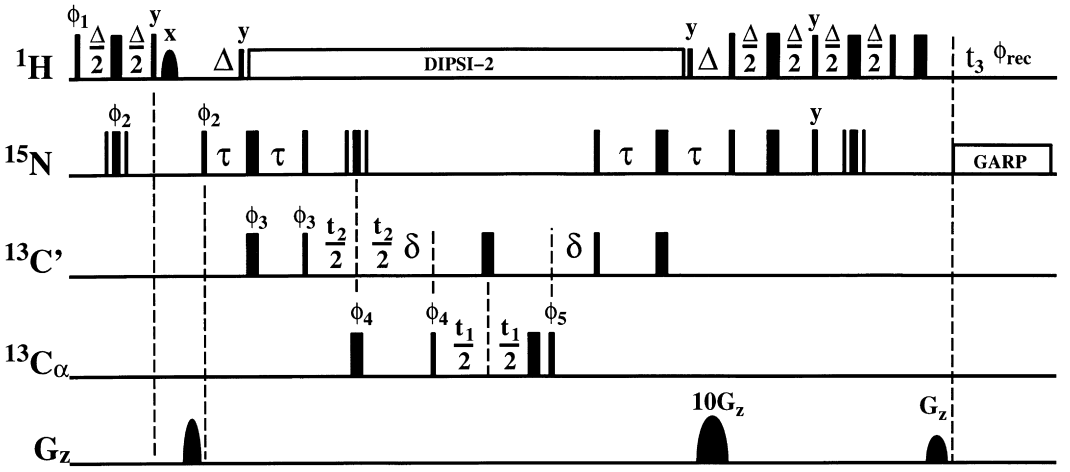

ϕ_1 =x; ϕ_2 = x, −x; ϕ_3 = 2(x), 2(−x) + TPPI(t_2); ϕ_4 = 4(x), 4(−x) + TPPI(t_1);

ϕ_5 =x+BSP; ϕ_{rec} = x, 2(−x), x, −x, 2(x), −x.

Δ = 5.4 ms, τ = 13.5 ms, δ = 7 ms.

Fig. 19. Pulse sequences of the 3D HN(CO)CA (a) and the 3D H(N)COCA (b) experiments.

displayed in Fig. 19a is:

$$\text{3D HN(CO)CA } H^N \rightarrow N \rightarrow C' \rightarrow C_\alpha(t_1) \rightarrow C' \rightarrow N(t_2) \rightarrow H^N(t_3)$$

$$f = \sin^4(\pi^1 J_{N,HN}\Delta)\exp(-2\Delta/T_{2HN})\sin^2(2\pi^1 J_{C',N}\tau) \exp(-4\tau/T_{2N})$$

$$\sin^2(\pi^1 J_{C',C\alpha}\delta)\exp(-(t_1 + 2\delta)/T_{2C'})\cos(\pi^1 J_{C\alpha,C\beta}t_1) \exp(-t_1/T_{2C\alpha}) \quad (16a)$$

If the H(N)COCA experiment (Fig. 19b) is preferable for resolution reasons, COS-INEPT transfers could be used for both the C′, N and N, H^N transfers. However, this is not advisable since relaxation losses prevent a sensitivity gain in the C′, N step (cf. chapter 3.4). The H(N)COCA experiment is therefore less sensitive than the HN(CO)CA. A COS-INEPT step can still be used for the N, H^N transfer to suppress the solvent. The transfer amplitude is almost identical to Eq. (16a):

$$\text{3D H(N)COCA } H^N \rightarrow N \rightarrow C' \rightarrow C_\alpha(t_1) \rightarrow C'(t_2) \rightarrow N \rightarrow H^N(t_3)$$

$$f(\text{Eq.(16a)})*\exp(-t_2/T_{2C'}) \quad (16b)$$

The duration of 8 ms for the delay δ used for the C′, C_α transfer optimal for $^1J_{C',C\alpha} \approx 55$ Hz and assuming a transverse C′ T_2 relaxation time of 50 ms (see Fig. 21). The transfer amplitude for the H(N)COCA experiment, Eq. (16b), differs from that of the HN(CO)CA experiment only in a relaxation term for C′ during t_2. This term occurs because the chemical shift of C′ evolves during a real time evolution, compared to a constant time chemical shift evolution of N in the HN(CO)CA. Real time evolution is acceptable because the carbonyl magnetization decays only slowly.

The resolution for recording the ^{15}N chemical shift during t_2 can be doubled by utilizing both of the N,C′ transfer steps ($2\tau = 1/(2J_{N,C'})$) for chemical shift evolution, with a slight modification of the pulse sequence (‘‘full-sweep constant time’’ evolution, FCT) [172–174] e.g. using HMQC steps for the N → C′ and C′ → C_α transfer, the resolution in the nitrogen dimension can be doubled in the HN(CO)CA experiment [173]. In an analogous manner, the C′ resolution can be doubled in the alternative H(N)COCA experiment by making full use of the duration 2δ for C′ shift evolution.

4.3. 3D HN(CA)CO

The HN(CA)CO experiment [55] correlates the chemical shifts of $H^N(i)$, $N(i)$ and $C'(i)$, the H(N)CACO experiment [57] those of $H^N(i)$, $C_\alpha(i)$ and $C'(i)$. In analogy to the HNCA experiment, cross peaks involving the resonances of $C'(i-1)$ and $C_\alpha(i-1)$) can also be observed, depending on the relaxation properties of the protein. Owing to the low sensitivity of the experiment, only a fraction of these correlations is normally observed. Whether $^{13}C_\alpha$ or ^{15}N chemical shift evolution is preferable depends on the resolution of the correlations $H^N(i)$, $C_\alpha(i)$ or $H^N(i)$, $N(i)$, which are also projections of the HNCA experiment. For most proteins, the resolution of the $H(i)$, $N(i)$ correlation is far superior to the $H^N(i)$, $C_\alpha(i)$ correlation, and the HN(CA)CO experiment is therefore preferable. As an additional advantage, a COS backtransfer N → H^N leads to a gain in sensitivity of ≈ 2 in the HN(CA)CO experiment, which cannot be realized in the H(N)CACO.

The HN(CA)CO experiment (Fig. 20) is derived from the HNCA experiment. Starting on the amide protons, magnetization is transferred via the amide nitrogens to the C_α spins. For the following magnetization transfer between the C_α and the C′ spins either an HMQC- or an HSQC-type experiment can be used. In the HMQC based experiment (Fig. 20a), the C_α magnetization is transversal during a CT delay of duration $2(\delta + \eta) = 1/^1J_{C\alpha,C\beta} \approx 24$ ms, thus refocusing the homonuclear C,C couplings. This results in inverted signals for Gly C_α cross peaks. A fraction of the constant time delay (2η) is also used for chemical shift evolution of the carbonyls in a CT evolution time t_1. The resolution in this dimension can be increased by ‘‘mirror image’’ linear prediction [175]. During the back transfer of the magnetization, amide nitrogen chemical shift evolves during the delay 2τ, which is needed for the refocusing of the C_α, N coupling. The COS-INEPT back transfer N → H is combined with a heteronuclear gradient echo.

a) 3D HN(CA)CO (HMQC)

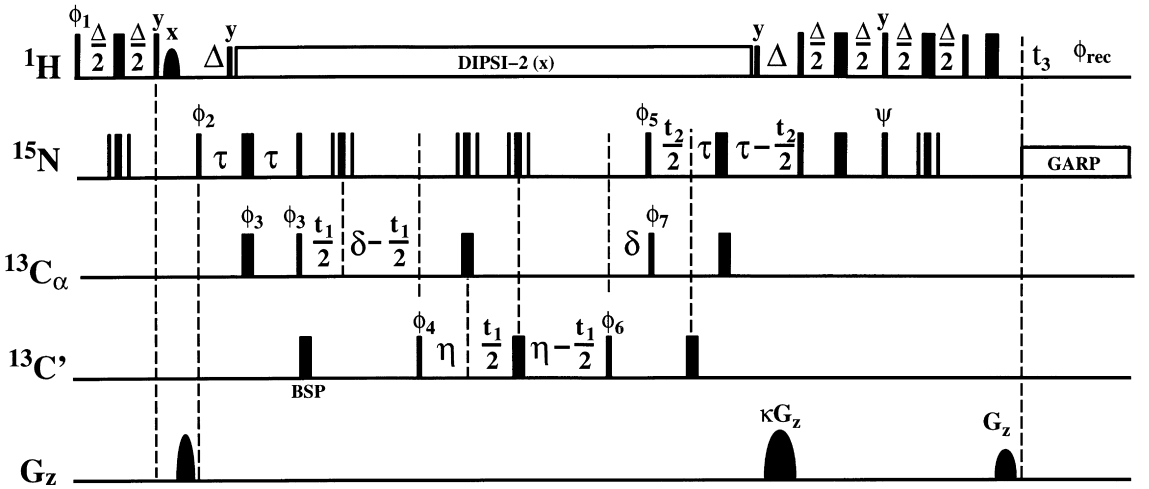

κ = +/–10; ψ = +/–y; ϕ_1 = x; ϕ_2 = 2(x), 2(–x); ϕ_3 = x ; ϕ_4 = x + BSP; ϕ_5 = x;
ϕ_6 = 4(x), 4(–x) + TPPI(t_1); ϕ_7 = x, –x; ϕ_{rec} = x, 2(–x), x, –x, 2(x), –x.
Δ = 5.4 ms, τ = 11 ms, δ = 6.8 ms, η = 5.5 ms.

b) 3D HN(CA)CO (HSQC)

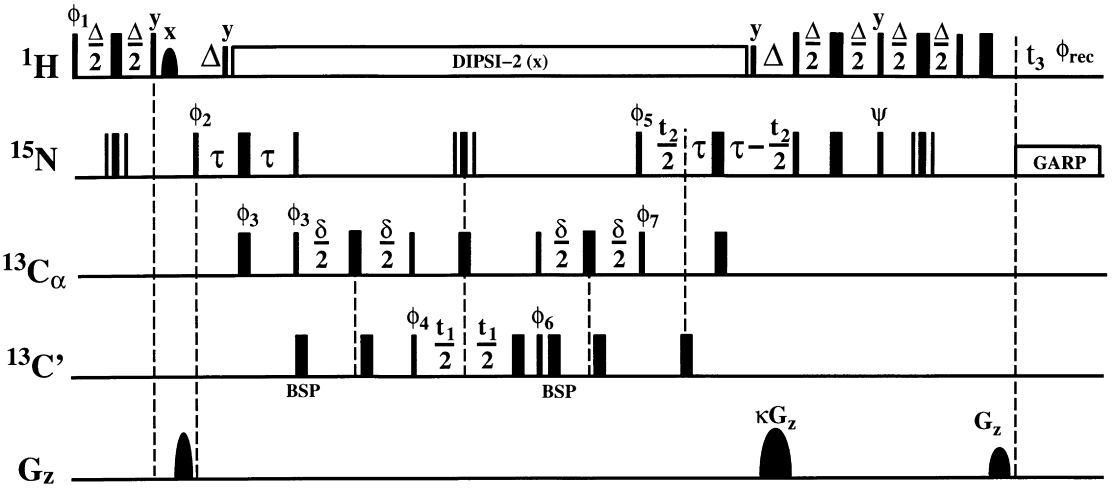

κ = +/–10; ψ = +/–y; ϕ_1 = x; ϕ_2 = x, –x; ϕ_3 = x ; ϕ_4 = x + BSP; ϕ_5 = x;
ϕ_6 = 4(x), 4(–x) + TPPI(t_1); ϕ_7 = 2(x), 2(–x), ϕ_{rec} = x, 2(–x), x, –x, 2(x), –x.
Δ = 5.4 ms, τ = 11 ms, δ = 6.8 ms, η = 5.5 ms.

Fig. 20. Pulse sequences for the a) HMQC-based 3D HN(CA)CO and b) HSQC-based 3D HN(CA)CO experiment.

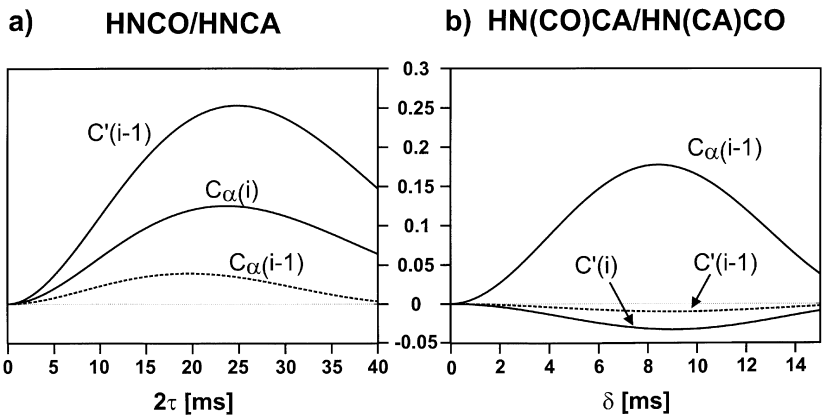

Fig. 21. Transfer amplitudes of experiments used for the assignments of H^N, N, C_α and C' of proteins: HNCO, HNCA, HN(CO)CA and HN(CA)CO. (a) Transfer amplitude of the HNCO (Eq. (14)) and HNCA experiment (Eq. (15)) as a function of the CT delay 2τ, used for evolution of $^1J_{C\alpha,N}$ and $^2J_{C\alpha,N}$ (dashed lines) couplings. (b) Transfer amplitude of the HN(CO)CA (Eq. (16)) and HN(CA)CO experiment (Eq. (17)) as a function of delay δ, used for evolution of $^1J_{C\alpha,C'}$. Transfer amplitudes for cross peaks to $C_\alpha(i-1)$ or $C'(i-1)$ caused by $^2J_{C\alpha,C'}$ are indicated by dashed lines. Parameters used: $^1J_{H,N} = 92$ Hz, $^1J_{C',N} = 15$ Hz, $^1J_{C\alpha,N} = 11$ Hz, $^2J_{C\alpha,N} = 7$ Hz, $^1J_{C,C} = 35$ Hz, $^1J_{C',C\alpha} = 55$ Hz, $T_{2HN} = 50$ ms, $T_{2N} = 50$ ms, $T_{2C\alpha} = 20$ ms, $T_{2C} = 50$ ms, $\Delta = 5.4$ ms, $\tau = 12$ ms, $2(\delta + \eta) = 24$ ms, $2\eta = 8$ ms.

Analogously to the HNCA experiment two cross peaks are expected. The intraresidual peak correlating to $C_\alpha(i)$ originates from $N \rightarrow C_\alpha$ transfer via the $^1J_{C\alpha,N}$ coupling and the sequential cross peak to $C_\alpha(i-1)$ originates from $N \rightarrow C_\alpha$ transfer via the $^2J_{C\alpha,N}$ coupling. The corresponding transfer amplitudes are:

$$\text{3D HN(CA)CO(HMQC)} \qquad H^N \rightarrow N \rightarrow C_\alpha$$

$$\sin^4(\pi^1 J_{N,HN}\Delta)\exp(-2\Delta/T_{2HN})\exp(-4\tau/T_{2N})$$

$$\rightarrow C'(t_1) \rightarrow C_\alpha \rightarrow N(t_2) \rightarrow H^N(t_3)$$

$$\sin^4(\pi^1 J_{N,HN}\Delta)\exp(-2\Delta/T_{2HN})\exp(-4\tau/T_{2N})$$

$$f(\tau)*\sin^2(\pi^1 J_{C'C_\alpha}\delta)\exp(-2\eta/T_{2C'})$$

$$\exp(-2(\delta+\eta)/T_{2C_\alpha})$$

$$\textit{for } C_\alpha(i): \quad f(\tau) = \sin^2(2\pi^1 J_{C\alpha,N}\tau)\cos^2(2\pi^2 J_{C\alpha,N}\tau)$$

$$\textit{for } C_\alpha(i-1): \; f(\tau) = \sin^2(2\pi^2 J_{C\alpha,N}\tau)\cos^2(2\pi^1 J_{C\alpha,N}\tau) \qquad (17)$$

The C_α,C' transfer can alternatively be implemented as a HSQC (Fig. 20b). This should be favorable with respect to relaxation. However, more pulses have to be applied compared to the HMQC-type implementation. In our hands, the HMQC-type experiment yields better sensitivity than the HSQC-based implementation.

The transfer amplitudes for the experiments discussed so far are compared in Fig. 21. Useful delays for a protein of $\approx$ 20 kD molecular weight are: $2\tau = 26$ ms (HNCO) or $2\tau = 24$ ms (HNCA), $\delta = 8$ ms (HN(CA)CO and HN(CO)CA). It can be seen from Fig. 21 that the intensity of C' cross peaks in the HN(CA)CO is only about 10% of that in the HNCO. This is mainly because of the fast relaxation of transverse C_α magnetization during the CT delay $2(\delta + \eta) \approx 24$ ms. This loss in sensitivity is even more pronounced for proteins with shorter T_2, rendering the HN(CA)CO experiment impractical in such cases. However, HNCACO-type experiments are very useful if applied to a deuterated sample in combination with ^{2}H-decoupling (see Section 5.8).

4.4. Reduced dimensionality experiments

In the triple resonance experiments described so far, *n* types of chemical shifts are recorded in an *n*-dimensional experiment. As an alternative, reduced dimensionality triple resonance experiments have been proposed [78–82], that record *n* chemical shifts in an $(n-1)$-dimensional experiment. The simultaneous recording of the chemical shift can be done either by evolution of zero and double quantum

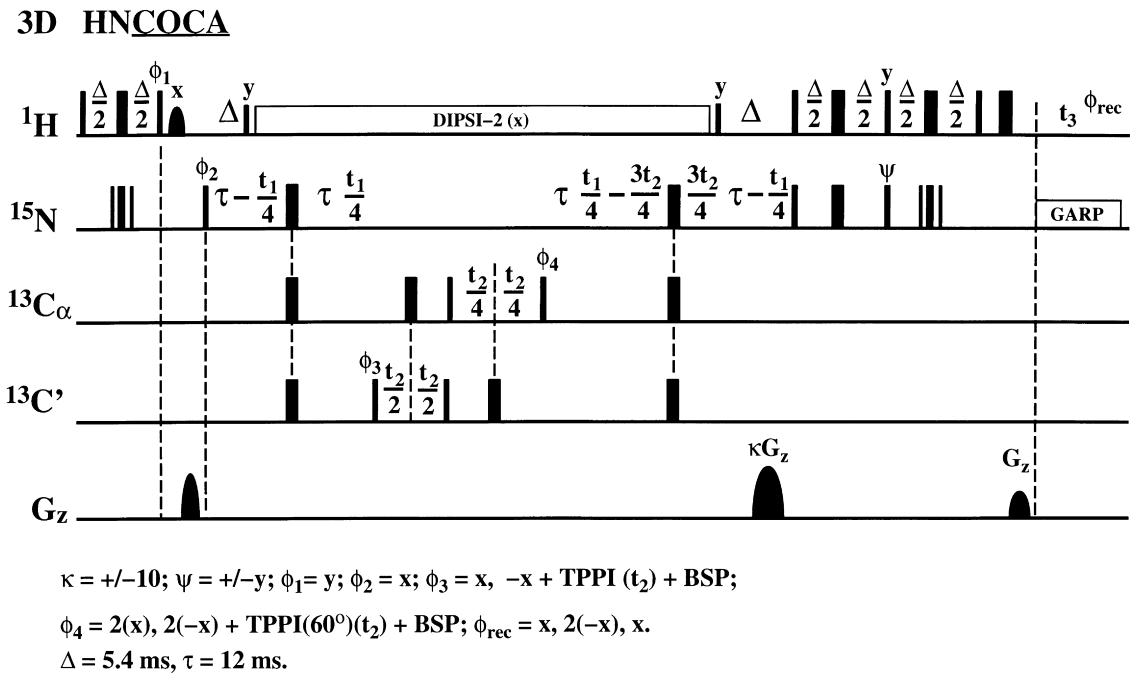

Fig. 22. Pulse sequence for a reduced dimensionality 3D HN*COCA* experiment. The chemical shifts of the C′ and C_α spins are recorded in simultaneous evolution of single quantum coherences during t_2. TPPI on ϕ_4 is done in steps of 60° in order to shift the center of the C_α chemical shifts such that resonance overlap in the ^{13}C dimension is reduced [176].

coherences or by simultaneous incrementing of two single quantum evolution times. As the simultaneous chemical shift recording leads to a peak doublet in the respective frequency domain, automatic peak picking will be facilitated. In addition, for evolution of DQ/ZQ coherences the relaxation rates of these coherences for directly bound pairs of spins like H,C or H,N are smaller for molecules in the slow tumbling limit than those of single quantum coherences [162,170]. In contrast, the sensitivity of these experiments is reduced by a factor $1/\sqrt{2}$ compared to the corresponding 3D single quantum (SQ) experiment in which only SQ of either of the two spins evolves. This is because the cross peak intensity is split into two peaks (loss of signal-to-noise: 1/2), however a factor $\sqrt{2}$ is gained as a result of the lower dimensionality of the experiment. A modified version of these experiments has been introduced recently, which in part yields improved sensitivity by utilizing symmetrization with respect to a reference peak [176]. Another drawback of this strategy is that the chemical shifts of the individual spins have to be calculated from the frequencies of the zero or double quantum coherences. The spectra used for resonance assignment can therefore not be compared directly to the isotope-edited NOESY spectra used to derive distance information. As an example, the pulse sequence of the reduced dimensionality 3D HNCOCA experiment is shown in Fig. 22. The experiment was originally named 3D COHNNCA. However, in following the previously mentioned nomenclature for triple resonance experiments we prefer the name HNCOCA, where the underlined nuclei correspond to simultaneous evolution of chemical shifts defining the reduced dimensionality of this experiment. Compared to the original experiment, in the pulse sequence shown in Fig. 22 sensitivity enhancement is combined with a heteronuclear $^{15}N,^{1}H$ gradient echo for improved solvent suppression.

In the out-and-back pulse sequence, magnetization is transferred from the amide proton to the amide nitrogen, followed by simultaneous HMQC-type transfer from ^{15}N to $^{13}C_\alpha$ and to $^{13}C'$. The chemical shift for the $^{13}C'$ and $^{13}C_\alpha$ spins is recorded

simultaneously. However, because $^{13}C_\alpha$ relaxation times are much shorter than those of $^{13}C'$, and, in addition, homonuclear C,C couplings can evolve for the $^{13}C_\alpha$ spin, its chemical shift evolution is scaled by 1/2 compared to the $^{13}C'$ chemical shift. The ^{15}N chemical shift evolution exploits the out and the back part of the magnetization transfer to obtain optimum resolution as was proposed by Madsen and Sørensen [177]. The transfer amplitude given in Eq. (18) also includes the terms for chemical shift evolution in order to indicate the corresponding chemical shift modulation of the cross peaks observed in the experiment.

3D HNCOCA

$$H^N \rightarrow N(t_1/2) \rightarrow CO(t_2)/CA(t_2/2) \rightarrow N(t_1/2) \rightarrow H^N(t_3)$$

$$\sin^4(\pi^1 J_{N,HN}\Delta)\exp(-2\Delta/T_{2HN})\exp(-4\tau/T_{2N})$$
$$\cos(\Omega_{Nt1})\cos(\Omega_{C'(i-1)t2})\exp(-(t_2/T_{2C'})*f(\tau,t_2),$$

where $f(\tau,t_2)$ for cross peaks observed at different chemical shifts is given by:

$$\Omega_{C'(i-1)}:$$
$$\sin^2(2\pi^1 J_{C'(i-1),N}\tau)\cos^2(2\pi^1 J_{C\alpha(i),N}\tau)$$
$$\cos^2(2\pi^2 J_{C\alpha(i-1),N}\tau) \quad (18a)$$

$$\Omega_{C'(i-1)} \pm (1/2)\Omega_{C\alpha(i)}:$$
$$+\cos(\Omega_{C\alpha(i)}t_2/2)\exp(-t_2/2T_{2C\alpha})$$
$$\cos(\pi^1 J_{C\alpha,C\beta}(t_2/2))\sin^2(2\pi^1 J_{C\alpha(i),N}\tau)$$
$$\sin^2(2\pi^1 J_{C'(i-1),N}\tau)\cos^2(2\pi^2 J_{C\alpha(i-1),N}\tau) \quad (18b)$$

$$\Omega_{C'(i-1)} \pm (1/2)\Omega_{C\alpha(i-1)}:$$
$$+\cos(\Omega_{C\alpha(i-1)}t_2/2)\exp(-t_2/2T_{2C\alpha})$$
$$\cos(\pi^1 J_{C\alpha,C\beta}(t_2/2))$$
$$*\sin^2(2\pi^2 J_{C\alpha(i-1),N}\tau)\sin^2(2\pi^1 J_{C'(i-1),N}\tau)$$
$$\cos^2(2\pi^1 J_{C\alpha(i),N}\tau) \quad (18c)$$

$$\Omega_{C'(i-1)} \pm (1/2)\Omega_{C\alpha(i1)} \pm \Omega_{C\alpha(i-1)}:$$
$$-\cos(\Omega_{C\alpha(i)}t_2/2)\cos(\Omega_{C\alpha(i-1)}t_2/2)$$
$$\exp(-t_2/T_{2C\alpha})\cos^2(\pi^1 J_{C\alpha,C\beta}(t_2/2))$$
$$*\sin^2(2\pi^1 J_{C\alpha(i),N}\tau)\sin^2(2\pi^1 J_{C'(i-1),N}\tau)$$
$$\sin^2(2\pi^2 J_{C\alpha(i-1),N}\tau) \quad (18d)$$

This transfer amplitude encodes a number of doublet peaks in the t_2 dimension centered at the chemical shift of the C' spin, because TPPI is applied to phase ϕ_3. The terms Eq. (18b) and Eq. (18c) correspond to ω_2 cross peaks at the sum and difference of the chemical shifts of $C'(i-1)$ and $C_\alpha(i)$, and $C'(i-1)$ and $C_\alpha(i-1)$, respectively (where the C_α chemical shifts are scaled as mentioned before). Eq. (18a) is a cross peak at the chemical shift of $C'(i-1)$, where no transfer to C_α spins is accomplished. Term Eq. (18d) yields a doublet of doublets, however with much less signal-to-noise than in Eqs. (18a)–(18c). Owing to the splitting into four cross peaks the signal-to-noise for cross peaks arising from Eq. (18d) is scaled by 0.25 and 0.5 compared to Eqs. (18a) and (b), (c), respectively. (Peaks arising from this term are not desirable and can be further reduced in intensity by choosing a delay τ shorter than 13.5 ms.) As the doublets are symmetric with respect to the $^{13}C'(i-1)$ chemical shift a symmetrization routine can be applied to improve the signal-to-noise of the spectrum and thus facilitate the identification of the corresponding pairs of cross peaks.

Theoretically, from this single experiment all the backbone chemical shifts could be extracted. However, in practice, this is unlikely because of the low sensitivity of the experiment, especially for larger proteins. The sensitivity has to be compared with a 3D HNCA and a 3D HNCO experiment which still convey more spectroscopic information since potential overlap is reduced in these experiments compared to the reduced dimensionality HNCOCA experiment. Comparing the signal-to-noise ratio in the HNCOCA experiment to HNCA and HNCO experiments with the same experimental time (using Eqs. (14) and (16a) and assuming the same values for J and T_2) the signal-to-noise is reduced to 34% and 40% for the $^{13}C'(i-1)$ and the $^{13}C_\alpha(i)/^{13}C_\alpha(i-1)$ cross peaks,

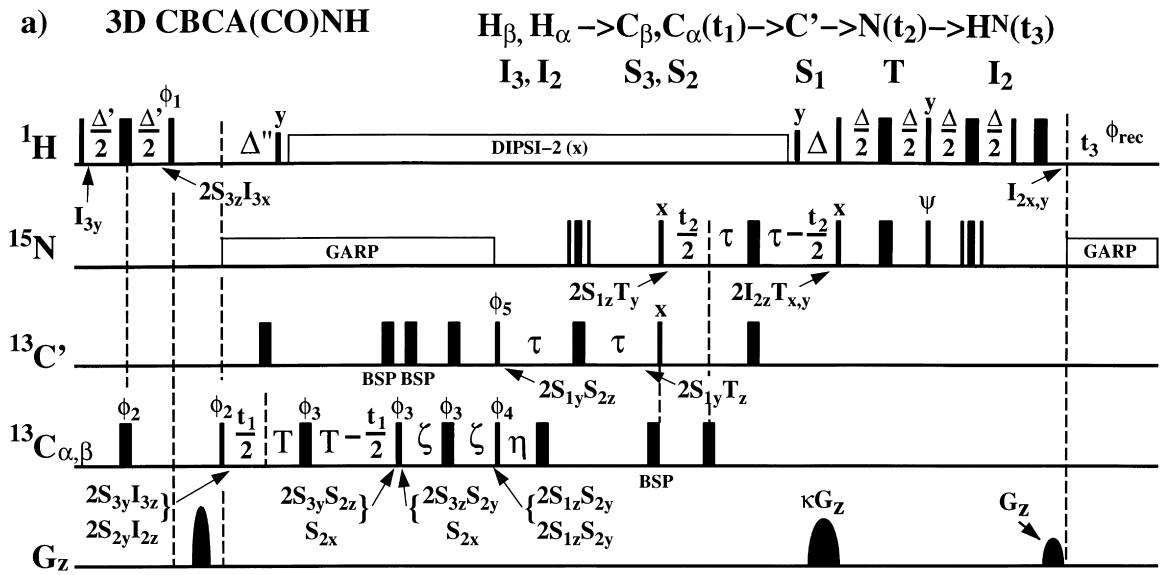

κ = +/–10; ψ = +/–y; ϕ_1= y; ϕ_2= x, –x + TPPI(t_1); ϕ_3 =x;

ϕ_4 =x; ϕ_5 = 2(x), 2(–x) ; ϕ_{rec}= x, 2(–x), x.

Δ'=3.6 ms, Δ''=2.4 ms, Δ=5.4 ms, τ=13.5 ms, T=3.6 ms, ζ=3.4 ms, η=4.5 ms.

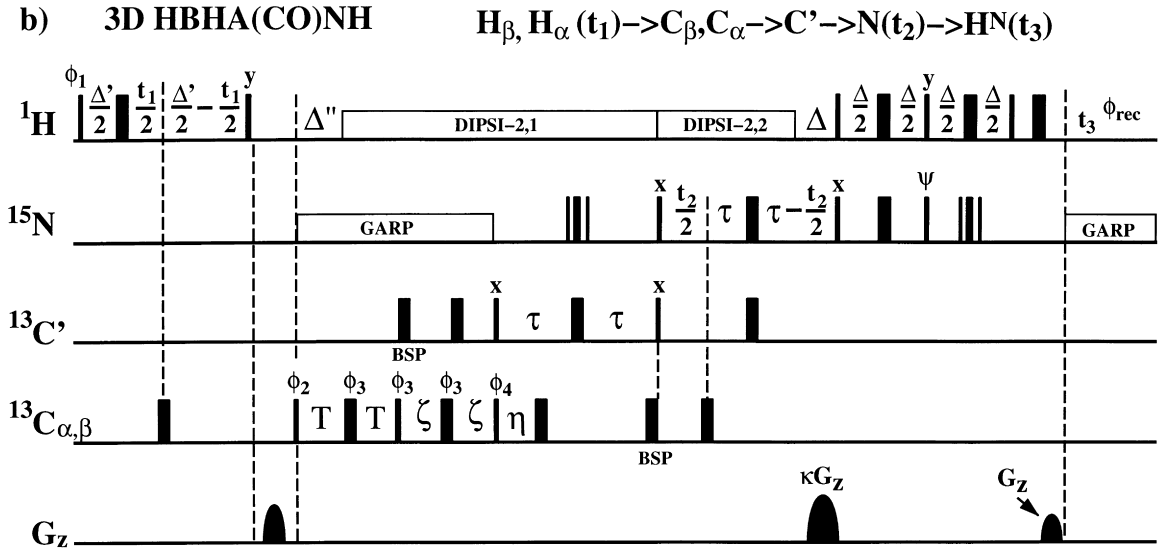

κ = +/–10; ψ = +/–y; ϕ_1= x, –x + TPPI(t_1); ϕ_2= 2(x), 2(–x);

ϕ_3 = x; ϕ_4 = x; ϕ_{rec}= x, 2(–x), x.

Δ'=3.6 ms, Δ''=2.4 ms, Δ=5.4 ms, τ=13.5 ms, T=3.6 ms, ζ=3.4 ms, η=4.5 ms.

Fig. 23.

respectively. This demonstrates the poor sensitivity of this class of pulse sequences compared to the conventional triple resonance experiments.

3D $H_{\alpha/\beta}C_{\alpha/\beta}$(CO)NH was also introduced as a reduced dimensionality experiment, that has the potential to yield ^{1}H and ^{13}C chemical shifts for the C_α and C_β carbons of the residues (i) and (i-1) in combination with the amide $H^N(i)$ and N(i) chemical shifts [80]. However, similar considerations regarding the S/N compared to the SQ-versions apply.

5. Combined backbone and side-chain assignment

In principle, the experiments described in the previous section can yield complete backbone assignments and establish the sequential connectivities. However, overlap even in 3D spectra results in ambiguities. Therefore, an additional assignment strategy has been developed based on the use of the chemical shifts of the $C_{\alpha,\beta}$ and $H_{\alpha,\beta}$ resonances for the sequential assignment. As the chemical shifts of the side-chain carbons are characteristic for the amino acid type, this information can also be utilized to position sequentially connected fragments within the amino acid sequence. A number of computer programs have been developed for automated assignments that make use of this strategy [178–182].

Experiments described in this chapter employ COS transfers and a heteronuclear gradient echo for water suppression in the final N,H back transfer. This is especially important for experiments detecting aliphatic protons, as in the HCCH-TOCSY. Using the heteronuclear gradient echo, this experiment can be recorded on protein samples in H_2O solution, rendering a second protein sample in D_2O superfluous.

5.1. 3D CBCA(CO)NH

The 3D CBCA(CO)NH experiment [58] (Fig. 23a) is a transfer experiment, which uses a relay-COSY [106] step $C_\beta/C_\alpha \rightarrow C_\alpha$ to correlate the chemical shifts $H^N(i)$, N(i), $C_\alpha(i-1)$ and $C_\beta(i-1)$. Thus, magnetization is transferred from $H_{\alpha,\beta}$ to the directly bound $C_{\alpha,\beta}$ followed by CT chemical shift evolution of $C_{\alpha,\beta}(t_1)$. After the relay-COSY step, the C_β,C_α coupling is refocused and the magnetization is transferred from C_β/C_α to the amide nitrogen in two INEPT steps, followed by CT chemical shift evolution of the amide nitrogens (t_2). The magnetization is detected (t_3) after transfer to the amide protons using a COS-INEPT sequence. To achieve an efficient decoupling of the protons during the pulse sequence, the DIPSI-2 decoupling sequence can be applied in the center of the H_α, H_β region while carbon spins are transverse and centered in the H^N region when amide nitrogen magnetization is transverse. The proton carrier frequency could be switched before the C′,N coherence transfer. However, this switching of the ^{1}H-carrier frequency might interfere with water suppression and it is therefore not recommended. Note, that in transfer experiments where magnetization also can originate from protons with chemical shifts close to the water frequency water-flip-back (as described in Section 3.5) cannot be employed.

In analogy to the H(N)COCA vs. HN(CO)CA experiments, a 3D CBCACO(N)H sequence is preferable for proteins that exhibit better resolution in the $H^N(i)$,$C'(i-1)$ correlation compared to the $H^N(i)$,N(i) correlation. In any case, ''mirror image'' linear prediction can be used during processing of both t_1 and t_2, because both are CT evolution times.

The transfer amplitudes for C_β and C_α cross peaks in the CBCA(CO)NH experiment depend on the carbon multiplicity of the carbon spins. For a generalized ^{13}C spin system C_α-$(C_\beta)_m$-$(C_\gamma)_p$, the transfer amplitudes are given by Eq. (19a). m is 0 for glycine and 1 for all other amino acids; n is the proton multiplicity of the starting ^{13}C spin. The factor $f(T,\zeta)$, which is different for C_α and C_β spins, is given by Eqs. (19b) and (19c).

3D CBCA(CO)NH $H_{\alpha,\beta} \rightarrow C_{\alpha,\beta}(t_1) \rightarrow C_\alpha \rightarrow C'$

$\rightarrow N(t_2) \rightarrow H^N(t_3)$

Fig. 23. (a) Pulse sequence for the 3D CBCA(CO)NH experiment that yields chemical shifts of four nuclei per amide: $H^N(i)$, $C_\alpha(i-1)$, $C_\beta(i-1)$ and N(i). Note the application of additional selective carbonyl inversion pulses (marked ''BSP'') to eliminate Bloch–Siegert phase shifts. The evolution of product operation during the course of the pulse sequence is indicated. (b) The related HBHA(CO)NH experiment yields the corresponding $H_\alpha(i-1)$ and $H_\beta(i-1)$ chemical shifts.

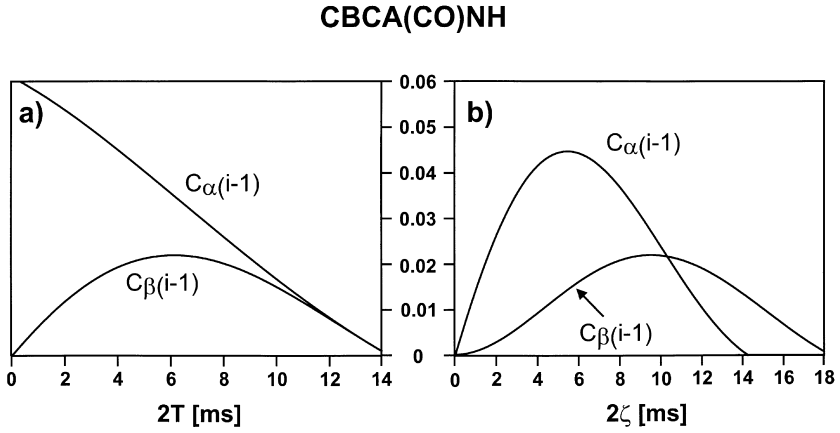

Fig. 24. Transfer amplitudes for C_α and the C_β cross peaks in the CBCA(CO)NH experiment as a function of the CT delays $2T$ (a) and 2ζ (b). The graphs were obtained from Eq. (19) for for a typical spin system $C_\alpha H\text{-}C_\beta H_2\text{-}C_\gamma$ ($n = 1$ for C_α, $n = 2$ for C_β, $m = 1$ and $p = 1$) using the parameters: ${}^1J_{H,N} = 92$ Hz, ${}^1J_{H,C} = 135$ Hz, ${}^1J_{C'N} = 15$ Hz, ${}^1J_{C\alpha,N} = 11$ Hz, ${}^2J_{C\alpha,N} = 7$ Hz, ${}^1J_{C,C} = 35$ Hz, ${}^1J_{C',C\alpha} = 55$ Hz, $T_{2HN} = 50$ ms, $T_{2N} = 50$ ms, $T_{2C}\alpha,\beta = 20$ ms, $T_{2H}\alpha,\beta = 20$ ms, $T_{2C'} = 50$ ms, $\Delta = 5.4$ ms, $\Delta' = 3.8$ ms, $\Delta'' = 2$ ms, $\tau = 11$ ms, $2T = 6.5$ ms, $\zeta = 4.5$ ms.

Transfer amplitudes:

$$f(T,\zeta) = \sin(\pi {}^1J_{H,C}\Delta')\sin(\pi {}^1J_{H,C}\Delta'')\cos^{n-1}(\pi {}^1J_{H,C}\Delta'')\exp(-\Delta'/T_{2H})\sin(2\pi {}^1J_{C',C\alpha}\zeta)\sin(2\pi {}^1J_{C',C\alpha}\eta)\exp(-2T/T_{2C})\exp(-2\zeta/T_{2C})\sin^2(2\pi {}^1J_{C',N}\tau)\exp(-2\tau/T_{2C'})\exp(-2\tau/T_{2N})\sin^2(\pi {}^1J_{N,HN}\Delta)\exp(-\Delta/T_{2HN}) \quad (19a)$$

For the cross peak originating from $H_\alpha \rightarrow C_\alpha$, $f(T,\zeta)$ is given by:

$$f(T,\zeta) = \cos^m(2\pi {}^1J_{C\alpha,C\beta}T)\cos^m(2\pi {}^1J_{C\alpha,C\beta}\zeta) \quad (19b)$$

and for the cross peak originating from the transfer $H_\beta \rightarrow C_\beta$:

$$f(T,\zeta) = \sin(2\pi {}^1J_{C\alpha,C\beta}T)\cos^p(2\pi {}^1J_{C\beta,C\gamma}T)\sin(2\pi {}^1J_{C\alpha,C\beta}\zeta) \quad (19c)$$

Useful transfer efficiencies for both transfer pathways are obtained using $\Delta' = 3.8$ ms, $\Delta'' = 2.0$ ms, $2T \approx 1/(4J_{C,C}) = 6.5$ ms, $2\zeta \approx 9$ ms, $2\eta = 1/(2{}^1J_{C'\,C\alpha}) = 9$ ms and $\tau = 11$ ms. The dependence of the transfer amplitude on the duration of the CT delays $2T$ and 2ζ is shown in Fig. 24 for C_α- and C_β cross peaks in the spin system $C_\alpha H\text{-}C_\beta H_2\text{-}C_\gamma$ ($m = 1$, $p = 1$ and $n = 1, 2$ for $C_{\alpha,\beta}$) which reflects the side chain spin topology of most amino acids.

The CBCA(CO)NH experiment is easily modified to record the $H_{\alpha,\beta}(i-1)$ chemical shifts instead of the carbon chemical shifts in the HBHA(CO)NH [61] experiment (Fig. 23b). In this experiment the carbon evolution time t_1 is replaced by chemical shift evolution of the aliphatic protons during Δ' in a ''semi-constant-time'' evolution time. For the implementation of this evolution time, see the discussion of the HCCH-TOCSY experiment (Fig. 33, Section 5.5). Experiments with evolution of proton chemical shifts are less sensitive than their equivalents that correlate the carbon chemical shifts. This is mainly because of the fast relaxation of the protons during the chemical shift evolution during t_1. However, the chemical shifts of side-chain protons are important in combination with the carbon assignments (e.g. from CBCA(CO)NH experiments) for identifying spin systems in the HCCH-TOCSY experiment.

5.2. 3D CBCANH

The CBCANH experiment [59] (Fig. 25) correlates the N and H^N resonance of each amino acid with aliphatic resonances of both the same amino acid and the preceding amino acid. Thus, four cross peaks

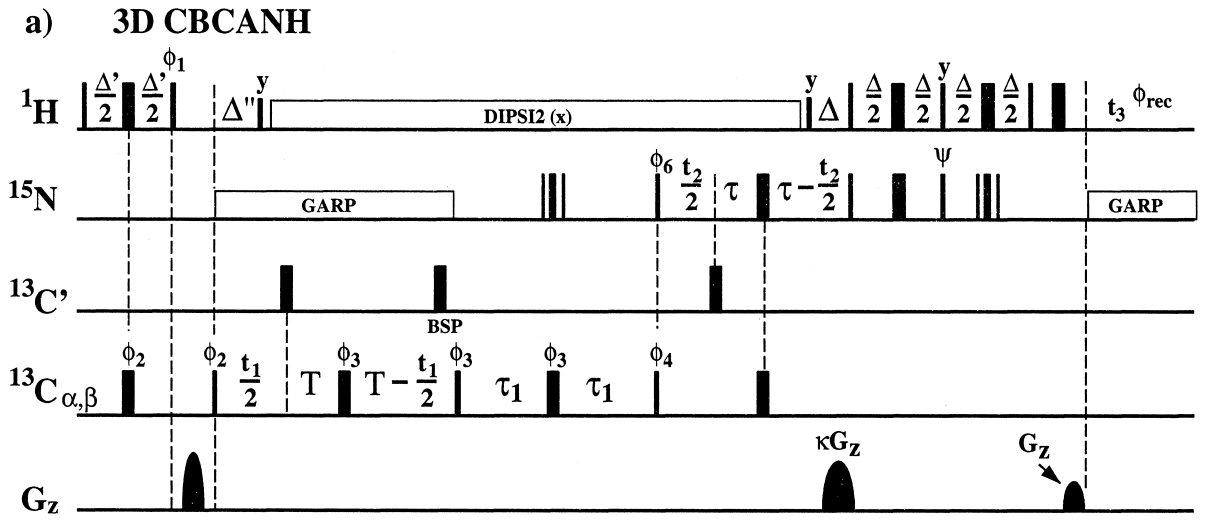

κ = +/10; ψ = +/y; ϕ_1=y; ϕ_2= x, x + TPPI(t_1); ϕ_3 = x;
ϕ_4 = x; ϕ_6 = 2(x), 2(x); ϕ_{rec}= x, 2(x), x.
Δ' = 3.6 ms, Δ''= 2.0 ms, Δ = 5.4 ms, τ_1 = 11 ms, τ = 11 ms, T = 3.6 ms.

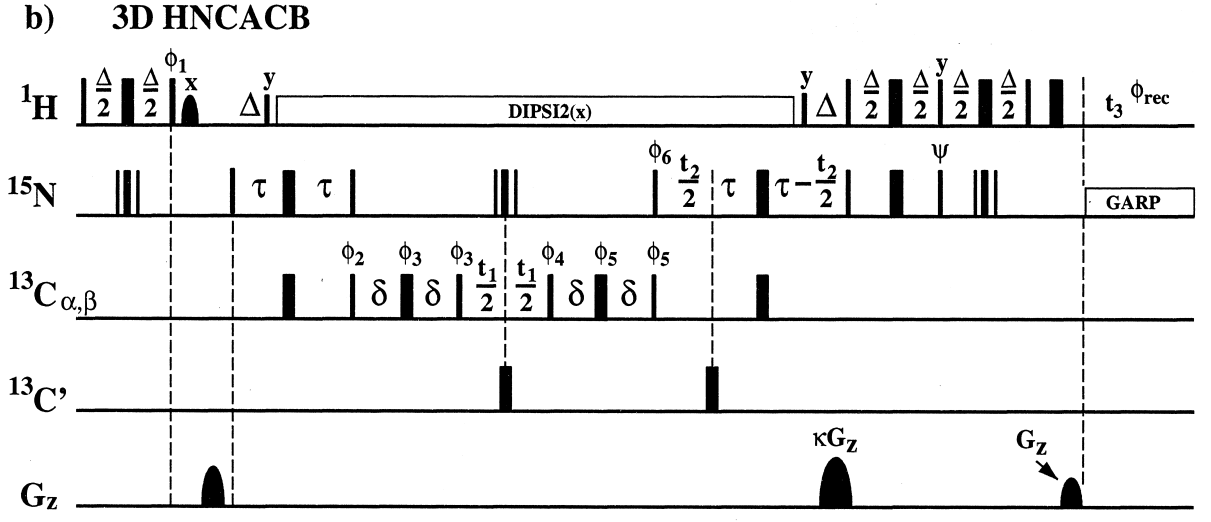

κ = +/10; ψ = +/y; ϕ_1= y; ϕ_2= x, x + TPPI(t_1); ϕ_3 = x + TPPI(t_1);
ϕ_4 = y +BSP; ϕ_5 = x+BSP; ϕ_6 = 2(x), 2(x); ϕ_{rec}= x, 2(x), x.
Δ = 5.4 ms, τ = 11 ms, δ = 3.6 ms.

Fig. 25. Pulse sequence for the sensitivity-enhanced (a) 3D CBCANH and (b) 3D HNCACB experiment. Note, that in contrast to the CBCANH experiment water-flip-back can be employed in the out-and-back type HNCACB experiment by applying the water-selective pulse shown in the pulse sequence (b).

are obtained for each amino acid, which connect the chemical shifts of $H^N(i)$, $N(i)$ with the chemical shifts of $C_\alpha(i)$, $C_\beta(i)$ and $C_\alpha(i-1)$, $C_\beta(i-1)$. This cross-peak information allows a complete sequential assignment of the peptide chain, provided there is no overlap in the $H^N(i)$, $N(i)$ correlation. Otherwise, a combination of CBCANH and CBCA(CO)NH or of CBCANH, CBCACO(N)H and HNCO is used for the assignment. The CBCANH experiment starts with an INEPT-type transfer of magnetization from the aliphatic protons to the C_α and C_β spins and chemical shift evolution of the carbons, as in the CBCA(CO)NH experiment. In the following relay step, the magnetization transfer $C_\beta \rightarrow C_\alpha$ and $C_\alpha \rightarrow C_\alpha$ is selected. From the C_α, the magnetization is transferred in two INEPT steps to the amide resonance of the same amino acid (via $^1J_{C\alpha,N}$) and of the next amino acid (via $^2J_{C\alpha,N}$). Amide chemical shift is recorded in a CT evolution time t_2 of duration $2\tau \approx$ 22 ms, which is chosen to yield good transfer via both couplings. After a COS-INEPT transfer from N to H^N, the amide protons are detected in t_3.

In a ^{13}C spin system C_α-$(C_\beta)_m$-$(C_\gamma)_p$ (m and p are the multiplicities of C_β and C_γ carbons, respectively – m equals 0 for glycine and 1 otherwise), the transfer amplitudes for the pathways originating from $C_\beta(i)$, $C_\beta(i-1)$, $C_\alpha(i)$, and $C_\alpha(i-1)$ are (n is the H-multiplicity of the carbons):

3D CBCANH $\quad H_{\alpha,\beta} \rightarrow C_{\alpha,\beta}(t_1) \rightarrow C_\alpha \rightarrow N(t_2)H^N(t_3)$

$$\sin(\pi^1 J_{C,H}\Delta')\sin(\pi^1 J_{C,H}\Delta'')\cos^{n-1}(\pi^1 J_{H,C}\Delta'')$$
$$\exp(-\Delta'/T_{2H})f(T,\tau_1,\tau)$$
$$\exp(-2(T+\tau_1)/T_{2C})\exp(-2\tau/T_{2N})$$
$$\sin^2(\pi^1 J_{N,HN}\Delta)\exp(-\Delta/T_{2HN}) \qquad (20a)$$

The term $f(T,\tau_1,\tau)$ of the transfer function depends on the type of cross peak:

$C_\alpha(i)$:
$$f(T,\tau_1,\tau) = \cos^m(2\pi^1 J_{C\alpha,C\beta}T)\cos^m(2\pi^1 J_{C\alpha,C\beta}\tau_1)$$
$$\sin(2\pi^2 J_{C\alpha,N}\tau_1)\cos(2\pi^1 J_{C\alpha,N}\tau_1)$$
$$\sin(2\pi^2 J_{C\alpha,N}\tau)\cos(2\pi^1 J_{C\alpha,N}\tau) \qquad (20b)$$

$C_\alpha(i-1)$:
$$f(T,\tau_1,\tau) = \cos^m(2\pi^1 J_{C\alpha,C\beta}T)\cos^m(2\pi^1 J_{C\alpha,C\beta}\tau_1)$$
$$\sin(2\pi^2 J_{C\alpha,N}\tau_1)\cos(2\pi^1 J_{C\alpha,N}\tau_1)$$
$$\sin(2\pi^2 J_{C\alpha,N}\tau)\cos(2\pi^1 J_{C\alpha,N}\tau) \qquad (20c)$$

$C_\beta(i)$:
$$f(T,\tau_1,\tau) = \sin(2\pi^1 J_{C\alpha,C\beta}T)\cos^p(2\pi^1 J_{C\beta,C\gamma}T)$$
$$\sin(2\pi^1 J_{C\alpha,C\beta}\tau_1)$$
$$\sin(2\pi^1 J_{C\alpha,N}\tau_1)\cos(2\pi^2 J_{C\alpha,N}\tau_1)$$
$$\sin(2\pi^1 J_{C\alpha,N}\tau)\cos(2\pi^2 J_{C\alpha,N}\tau) \qquad (20d)$$

$C_\beta(i-1)$:
$$f(T,\tau_1,\tau) = \sin(2\pi^1 J_{C\alpha,C\beta}T)\cos^p(2\pi^1 J_{C\alpha,C\gamma}T)$$
$$\sin(2\pi^1 J_{C\alpha,C\beta}\tau_1)$$
$$\sin(2\pi^2 J_{C\alpha,N}\tau_1)\cos(2\pi^1 J_{C\alpha,N}\tau_1)$$
$$\sin(2\pi^2 J_{C\alpha,N}\tau)\cos(2\pi^1 J_{C\alpha,N}\tau) \qquad (20e)$$

To achieve good signal-to-noise for all types of cross peaks, the delays in the CBCANH experiment are chosen as follows: $\Delta' = 3.8$ ms, $\Delta'' = 2.0$ ms, $2T \approx 1/(4J_{C,C}) = 7$ ms, $2\tau_1 = 22$ ms and $2\tau = 22$ ms. Simulated transfer amplitudes for the four transfer pathways are depicted in Fig. 26 as a function of the delay $2\tau_1$. Note that the C_α-cross peaks of all amino acids but glycine have opposite sign compared to the C_β cross peaks, which is helpful for both manual and automated assignment.

As an alternative to the CBCANH, the HNCACB experiment [60] uses an ''out-and-back'' magnetization transfer (Fig. 25b):

$$H^N \rightarrow N \rightarrow C_\alpha \rightarrow C_{\alpha,\beta}(t_1) \rightarrow C_\alpha \rightarrow N(t_2) \rightarrow H^N(t_3).$$

This experiment is more sensitive than CBCANH mainly because ^{13}C magnetization is transverse only during about half the time in the HNCACB ($4\delta + t_1 \approx 15$ ms) compared to the CBCANH

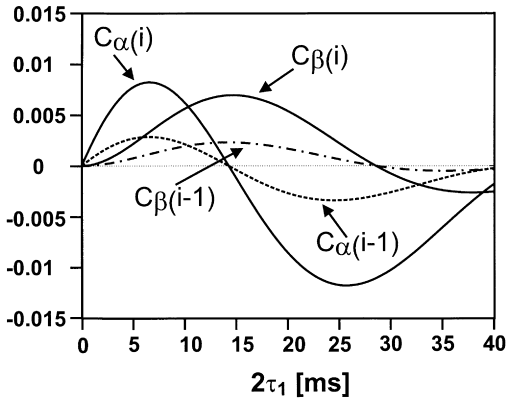

Fig. 26. Transfer amplitudes as a function of the delay $2\tau_1$ for the four magnetization transfer pathways correlating $C_\beta(i)$, $C_\alpha(i)$, $C_\beta(i-1)$ and $C_\alpha(i-1)$ in the CBCANH experiment. Simulations are according to Eq. (20) for a spin system $C_\alpha H\text{-}C_\beta H_2\text{-}C_\gamma$ ($n = 1$ for C_α, $n = 2$ for C_β, $m = 1$ and $p = 1$) using: $^1J_{H,N} = 92$ Hz, $^1J_{H,C} = 135$ Hz, $^1J_{C\alpha,N} = 11$ Hz, $^2J_{C\alpha,N} = 7$ Hz, $^1J_{C,C} = 35$ Hz, $T_{2HN} = 50$ ms, $T_{2N} = 50$ ms, $T_{2H\alpha,\beta} = 20$ ms, $T_{2C\alpha,\beta} = 20$ ms, $\Delta = 5.4$ ms, $\Delta' = 3.8$ ms, $\Delta'' = 2$ ms, $\tau_1 = \tau = 11$ ms, $T = 4.5$ ms.

($2TH + 2\tau_1 \approx 30$ ms). However, a disadvantage of this experiment is that the carbon chemical shifts recorded during t_1 are modulated by C,C couplings. This is especially critical for C_β cross peaks, which can have up to three carbon coupling partners. In the following we derive the relative signal-to-noise ratios for the $C_\beta(i)$, $N(i)$, $H^N(i)$ cross peak in the two experiments as a function of ^{13}C T_2 times in order to compare their relative sensitivity.

The transfer efficiency for the $C_\beta(i)$ cross peak in the HNCACB experiment is given by:

$$\sin^4(\pi^1 J_{HN,N}\Delta)\exp(-2\Delta/T_{2HN})\sin^2(2\pi^1 J_{C\alpha,N}\tau)$$

$$\cos^2(2\pi^2 J_{C\alpha,N}\tau)\exp(-4\tau/T_{2N}),$$

$$\sin^2(\pi^1 J_{C\alpha,C\beta}2\delta)\exp(-4\delta/T_{2C\alpha})$$

$$* \frac{1}{t_1^{max}} \int_0^{t_1^{max}} \cos(\pi^1 J_{C\alpha,C\beta}t_1)$$

$$\cos^p(\pi^1 J_{C\beta,C\gamma}t_1)e^{-t_1/T_{2C_\beta}}\,dt_1 \qquad (21)$$

The parts of the transfer amplitudes for the carbon magnetization that differ between the CBCANH ($2T$ and $2\tau_1$) and the HNCACB (4δ and t_1) pulse sequences are given in Eq. (22a) for the $C_\beta(i)$ cross peak in a spin system C_α-(C_β)-$(C_\gamma)_p$ assuming $T_{2C\alpha} = T_{2C\beta} = T_{2C}$:

$$S_{CT}^{CBCANH} = \sin(2\pi^1 J_{C\alpha,C\beta}T)\cos^p(2\pi^1 J_{C\beta,C\gamma}T)$$

$$\sin(2\pi^1 J_{C\alpha,C\beta}\tau_1)\exp(-2(T+\tau_1)/T_{2C})\exp(-2\tau/T_{2N})$$

$$S_{RT}^{HNCACB} = \sin^2(2\pi^1 J_{C\alpha,C\beta}\delta)\exp(-4\delta/T_{2C})$$

$$* \frac{1}{t_1^{max}} \int_0^{t_1^{max}} \cos(\pi^1 J_{C\alpha,C\beta}t_1)\cos^p(\pi^1 J_{C\beta,C\gamma}t_1)$$

$$\times e^{-t_1/T_{2C_\beta}}\,dt_1 \qquad (22a)$$

Comparing the two implementations for different T_{2C} (20 ms and 10 ms) and T_{2N} (80 and 50 ms) using optimized delays (for $T_{2C} = 20/10$ ms $T_{2N} = 80/50$ ms: $2\delta = 87$ ms, $2T = 7$ ms, $2\tau_1 = 22/20$ ms, $2\tau_1 = 22$ ms, $t_1^{max} = 1/(4J_{CC})$) yields:

	T_{2C}, T_{2N}	$p = 1$	$p = 2$
S_{HNCACB}/S_{CBCANH}	20 ms, 80 ms	1.66	2.13
	10 ms, 50 ms	1.70	2.26

(22b)

Because of the better resolution, the CBCANH is recommended for proteins with ^{13}C T_2 relaxation times of around 20 ms, while for proteins with shorter ^{13}C T_2 times the HNCACB experiment will be advantageous, although resolution has to be sacrificed. In combination with ^2H labelling, the HNCACB with constant-time ^{13}C chemical shift evolution becomes the experiment of choice (see Section 5.8).

In summary, without the use of deuteration the CBCANH experiment yields acceptable signal-to-noise for ^{13}C T_2 relaxation times $>$ 20 ms and is therefore the recommended implementation. For shorter T_2 relaxation times, both experiments will not yield reasonable signal-to-noise ratios. However, in combination with ^2H labelling HNCACB will be the experiment of choice, and has been proven very useful especially in combination with a constant-time ^{13}C chemical shift evolution (see Section 5.8).

5.3. 3D (H)CC(CO)NH-TOCSY

The relay-COSY transfer C_β, $C_\alpha \rightarrow C_\alpha$, which is used in the CBCA(CO)NH and CBCANH experiments, is efficient for proteins up to 20 kD molecular

weight. For smaller proteins with more favorable relaxation properties, it is also possible to transfer magnetization from all side-chain resonances to the C_α nucleus by homonuclear C,C-TOCSY transfer and via C' and N to the amide protons. Such experiments are less sensitive than the relay-COSY experiments, because magnetization originating from all nuclei is distributed into the whole spin system, with only a small part being transferred to the C_α. Further, it is hard to find a mixing time τ_m that yields good transfer for all aliphatic side-chain carbons of all amino acids to their C_α carbon [183].

Very similar (H)CC(CO)NH experiments have been proposed by several groups [62–65] that all transfer magnetization via a pathway $H \rightarrow C \rightarrow C \rightarrow C_\alpha$, followed by INEPT steps to transfer the magnetization via C' and N to the amide proton. For the successful implementation of such sequences it is essential to transfer the coherence from the C_α to the C' spin as fast as possible. The time necessary for this transfer is $2f = 1/(2J(C_\alpha,C'))$ if the homonuclear C,C-TOCSY is followed by a C_α,C' selective INEPT transfer step. The low transfer efficiency of these experiments can be increased by the use of a tailored TOCSY (TACSY) transfer for the $C_\alpha \rightarrow C'$ transfer. To achieve tailored TOCSY transfer between the two frequency bands of the C_α and the C- spins, **PL**anar do**U**ble band **S**elective **H**omonuclear TACSY (PLUSH TACSY) sequences have been developed [184,185] (see the following and Section 5.4). Two implementations of the (H)CC(CO)NH experiment are compared in Fig. 27. Again, the chemical shift evolution of $^{13}C'$ instead of ^{5}N in an (H)CCCO(N)H-TOCSY experiment could be implemented alternatively.

The transfer amplitude of the (H)CC(CO)NH-TOCSY experiment is very similar to the CBCA-(CO)NH experiment, only the transfer efficiency of the C,C transfer step differs. The transfer function $T(C_k,C_1)$ describes the efficiency for the transfer of in-phase coherence from the spin C_k to spin C_1. For the pulse sequence Fig. 27a we obtain in a spin system C_α-(C_β)-$(C_\gamma)_p$ with proton multiplicities n:

$$\text{3D(H)CC(CO)NH} \qquad H_{\text{aliph.}} \rightarrow C_{\text{aliph}}(t_1) \rightarrow C_\alpha \rightarrow C \rightarrow N(t_2) \rightarrow H^N(t_3)$$

$$\sin(\pi^1 J_{C,H}\Delta')\sin(\pi^1 J_{C,H}\Delta'')\cos^{n-1}(\pi^1 J_{H,C}\Delta'')$$

$$\exp(-\Delta'/T_{2H})$$

$$\left[\sum_{k=\alpha,\beta,\gamma\ldots} T(C_k, C_\alpha)\right]\exp(-\tau_m/T_{1\rho C})$$

$$\sin(2\pi^1 J_{C',C_\alpha}\zeta)\cos(2\pi^1 J_{C\alpha,C\beta}\zeta)$$

$$\exp(-(\Delta'' + t_1 + 2\zeta)/T_{2C})$$

$$\sin(2\pi^1 J_{C',C_\alpha}\eta)\sin^2(2\pi^1 J_{C',N}\tau)$$

$$\exp(-2\tau/T_{2C'})\exp(-2\tau/T_{2N})$$

$$\sin^2(\pi^1 J_{N,HN}\Delta)\exp(-\Delta/T_{2HN}) \tag{23a}$$

Note that in the pulse sequences of Fig. 27a anti-phase coherence of the type $2C_{\beta z}C_{\alpha y}$ at the end of the C, C-TOCSY sequence can refocus during 2ζ and can therefore add to the signal described by Eq. (23a).

The transfer amplitude of the sequence in Fig. 27b can be calculated assuming that C_α and C' are both transverse for $\tau_1/2$ during the $C_\alpha \rightarrow C'$ transfer:

$$\sin(\pi^1 J_{C,H}\Delta')\sin(\pi^1 J_{C,H}\Delta'')\cos^{n-1}(\pi^1 J_{C,H}\Delta'')$$

$$\exp(-\Delta/T_{2H'})$$

$$\left[\Sigma_{k=\alpha,\beta,\gamma\ldots} T(C_k, C_\alpha)\right]$$

$$\exp(-(\Delta'' + t_1)/T_{2C})\exp(-\tau_m/T_{1\rho C})$$

$$\frac{1}{2}\left[1 - \cos(\pi^1 J_{C',C_\alpha}\tau_1)\right]\exp(-\tau_1/(2T_{1\rho C}))$$

$$\exp(-\tau_1/(2T_{1\rho C'}))$$

$$\sin^2(2\pi^1 J_{C',N}\tau)\exp(-2\tau/T_{2C'})\exp(-2\tau/T_{2N})$$

$$\sin^2(\pi^1 J_{N,HN}\Delta)\exp(-\Delta/T_{2HN}) \tag{23b}$$

In the pulse sequences depicted in Fig. 27, chemical shift evolution of the fast-relaxing aliphatic carbons occurs during t_1. By utilizing the delay Δ'', t_1 can be implemented as a semi-constant-time evolution (see Section 5.5.1) to minimize the duration during which

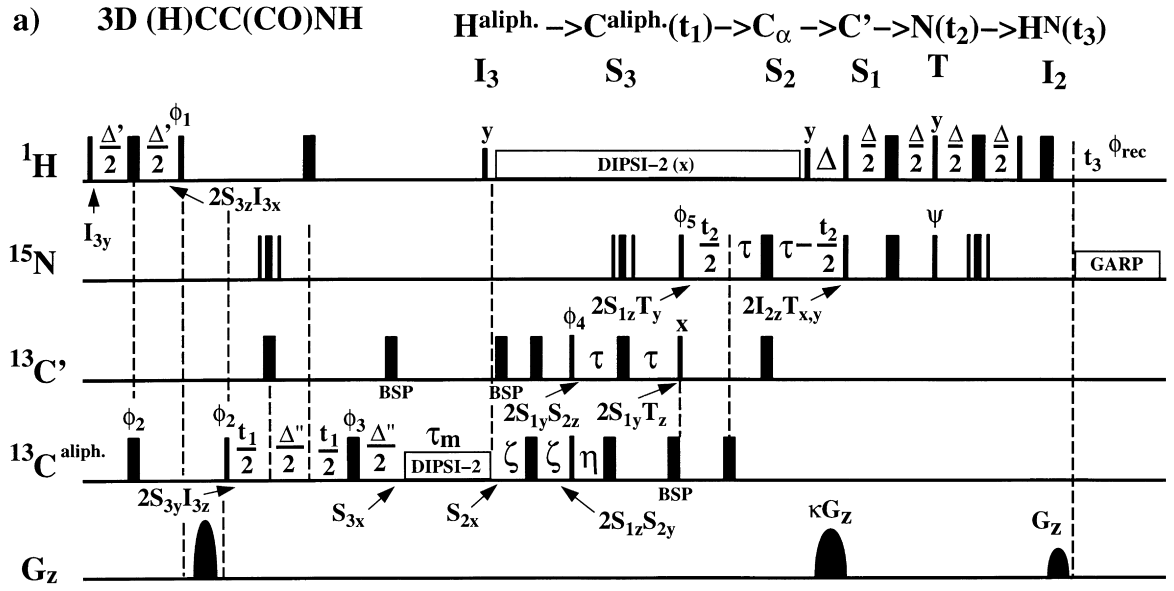

κ = +/–10; ψ = +/–y; ϕ_1=y; ϕ_2=2(x), 2(–x) + TPPI(t_1); ϕ_3 = x;

ϕ_4 = x; ϕ_5 = x, –x; ϕ_{rec}= x, 2(–x), x.

Δ'=3.6 ms, Δ"=2.4 ms, Δ=5.4 ms, τ=13.5 ms, ζ=3.4 ms, η=4.5 ms.

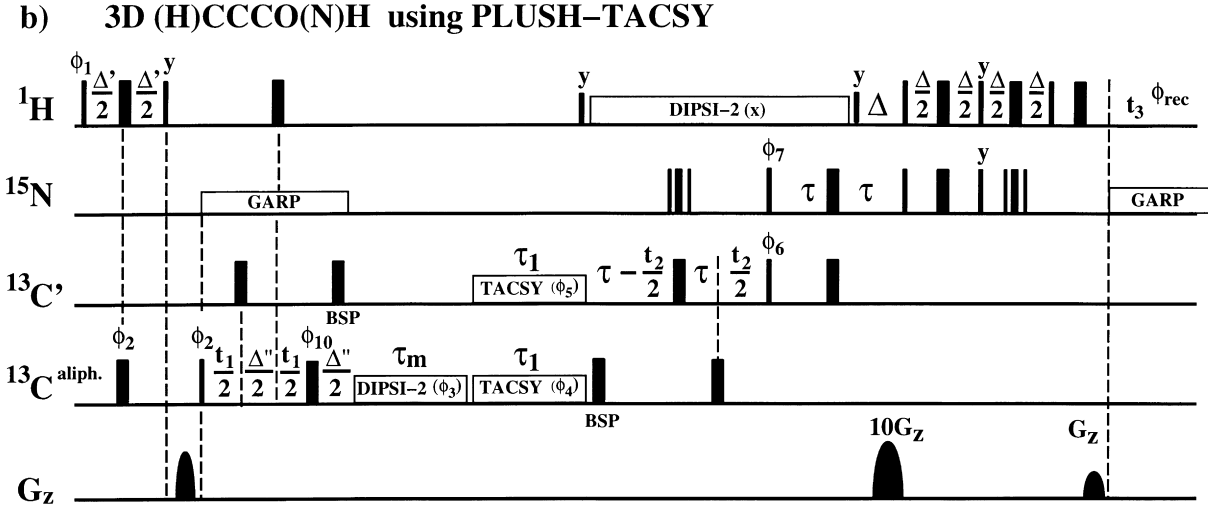

ϕ_1= x; ϕ_2= x, –x + TPPI(t_1); ϕ_3 = x; ϕ_4 = x; ϕ_5 = x; ϕ_6 = 2(x), 2(–x) + TPPI(t_2);

ϕ_7= 4(x), 4(–x); ϕ_{10} = x; ϕ_{rec}= x, 2(–x), x, –x, 2(x), –x.

Δ'=3.6ms, Δ"=2.4ms, Δ=5.4ms, τ_1=18ms, τ=13ms.

Fig. 27. Implementations of the (H)CC(CO)NH-TOCSY experiment. (a) Conventional version using INEPT transfers for the steps $C_\alpha \rightarrow C' \rightarrow N$ and a COS-INEPT for the $N \rightarrow H^N$ transfer; (b) The $C_\alpha \rightarrow C'$ transfer in (a) is replaced by a tailored TOCSY sequence (PLUSH TACSY).

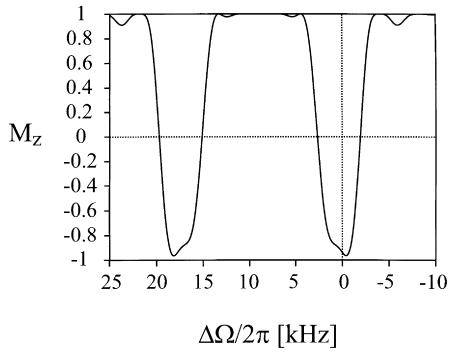

Fig. 28. Inversion profile of a G2 pulse: M_z magnetization as a function of resonance offset $\Delta\Omega$ after application of a shaped G2 pulse (G2 = $G^{270}G^{270}$). G2 is applied with the carrier frequency placed in the middle of C_α resonance frequencies. Thus, in order to fulfil the Hartmann–Hahn condition between the C_α and C' spins on a 600 MHz spectrometer, the G2 pulse must then be both phase- and amplitude-modulated with $\Delta\Omega/2 = 8930$ Hz. The pulse duration is $\tau_p = 559.91$ μs and the pulse is applied at a field strength $\gamma B_1^{max}/(2\pi) = 9516$ Hz

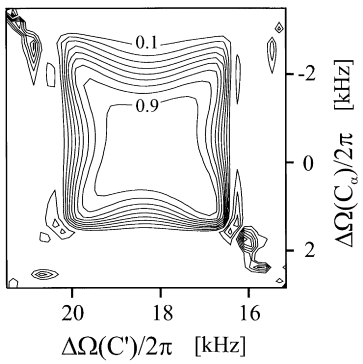

Fig. 29. Simulated transfer efficiency $T(C_\alpha,C')(\Delta\Omega)$ for the coherence transfer $C_\alpha \leftarrow\rightarrow C'$ as a function of the offset $\Delta\Omega$ between C_α and C' spins. A simulation of the PLUSH-TACSY mixing scheme consisting of an MLEV-16 expansion of the G2 pulse of Fig. 28 applied at the center of the C_α spectral width is shown.

the carbon spins are transverse. From the term $\frac{1}{2}[1 - \cos(\pi^1 J_{C'C\alpha}\tau_1)]$ in Eq. (23b), the optimal mixing time for the heteronuclear $C_\alpha \rightarrow C'$-TOCSY is calculated as $\tau_1 = 1/^1J_{C',C\alpha} \approx 18$ ms. The $C_\alpha \rightarrow C'$-TOCSY is implemented using a PLUSH TACSY sequence [185], because the chemical shift difference $\Delta\Omega$ between the C_α and C' spectral regions is too large to be covered by a normal TOCSY sequence. The doubly band selective PLUSH TACSY sequence eliminates chemical shift within the C_α and C' frequency bands. Therefore the Hartmann–Hahn condition, which is required for TOCSY or TACSY transfer, is fulfilled for these nuclei. The PLUSH TACSY sequence consists of a frequency-selective shaped inversion pulse G2, which is composed of two Gaussian pulses. In order to achieve band-selective inversion at $\pm\Delta\Omega/2$, this pulse shape is amplitude-modulated by $\cos(2\pi\Delta\Omega/2t)$. $\Delta\Omega$ is the chemical shift difference between the C_α and C' spectral regions. To obtain a planar mixing Hamiltonian of the form $H^{eff} = \pi J(S_{kz}S_{lz} + S_{ky}S_{ly})$ (S_k and S_l being the spin operators for the C_α and C' spins, respectively) the G2 inversion pulse can be constructed by combination of two $n * 90°$ rotations. For example, two self-refocusing 270° Gaussian pulses can be used, where G2 = $G^{270}G^{270}$. The G2 pulse is then expanded by an MLEV-16 supercycle. For a 600 MHz instrument, the duration of G2 = $G^{270}G^{270}$ – with G^{270} being a Gaussian shape at 5% truncation – is $\tau_p = 559.91$ μs applied at a field strength $\gamma B_1^{max}/(2\pi) = 9516$ Hz with phase- and amplitude-modulation frequencies of $\Delta\Omega/2 = 8930$ Hz. Using an MLEV-16 supercycle of this G2 pulse, TACSY transfer between the C_α and C' nuclei is achieved, while the C_β nuclei are effectively decoupled from the C_α spins.

From the inversion profile of the G2 pulse, shown in Fig. 28, it is obvious that the two side bands of the amplitude modulation influence each other to some degree, but the inversion of both spectral regions is still acceptable. The quality of the inversion can be optimized by variation of the truncation level of the Gaussian pulse shape used for G2 [185]. A simulation of the C_α, C' coherence transfer (Fig. 29) shows good transfer for the C_α, C'-TOCSY. This was also found experimentally comparing the respective H(CC)(CO)NH experiments. Accordingly, the pulse sequence depicted in Fig. 27b can be expected to be the most sensitive implementation of the (H)CC(CO)NH-TOCSY experiment.

5.4. 3D H(CC)(CO)NH-TOCSY

The H(CC)(CO)NH-TOCSY experiment is closely related to the (H)CC(CO)NH-experiment. The pulse sequences depicted in Fig. 30 differ from published pulse sequences [62] in the use of a combined hetero- and homonuclear TOCSY for the transfer

$H \rightarrow C \rightarrow C_\alpha$. This combined TOCSY transfer has also been proposed by Zuiderweg et al. for the HCCH-TOCSY [186]. The advantage of the combined transfer stems from the minimization of times during which the fast-relaxing proton and carbon nuclei are transverse.

The proton chemical shift evolution occurs during the RT evolution time t_1, because the heteronuclear TOCSY transfers in-phase magnetization $I_x \rightarrow S_x$. For the same reason, the ^{15}N evolution occurs during the RT evolution time t_2 in the pulse sequence Fig. 30b, in contrast to the CT evolution in Fig. 30a. The transfer amplitudes of the pulse sequences in Fig. 30 for a $(H_nC)_k$–C_α–C'–N–H spin system are:

3D H(CC)(CO)NH (Fig.30a)

$$H_{aliph.}(t_1) \rightarrow C_{aliph.} \rightarrow C_\alpha \rightarrow C \rightarrow N(t_2) \rightarrow H^N(t_3)$$
$$[T(H_n, C)]\exp(-t_1/T_{2H})\exp(-\tau_1/(2T_{1\rho H}))$$
$$\left[\sum_{k=\alpha,\beta,\gamma,\ldots} T(C_k, C_\alpha)\right]\exp(-(\tau_2)/(2T_{1\rho,C}))$$
$$\sin(2\pi^1 J_{C',C\alpha}\zeta)\cos(2\pi^1 J_{C\alpha,C\beta}\zeta)\exp(-2\zeta/T_{2C\alpha})$$
$$\sin(2\pi^1 J_{C',C\alpha}\eta)\sin^2(2\pi J_{C,N}\tau)\exp(-2\tau/T_{2C'})$$
$$\exp(-2\tau/T_{2N})$$
$$\sin^2(\pi^1 J_{N,HN}\Delta)\exp(-\Delta/T_{2HN}) \qquad (24a)$$

3D H(CC)(CO)NH (Fig.30b) $H_{aliph.}(t_1) \rightarrow C_{aliph.}$
$$\rightarrow C_\alpha \rightarrow C \rightarrow N(t_2) \rightarrow H^N(t_3)$$
$$[T(H_n, C)]\exp(-t_1/T_{2H})\exp(-\tau_1/(2T_{1\rho H}))$$
$$\left[\sum_{k=\alpha,\beta,\gamma,\ldots} T(C_k, C_\alpha)\right]\exp(-(\tau_2)/(2T_{1\rho C}))$$
$$\frac{1}{2}[1 - \cos(\pi^1 J_{C^1,C\alpha}\tau_3)\exp(-\tau_3/(2T_{1\rho C}))$$
$$\exp(-\tau_3/(2T_{1\rho C}))$$
$$1/2[1 - \cos(\pi^1 J_{C^1,N}\tau_4)\exp(-\tau_4/(2T_{1\rho N}))$$
$$\exp(-\tau_4/(2T_{1\rho C}))$$
$$\sin(\pi^1 J_{N,HN}\Delta)\exp(-(\Delta + t_2)/T_{2N})$$
$$\sin(\pi^1 J_{N,HN}\tau_5)\exp(-\tau_5/(2T_{1\rho N}))\exp(-\tau_5/(2T_{1\rho HN})) \qquad (24b)$$

The transfer amplitude $T(H_n,C)$ is a function of the proton multiplicity of the carbons. As a compromise for all multiplicities, the mixing time τ_1 is chosen to be $\tau_1 \approx 0.77/^1J_{C,H} \approx 5.8$ ms. The mixing time of all other TOCSY transfers should be chosen slightly shorter than $1/J$ (cf. Eq. (24b)) to minimize relaxation losses: $\tau_3 = 18$ ms, $\tau_4 = 48$ ms, $\tau_5 = 10$ ms. With optimal mixing times of $1/J$ in a two-spin system, the heteronuclear TOCSY transfers take twice as long an INEPT transfer. For this reason, the pulse sequence of Fig. 30b is longer than that of Fig. 30a by 12 ms. The pulse sequences were compared using a sample of a Calmodulin/C20W complex ($\approx$ 19 kD). In spite of the longer duration, the sensitivity of the pulse sequence Fig. 30b is found to be $\approx$ 1.2 times higher compared to that in Fig. 30a. Representative traces from the respective experiments are shown in Fig. 31. Factors contributing to this sensitivity improvement are (i) the decoupling of the $J_{C\alpha,C\beta}$ coupling during the PLUSH TACSY transfer and (ii) better performance of TOCSY sequences in the presence of B_1 field inhomogeneity.

An H(CC)(CO)NH-TOCSY experiment optimized for application to fractionally deuterated proteins has recently been proposed by Gschwind et al.[165]. The pulse scheme also utilizes multiple-quantum line-narrowing because the carbon spins bound to the protons that are detected in this experiment are still effected by the dipolar coupling to the directly bound proton.

5.5. 3D H(C)CH-TOCSY

The HCCH-TOCSY experiment [70–73] is used to assign aliphatic ^1H,^{13}C spin systems and to link them to the sequentially assigned backbone resonances. In an $H_nC(i) - \ldots - H_mC(j)$-spin system a 3D H(C)CH-TOCSY experiment connects chemical shifts H(i), H(j) and C(j). This connectivity information yields the complete assignment of the ^1H and ^{13}C resonances, because the aliphatic proton chemical shifts of a given spin systems are found at the ^{13}C chemical shift of all the carbon frequencies involved in that spin system. However, the proton spin systems must then be traced in the 3D to find the ^{13}C frequencies that belong to the individual protons. In a 4D HCCH-TOCSY, all four involved chemical shifts can be

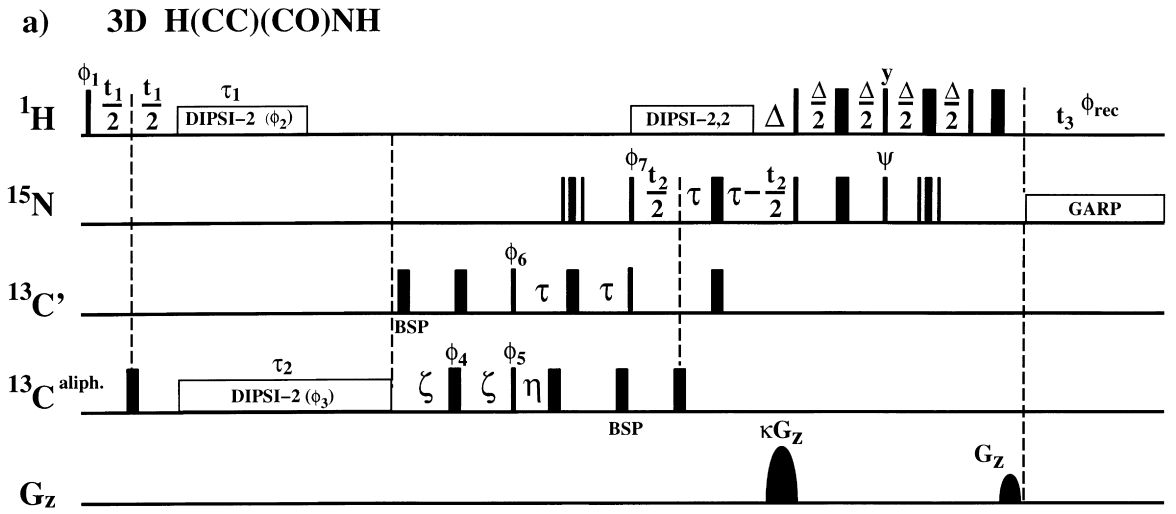

κ = +/−10; ψ = +/−y; ϕ_1= y, −y + TPPI(t_1); ϕ_2 = x; ϕ_3 = x; ϕ_4 = x;

ϕ_5 = 2(x), 2(−x); ϕ_6 =x; ϕ_7 = x; ϕ_{rec}= x, 2(−x), x.

Δ= 5.4 ms, τ= 13.5 ms, τ_1= 6 ms, τ_2= 12 ms, ζ= 3.4 ms, η= 4.5 ms.

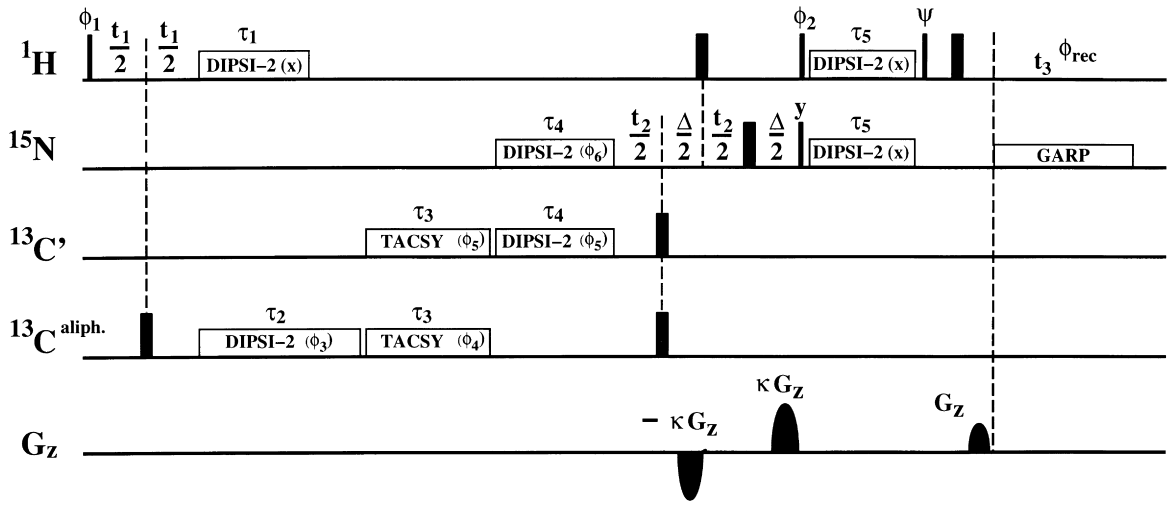

κ = +/−5; ψ = +/−y; ϕ_1= 2(y), 2(−y) + TPPI(t_1); ϕ_2= y; ϕ_3 = x, −x;

ϕ_4 = x; ϕ_5 = x; ϕ_6 = x; ϕ_{rec}= x, 2(−x), x.

Δ = 5.4 ms, τ_1= 6 ms, τ_2= 12 ms, τ_3= 18 ms, τ_4= 48 ms, τ_5= 9.5 ms.

Fig. 30. Implementations of 3D H(CC)(CO)NH-TOCSY experiments. (a) Pulse sequence derived from the pulse sequence shown in Fig. 27b. The H → C-TOCSY transfer can be combined with the C → C-TOCSY transfer, because there is no ^{13}C chemical shift evolution. (b) All INEPT transfers have been replaced by homo- and heteronuclear TOCSY transfers, including the N → H transfer, which is replaced by a planar heteronuclear TOCSY functioning as a COS-INEPT sequence.

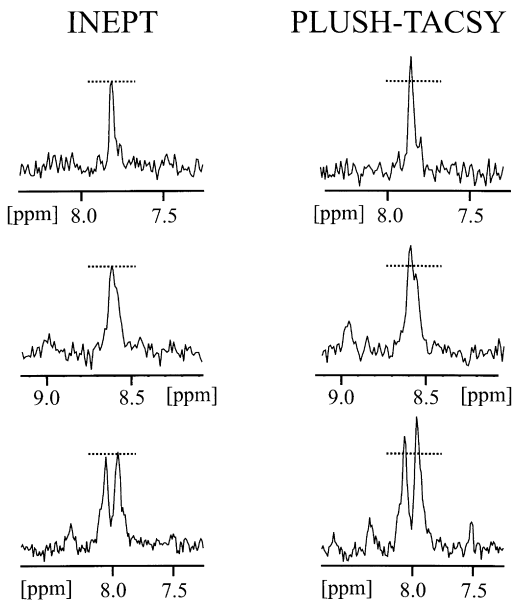

Fig. 31. Representative 1D traces of 2D H(CC)(CO)(N)H-TOCSY experiments acquired with the pulse sequence of Fig. 30a (INEPT) and Fig. 30b (PLUSH-TACSY) using a $\approx$ 1.5 mM sample of ^{13}C-, ^{15}N-labelled Calmodulin complexed with the unlabelled peptide C20W. The signal-to-noise of the ''all-TOCSY'' pulse sequence is $\approx$1.2 better compared to the conventional implementation using INEPT transfers.

extracted from each cross peak simultaneously. Fig. 32a shows the pulse sequence of the original H(C)CH-TOCSY [70], compared to a sensitivity-enhanced 3D H(C)CH-TOCSY experiment using a heteronuclear gradient echo for water suppression (Fig. 32b). The incrementation of the delays for ''semi-constant-time evolution'' [61,65] during t_1 is shown in the figure.

5.5.1. Semi-constant-time (''shared-time'') Evolution

In a semi-constant time evolution of chemical shifts, a constant delay Δ, that is necessary e.g. for the evolution of a coupling, is used for chemical shift evolution in addition to an incremented delay. In contrast to CT evolution, the total evolution segment does grow, however at a reduced rate with increasing t_1 (Fig. 33). The evolution is distributed such that for $t_1 = 0$ the duration of the evolution segment equals the delay Δ whereas for $t_1 = t_1^{\max}$ the duration of the evolution segment equals $t_1^{\max}$. As relaxation of the coherences involved takes place during Δ for $t_1 = 0$ and during $t_1^{\max}$ for $t_1 = t_1^{\max}$, the signal decay caused by relaxation effects is scaled by a factor $(t_1^{\max} - \Delta)/t_1^{\max}$ compared to a real-time implementation. In Fig. 33, the semi-constant time version for the initial H $\rightarrow$ C transfer of the pulse sequence of Fig. 32a is displayed (with Δ' being replaced by Δ).

The delays t_{1a}, t_{1b} and t_{1c} have to be incremented such that the evolution of chemical shift δ and of heteronuclear coupling is described by:

$$\begin{aligned} \delta: &\quad t_{1a} + t_{1b} - t_{1c} = t_1 \\ J: &\quad t_{1a} - t_{1b} + t_{1c} = \Delta \end{aligned} \tag{25a}$$

With the requirement that $t_1(0) = 0$, Eq. (25a) yields:

$$t_{1a}(0) = t_{1c}(0) = \Delta/2 \qquad \text{and} \qquad t_{1b}(0) = 0. \tag{25b}$$

For a FID along t_1 that is to be digitized by TD data points, two relations can be written for the increments Δt_{1a}, Δt_{1b}, Δt_{1c}, (Δt_1 = 1/SWH, where SWH is the spectral width in Hz):

$$\delta: \quad \Delta t_{1a} + \Delta t_{1b} - \Delta t_{1c} = \Delta t_1 \tag{25c}$$

$$J: \quad \Delta t_{1a} - \Delta t_{1b} + \Delta t_{1c} = 0$$

If the FID is digitized by TD complex points, it is required that t_{1c} (TD) $\geq$ 0;. this then yields (for t_{1c} (TD) = 0):

$$\Delta t_{1a} = \Delta t_1/2;$$

$$\Delta t_{1b} = \Delta t_1/2 + \Delta t_{1c} \text{ and } \Delta t_{1c} = -t_{1c}(0)/\mathrm{TD} \tag{25d}$$

Fulfilling Eqs. (25b) and (25d) assures chemical shift evolution with $t_1(0) = 0 < t_1 < t_1^{\max}$ and evolution of the coupling during Δ for all increments. Note, that Δt_{1c} is negative, reflecting the fact t_{1c} is decremented.

Comparing these results with the t_1 increments and delays of Fig. 32a, we obtain $t_{1a} = t_1/2 + \Delta'/2, t_{1b} = t_1/2(1 - \Delta'/t_1^{\max})$ and $t_{1c} = \Delta'/2(1 - t_1/t_1^{\max})$.

The transfer amplitude of the pulse sequence of Fig. 32a in an $H_nC(i) - \ldots - H_mC(j)$ spin system is (n is

a) 3D HC(C)H–TOCSY

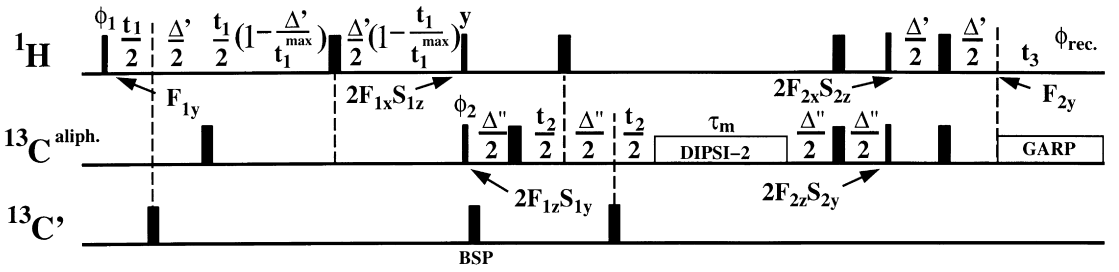

ϕ_1= x, −x + TPPI(t_1); ϕ_2 = 2(x), 2(−x)+ TPPI(t_2); ϕ_{rec}= x, 2(−x), x, −x, 2(x), −x.

Δ'=3.6 ms, Δ"=2.4 ms.

b) 3D DE H(C)CH–TOCSY

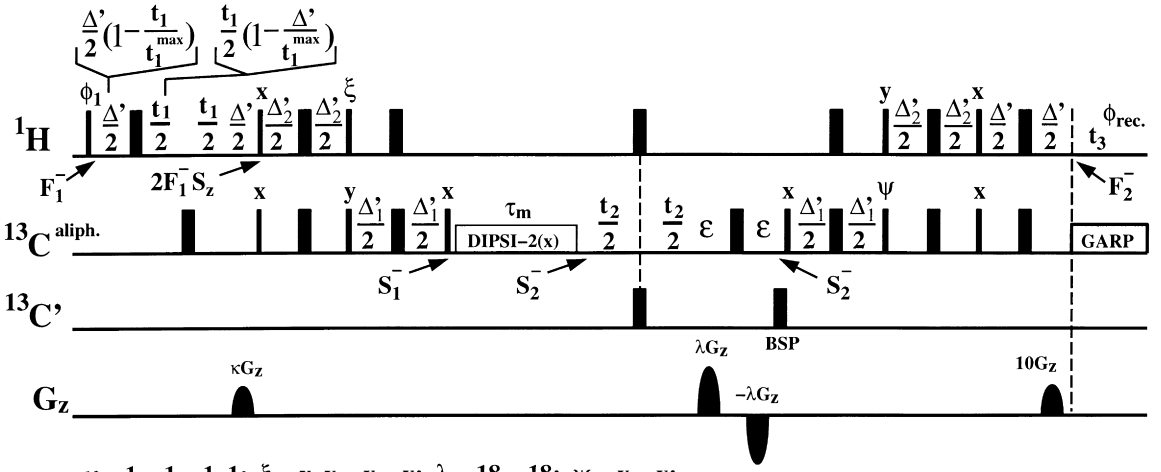

κ = 1, −1, −1, 1; ξ = y, y, −y, −y; λ = 18, −18; ψ = y, −y;

ϕ_1= 4(x), 4(−x); ϕ_{rec}=4(x), 4(−x).

Four successive scans are stored seperately.

Δ'= 3.8 ms, Δ'_1 = 2.3 ms, Δ'_2=1.7 ms.

Fig. 32. Pulse sequences for 3D HC(C)H-TOCSY experiments: (a) Conventional implementation: ^{1}H magnetization is transferred in a refocused INEPT to ^{13}C in-phase magnetization. After C,C-TOCSY mixing, the back-transfer is achieved in an analogous manner. The incrementation of delays required for shared-time evolution in t_1 is also indicated. Note that the C′ 180° pulse during the t_1 evolution period is not absolutely required, because $^2J_{H,C'}$ couplings are small. (b) Doubly sensitivity-enhanced 3D H(C)CH-TOCSY experiment with heteronuclear gradient echo for solvent suppression. The heteronuclear in-phase transfer is implemented with a *yxz*-ICOS-CT sequence [151]. Four different combination of gradients κ and λ and of phase settings ξ and ψ (corresponding to echo/antiecho pathways for both indirect dimensions) have to be recorded and stored in different memory locations. Modifications required for a semi-constant-time evolution during t_1 are indicated. The operator F is the sum of I operators denoting the proton spins.

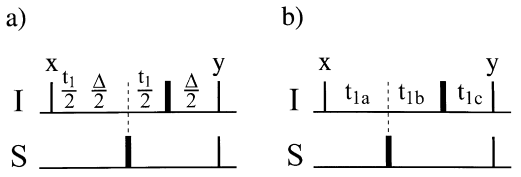

Fig. 33. Initial part of a pulse sequence with evolution of heteronuclear coupling J_{IS} during Δ and simultaneous chemical shift evolution of the I spins during t_1. (a) Conventional implementation (if Δ' is replaced by Δ and the scaling factors $(1 - \Delta'/t_1^{max})$ and $(1 - t_1/t_1^{max})$ are omitted, this corresponds to the initial HSQC step in the pulse sequence of Fig. 32a). (b) Semi-constant-time implementation; delays and increments are defined in the text.

the proton multiplicity of a carbon):

3D H(C)CH-TOCSY $\quad H(t_1) \rightarrow C \rightarrow C(t_2) \rightarrow H(t_3)$

$$\sin(\pi^1 J_{C,H}\Delta')\sin(\pi^1 J_{C,H}\Delta'')\cos^{n-1}(\pi^1 J_{C,H}\Delta'')$$

$$\exp(-(\Delta' + t_1)/T_{2H})$$

$$\left[\sum_{i\leq j} T(C_i, C_j)\right]\exp(-2\Delta'' + t_2)/T_{2C})\exp(-\tau_m/T_{1\rho C})$$

$$\sin(\pi^1 J_{C,H}\Delta')\sin(\pi^1 J_{C,H}\Delta'')\cos^{m-1}(\pi^1 J_{C,H}\Delta'')$$

$$\exp(-\Delta'/T_{2H}) \qquad (26a)$$

The transfer amplitude of the phase-modulating pulse sequence of Fig. 32b, which uses exclusively coherence order selective coherence transfers, is [151]:

$$f_{(H\leftrightarrow C)}\left[\sum_{i\leq j} T(C_i, C_j)\right]$$

$$\exp(-(2\varepsilon + 2\Delta_1' t_2)/T_{2C})\exp(-\tau_m/T_{1\rho C})f_{(H\leftrightarrow C)}$$

with

$$f_{(H\leftrightarrow C)} =$$

$$n/2\cos^{n-1}(\pi^1 J_{C,H}\Delta_2')\sin(\pi^1 J_{C,H}\Delta')\exp(-(\Delta' + \Delta_2'$$

$$+ t_1)/T_{2H})*[\sin(\pi^1 J_{C,H}\Delta_1')\cos^{n-1}(\pi^1 J_{C,H}\Delta_1')$$

$$+ \sin(\pi^1 J_{C,H}\Delta_2')] \qquad (26b)$$

$f_{(H\leftrightarrow C)}$ gives the transfer amplitude for the COS sequence. n is the multiplicity of the carbon spins. Note, that with the doubly sensitivity enhanced pulse sequence of Fig. 32b four combinations of echo/antiecho pathways have to be recorded in order to obtain sign discrimination for chemical shifts in both indirect dimensions.

To maximize magnetization transfer for all carbon multiplicities simultaneously, the delays are chosen as: $\Delta' = 3.8$ ms, $\Delta'' = 2.4$ ms, $\Delta'_2 = 1.7$ ms, $\Delta'_1 = 2.3$ ms. Sequence Fig. 32a is ≈ 1.6 ms shorter than sequence Fig. 32b and uses a smaller number of pulses. In contrast, Fig. 32b gains sensitivity in two enhancement steps and achieves optimal water suppression through the use of a heteronuclear gradient echo. The spectra for side-chain assignments can therefore be recorded on the sample that is also used for the backbone assignment (dissolved in H_2O). This will improve the comparability of chemical shift values extracted from both sets of spectra. The comparison of HCCH-TOCSY experiments on the protein rhodniin (11 kD) gave an average increase in signal-to-noise of 1.34 for the doubly sensitivity enhanced pulse sequence [153]. For larger proteins (>30 kD) the linewidths of side-chain carbon and proton resonances become close to the ^1J-coupling used for coherence transfer in the HCCH-TOCSY experiment. Therefore, an analogous HCCH-NOESY experiment has been suggested recently for very large proteins which employs $^{13}C,^{13}C$-NOESY transfer to correlate side-chain resonances [187].

5.6. Experiments for the assignment of aromatic resonances

Aromatic spin systems are very important for structure determination by NMR since these residues are usually located in the hydrophobic core of a protein. Therefore, they show many long range NOEs that provide important distance restraints to define the tertiary fold. The large number of long-range NOEs for aromatic protons makes assignment strategies based on J couplings preferable to NOE-based assignment strategies. The assignment of aromatic resonances is usually complicated because of strong coupling between ^1H and the ^{13}C spins within the aromatic ring system and short relaxation times. It is also not straightforward to connect the chemical shifts

of the aromatic spin system with those of the corresponding backbone resonances. Therefore, a variety of experimental schemes have been introduced that use an assignment strategy based on scalar couplings rather than on utilizing NOEs between the H_β-protons and the aromatic ortho-protons (H_δ).

Pulse sequences have been introduced that combine a heteronuclear correlation experiment with homonuclear H,H-TOCSY [188,189]. Also, HCCH-TOCSY type experiments optimized for aromatic spin systems have been proposed [190,191]. Heteronuclear dipolar relaxation between the directly coupled aromatic ^{1}H and ^{13}C spins is a main relaxation pathway, which decreases the sensitivity of aromatic ^{13}C, ^{1}H correlation experiments. Therefore a uniformly ^{13}C-, and ^{12}C-Phe-labelled sample was shown to be useful for the assignment of aromatic ^{1}H resonances and NOEs between Phe residues and the other residues of a protein [192].

In INEPT transfer based experiments [193,194] introduced by Kay's group, magnetization is transferred from H_β to C_β spins to the quaternary $^{13}C_\gamma$ nuclei using selective pulses for the aromatic C_γ spins, and adjusting the power level of the C_β pulses such that C_γ spins are not affected. In order to refocus the C_α,C_β couplings a 1,1 pulse [195,196] is employed with $\xi = 1/(2\Delta\Omega) - 4/\pi^* \tau_{\pi/2}(^{13}C)$ (Fig. 34), where $\tau_{\pi/2}$ (^{13}C) is the pulse width of the 90° (^{13}C) pulse and $\Delta\Omega$ is the resonance offset between the centers of the C_α and C_β resonance frequencies of aromatic amino acids. After carbon relay transfers to the protonated aromatic carbons, the magnetization is finally detected on the H_δ or H_ε protons (when the pulses shown in brackets in Fig. 34a are applied). The pulse sequence for this experiment is shown in Fig. 34a, the corresponding transfer amplitude is given in Eq. (27a).

Grzesiek and Bax have designed an experiment specifically for aromatic side-chains [197] that has as central step a Hartmann–Hahn type magnetization transfer between the aliphatic C_β- and the aromatic C_γ spins. In this experiment, ''AMNESIA'' (''Audio Modulation Nutation for Enhanced Spin Inter-Action''), the Hartmann–Hahn condition between C_β and the aromatic C_γ is achieved by an audio-modulated spin lock field.

A related type of experiment uses tailored TOCSY (PLUSH TACSY) transfer (see Section 5.4) between the aliphatic C_β- and the aromatic C_γ-spins followed by homonuclear ^{13}C-TOCSY to correlate the resonances in the aromatic ring to backbone resonances [184,185]. The pulse sequence is shown in Fig. 34b, the transfer amplitude is given in Eq. (27b) $T(C_\gamma,C_k)$ is the transfer efficiency for homonuclear sTOCSY transfer between the aromatic ^{13}C spins.

(HB)CB(CG, CD, CE)HE (Fig.34a)

$$H_\beta \rightarrow C_\beta(t_1) \rightarrow C_\gamma^{ar} \rightarrow C_\delta^{ar.} \rightarrow C_\varepsilon^{ar.} \rightarrow H_\varepsilon^{ar}(t_2)$$

$$\sin(\pi^1 J_{C,H}\Delta')\exp(-\Delta'/T_{2H})\sin(\pi^1 J_{C,H}\Delta'/2)$$

$$\cos(\pi^1 J_{C,H}\Delta'/2)$$

$$\sin(2\pi^1 J_{C\beta,C\gamma}2T)\exp(-2T/T_{2C\beta})$$

$$\sin(\pi^1 J_{C\beta,C\gamma}\tau_1)\sin(2\pi^1 J_{C\gamma,C\delta}\tau_1)\exp(-2\tau_1/T_{2C\gamma})$$

$$\sin(2\pi^1 J_{C\gamma,C\delta}\tau_2)\sin(2\pi^1 J_{C\delta,C\varepsilon}\tau_2)\exp(-2\tau_2/T_{2C\delta})$$

$$\sin(2\pi^1 J_{C\delta,C\varepsilon}\tau_3)\sin(\pi^1 J_{C\varepsilon,H\varepsilon}\Delta_1')\exp(-2\tau_3/T_{2C\varepsilon})$$

$$\sin(\pi^1 J_{C\varepsilon,H\varepsilon}\Delta_2')\exp(-\Delta_2'/T_{2H\varepsilon}) \qquad (27a)$$

(HB)CB(C, Caro)H (Fig.34b)

$$H_\beta \rightarrow C_\beta(t_1) \rightarrow C_\gamma^{ar} \rightarrow C^{ar.} \rightarrow H^{ar}(t_2)$$

$$\sin(\pi^1 J_{C,H}\Delta')\exp(-\Delta'/T_{2H})$$

$$\sin(\pi^1 J_{C,H}\Delta'/2)\cos(\pi^1 J_{C,H}\Delta'/2)\exp(-(\Delta'/2 + t_1)/T_{2C\beta})$$

$$\tfrac{1}{2}[1 - \cos(\pi^1 J_{C\beta,C\gamma}\tau_1)]\exp(-\tau_1/(2T_{1\rho C\beta}))$$

$$\exp(-\tau_1/(2T_{1\rho C\gamma}))$$

$$\left[\sum_{k=\delta,\varepsilon,\ldots} T(C_\gamma, C_k)\right]\exp(-(\tau_2)/T_{1\rho Caro})$$

$$\sin(\pi^1 J_{Caro,Haro}\Delta_1')\exp(-\Delta_1'/T_{2Caro})$$

$$\sin(\pi^1 J_{Caro,Haro}\Delta_2')\exp(-\Delta_2'/T_{2Haro}) \qquad (27b)$$

With respect to signal-to-noise the PLUSH-TACSY experiment seems to be the optimum

implementation for these aromatic experiments. However, if the aromatic proton resonances for a given residue overlap, it might be desirable to use the INEPT based experiments where the magnetization transfer can be directed specifically for observation of H_δ or H_ε, respectively.

5.7. Experiments for the assignment of specific side chain resonances

A number of experiments have been derived from the basic triple resonance experiments described so far in order to allow the identification of specific amino acid types. For example, the lack of an amide proton in prolines [83] or the unique occurrence of two H_α protons and the lack of a C_β carbon in glycines [84,85] have been utilized to design specific experiments for these residues. A modification of the HCA(CO)N experiment allows editing for residues following a proline and measuring the proline nitrogen chemical shifts. This information is not available from standard experiments and can therefore be helpful for establishing the sequential assignments to prolines. Further, pulse sequences have been introduced to assign specific polar and charged side chain spin systems, e.g. of Asp, Glu, Asn and Gln [88–92]. The pulse sequences are derived from backbone experiments like HNCO and are optimized for side chain spin systems. Two pulse sequences measuring the ^3J-coupling of side chain amides to aliphatic ^{13}C spins in the side chains of asparagine or glutamine residues (based on E.COSY [198] and quantitative J-correlation [92] type experiments, respectively) have been designed for the stereospecific assignments of side chain amide protons in order to better define the side chain conformation of these groups. A set of CBCA(CO)NH-based experiments exploit the different chemical shifts of aliphatic, aromatic or carbonyl C_γ-spins to identify side chain spin systems [91].

Arginine side-chains located on the surface of a protein are very important for the interaction with charged ligands, e.g. phosphotyrosine groups. However, the guanidinium H^N resonances are often broadened by conformational and chemical exchange and thus difficult to detect [199]. Usually, the H_ε amide protons are readily observed and under appropriate experimental conditions the other side chain resonances can also be observed. The assignment of the ^1H, ^{13}C and ^{15}N chemical shifts of the guanidinium group can be achieved by correlation to the corresponding aliphatic arginine side chain resonances. A number of experiments for ^{15}N-,$^{13}C/^{15}N$-, or $^{13}C/^{15}N$ ^2H-labelled samples have been proposed for this purpose [93–96].

5.8. Modified pulse sequences for ^2H- and ^{13}C, ^{15}N-labelled proteins

Recently, the use of fractional or complete deuterated protein samples has dramatically improved the performance of previously described triple resonance experiments on higher molecular weight proteins [200] (see also [201,202]). There are two advantages associated with deuterium labelling. First, because the main source of relaxation for ^{13}C spins in ^{13}C-labelled proteins is the directly bound proton, substituting the ^1H spin by ^1H ($\gamma_D/\gamma_D \approx 1/6.5$) greatly reduces the heteronuclear dipolar relaxation of the carbon spin. The ^{13}C T_2 is therefore increased by a factor of up to $I_H(I_H+1)\gamma_H^2/I_D(I_D+1)\gamma_D^2 = 15.8$ (I_H and I_D are the spin quantum numbers for ^1H and ^2H, respectively). This is important for most of the triple resonance experiments especially for the $^{13}C_\alpha$, because these experiments rely on magnetization transfer via the $^{13}C_\alpha$ spin, which is the fastest relaxing ^{13}C spin in the peptide fragment. Second, by use of deuteration, the density of ^1H spins is diluted, thus reducing the distribution of magnetization through homonuclear proton/proton relaxation pathways (spin diffusion) which is more efficient with increasing molecular weight. Therefore, by suppression of spin diffusion, the linewidths of the observed protons are narrower compared to a fully protonated spin system. For backbone [26,27] and H^N-detected side chain ^{13}C assignment experiments [76,77], a perdeuterated (100% ^2H-labelling for the side-chain protons) protein sample yields the best improvement of the relaxation rates. In this case, out-and-back type experiments have to be used or coherence transfer has to originate from ^{13}C with H^N being detected. Triple resonance experiments applied to deuterated proteins yield dramatic sensitivity improvements compared to fully protonated samples. Owing to the longer T_2, constant-time evolution periods can be employed for the evolution of the C_α chemical shifts.

a) aromatic $H_\beta C_\beta C_\gamma C_{\delta,\varepsilon} H_{\delta,\varepsilon}$

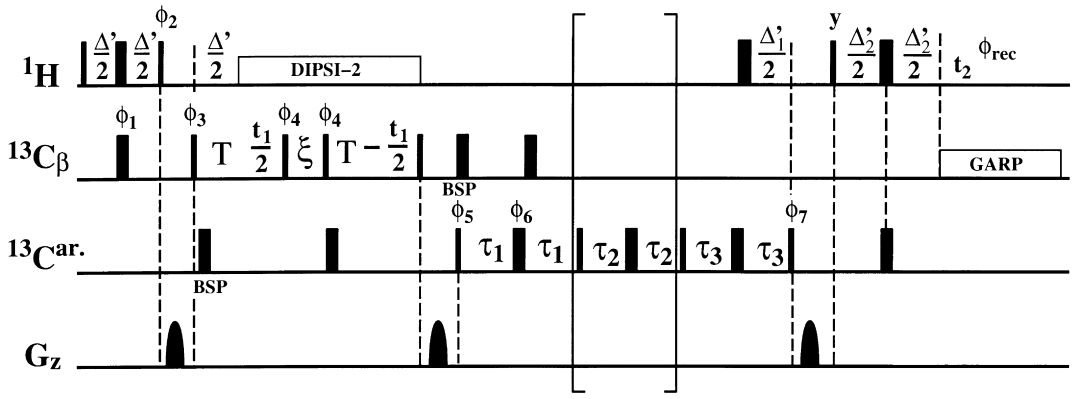

ϕ_1= x, −x; ϕ_2 = y, −y; ϕ_3 = x + TPPI (t_1); ϕ_4 = 2(x),2(y),2(−x),2(−y); ϕ_5 = x;

ϕ_6 =8(x), 8(y), 8(−x), 8(−y); ϕ_7 = 32(x), 32(−x);

ϕ_{rec} = 2[2(x,−x,−x,x),2(−x,x,x,−x)], 2[2(−x,x,x,−x),2(x,−x,−x,x)];

Δ'= 3.6 ms, Δ'_1 = 1.4 ms, Δ'_2=2.5 ms, T = 4.5 ms, τ_1= 2.7 ms, τ_2= 3.8 ms, τ_3= 2.1 ms,

$\xi = 1/(2\Delta\Omega) - 4/\pi * \tau_{\pi/2}(^{13}C_\beta)$.

b) $H_\beta C_\beta C_\gamma C^{ar.} H^{ar.}$ using PLUSH–TACSY

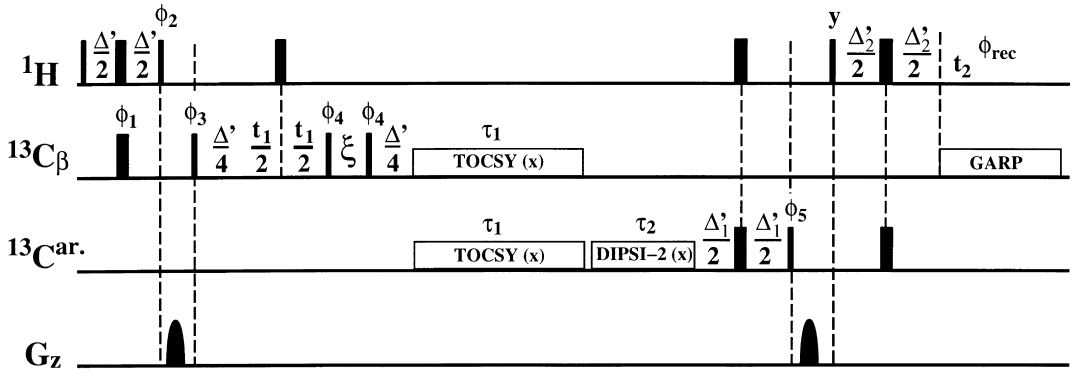

ϕ_1= 16(x), 16(−x); ϕ_2 = y; ϕ_3 = 8(x), 8(−x) + TPPI (t_1); ϕ_4 = x, −x, y, −y;

ϕ_5 =4(x), 4(−x); ϕ_{rec} = 2(x, −x),4(−x, x), 2(−x, x);

Δ'= 3.6 ms, Δ'_1 = 1.4 ms, Δ'_2=2.5 ms, τ_1= 25.6 ms, τ_2= 11.2 ms,

$\xi = 1/(2\Delta\Omega) - 4/\pi * \tau_{\pi/2}(^{13}C_\beta)$.

Fig. 34. Pulse sequences for $(H_\beta)C_\beta(C_\gamma C_\delta C_\epsilon)H_\epsilon$ experiments (a) INEPT based transfer (b) PLUSH-TACSY transfer (for details see text).

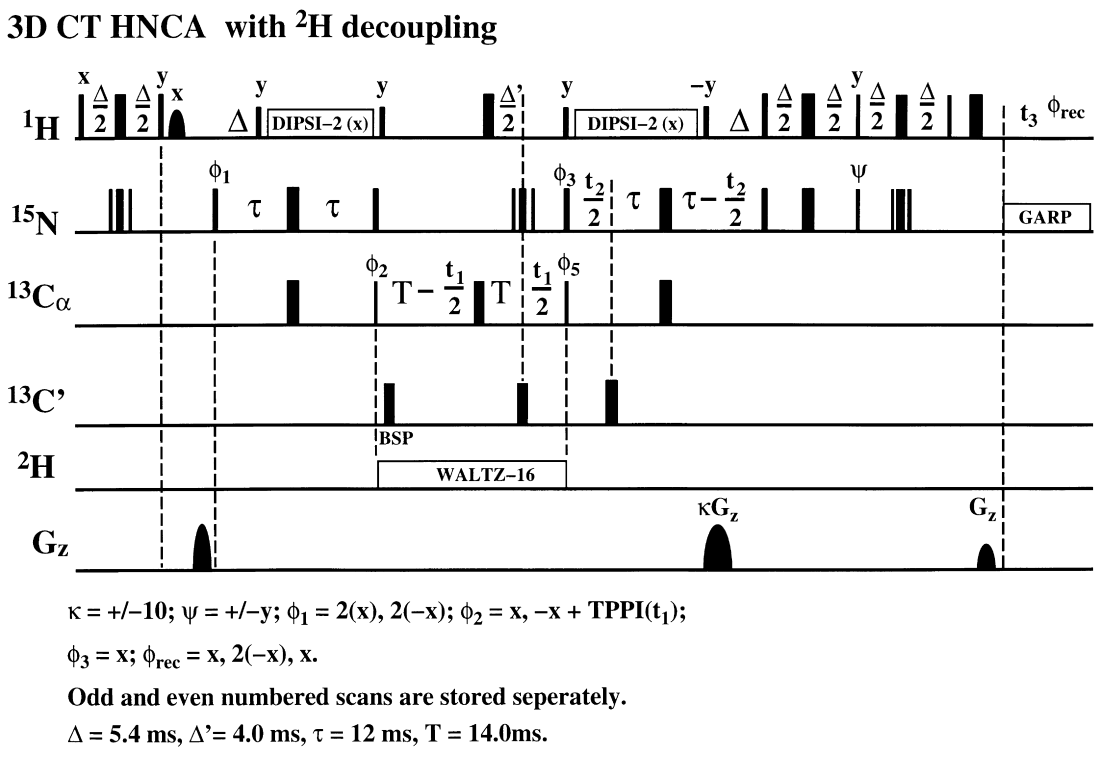

Fig. 35. Sensitivity-enhanced HNCA experiment with constant-time evolution of the $^{13}C_{\alpha}$ chemical shifts. During the constant-time evolution period, the ^{2}H,^{13}C scalar interaction is decoupled by high power ^{2}H decoupling. If applied to a fractionally deuterated protein sample, magnetization of ^{1}H bound $^{13}C_{\alpha}$-spins is purged by the 180° (^{1}H)-pulse applied during the constant-time period.

Although assignment experiments based on this approach yield excellent signal-to-noise, the extraction of structural restraints is limited because of the small number of observable NOEs. Two approaches have been proposed to cope with this problem: (a) selective reintroduction of ^{1}H in positions that yield a considerable number of structural restraints, e.g. selective protonation of hydrophobic amino acids [203–206], or selective protonation of methyl groups [205,207]; (b) the use of random fractional deuteration. A number of triple resonance experiments have been developed using random 75% fractionally deuterated proteins. Clearly, with increasing molecular weight, the deuteration level should be increased to enjoy the best possible gain in signal-to-noise in these assignment experiments [77,88]. In contrast, by using a 50% deuterated protein, all assignment-directed experiments and some of the NOE experiments could be recorded on a single sample, rather than on a set of different samples, which will show different chemical shifts caused by irreproducible sample conditions. The largest ^{2}H isotope shifts are observed for the chemical shifts of the directly bound ^{13}C spins. However, they are usually homogenous and depend mainly on the relevant carbon spin and its ^{2}H multiplicity.

Upon substitution of ^{1}H by ^{2}H, it becomes necessary to decouple the scalar coupling between the heteronucleus and the directly bound ^{2}H (Fig. 35). This is also necessary in order to reduce scalar relaxation of the second kind, because the ^{2}H T_1 relaxation times are rather short for macromolecules. Line broadening through this relaxation mechanism might otherwise compromise the benefits of the reduced dipolar interaction [26]. Experimentally, this decoupling is applied through the ^{2}H lock coil of the probe, by mixing the ^{2}H lock signal and the ^{2}H decoupling channel in an RF mixer, that can be switched via a pulse program command. It is therefore necessary to blank the lock receiver, and it is also recommended to

blank the lock transmitter signal in order to avoid crosstalk of the strong ^{2}H decoupling field (2 kHz) into the lock transmitter. These hardware requirements for ^{2}H decoupling are now commercially available.

Because relaxation times for $^{13}C_\alpha$ spins are dramatically increased as a result of deuteration (e.g. from 16.5 to 130 ms for a 37 kD complex [27]) constant time evolution can be used in many of the previously applied triple resonance experiments. This leads to much improved resolution, which is also desirable for larger proteins, where the increased number of cross peaks give rise to increased signal overlap in the spectra. As an example, the pulse sequence of a sensitivity-enhanced, ^{2}H decoupled, constant-time HNCA experiment [27] is shown in Fig. 35.

6. 3D and 4D NOESY/ROESY experiments

After the assignment of all or nearly all resonances of a protein, experiments for the extraction of structural parameters are analyzed. The most important parameter for NMR-based structure determination are ^{1}H,^{1}H distances which are derived from NOE intensities, and dihedral angles which are obtained from ^3J coupling constants. In this section, we will describe ^{13}C- and ^{15}N-edited NOESY experiments that are used for the measurement of NOE intensities, and experiments for the extraction of intra- and intermolecular NOEs for complexes of labelled and unlabelled molecules. Full coverage of the large number of sequences for measuring coupling constants would require another review. We therefore refer the reader to excellent reviews in the literature [208–211].

6.1. ^{13}C- and ^{15}N-edited NOESY/ROESY experiments

With increasing size of the molecules, overlap of cross peaks becomes a problem for the extraction of NOE intensities and internuclear distances from 2D NOESY spectra. This overlap can be removed by the introduction of additional frequency dimensions [23]. Resolving the NOESY spectrum along a heteronuclear dimension yields a large gain in resolution, while the number of peaks remains constant. The pulse sequence for the ^{15}N edited NOESY experiment (Fig. 36a) is composed of a 2D NOESY and a sensitivity-enhanced HSQC experiment using a heteronuclear gradient echo combined with water-flip-back. The sequence for the 3D ^{13}C edited NOESY experiment (Fig. 36b) is composed of a 2D NOESY and a ^{13}C, ^{1}H-HMQC pulse sequence. If NOEs between aliphatic and aromatic resonances are to be observed in the ^{13}C-edited experiment it is not recommended to use HSQC-type or COS-HSQC transfers. As only two carbon pulses are employed in HMQC based experiments, signal losses as a result of off-resonance effects are minimized in the HMQC implementation. If NOEs to amide protons are to be observed in the ^{13}C-edited NOESY, a sample in H_2O has to be used. For this application a pulse sequence optimized for sensitivity and solvent suppression has been proposed [212].

Cross peak intensities in these experiments do not only depend on the cross-relaxation rate, but also on the transfer amplitude of the heteronuclear correlation step. For accurate quantitation of the NOESY experiment, a HSQC or HMQC spectrum acquired under the same conditions as the NOESY has to be used in order to correct for the individual transfer efficiencies in the heteronuclear correlation step. However, this is not needed if NOE-derived distance restraints are only classified according to weak, medium, strong intensities in the NOESY experiment.

For proteins with more than 100 amino acids, NOESY overlap of cross peaks becomes a problem even in 3D heteronuclear edited NOESY experiments. A first approach to achieve better dispersion of the signals is to record the chemical shift of a second heteronucleus instead of that of the corresponding directly bound proton. This is done in 3D HMQC-NOESY-HMQC experiments and has been proposed for doubly ^{15}N-edited NOESY experiments [213,214]. However, compared to the 3D ^{1}H-edited NOESY experiment, an additional HMQC-step is necessary, which reduces the signal-to-noise ratio.

Much better resolution can be obtained by introducing the second heteronuclear chemical shift axis in addition to the proton chemical shift axis in doubly edited 4D NOESY experiments [215–219]. The most useful experiments are 4D ^{13}C, ^{13}C- and ^{13}C, ^{15}N-edited NOESY experiments. However, as a result of the additional frequency dimension and the longer pulse sequence, these experiments are less sensitive than their three-dimensional analogues. Nevertheless,

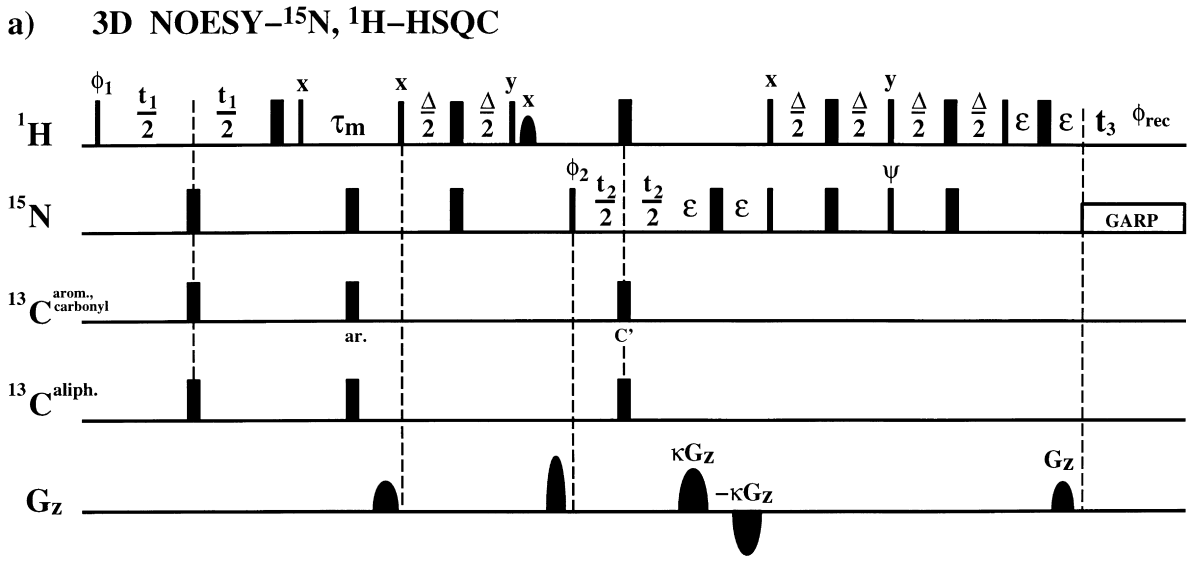

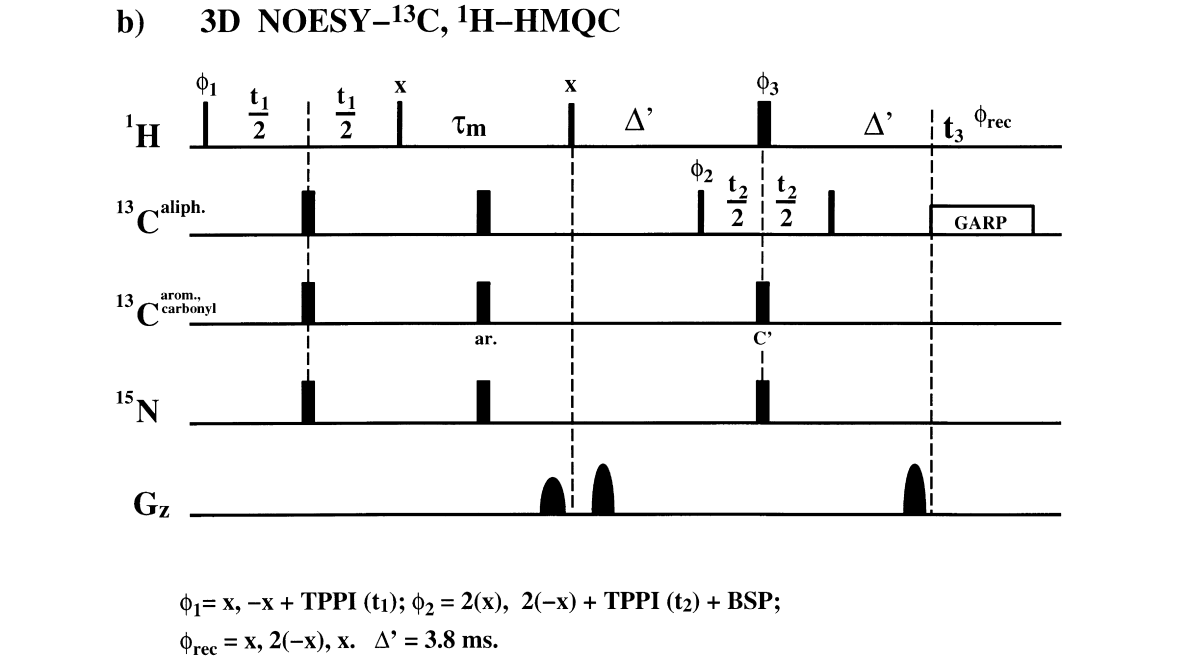

Fig. 36. Pulse sequences for ^{13}C- and ^{15}N-edited NOESY experiments a) 3D NOESY-^{15}N,^{1}H-HSQC with sensitivity enhancement. This experiment is preferably recorded on a ^{15}N labelled sample, in which case the ^{13}C pulses can be omitted. The proton pulse phase $\phi_1 = 45°$ is part of the water-flip-back scheme. (This achieves similar efficiency for the radiation damping during the NOESY mixing time in the two FIDs recorded with and without 90° shifted TPPI phase. (b) The 3D NOESY-^{13}C,^{1}H-HMQC is preferably applied to a D_2O solution of the protein.

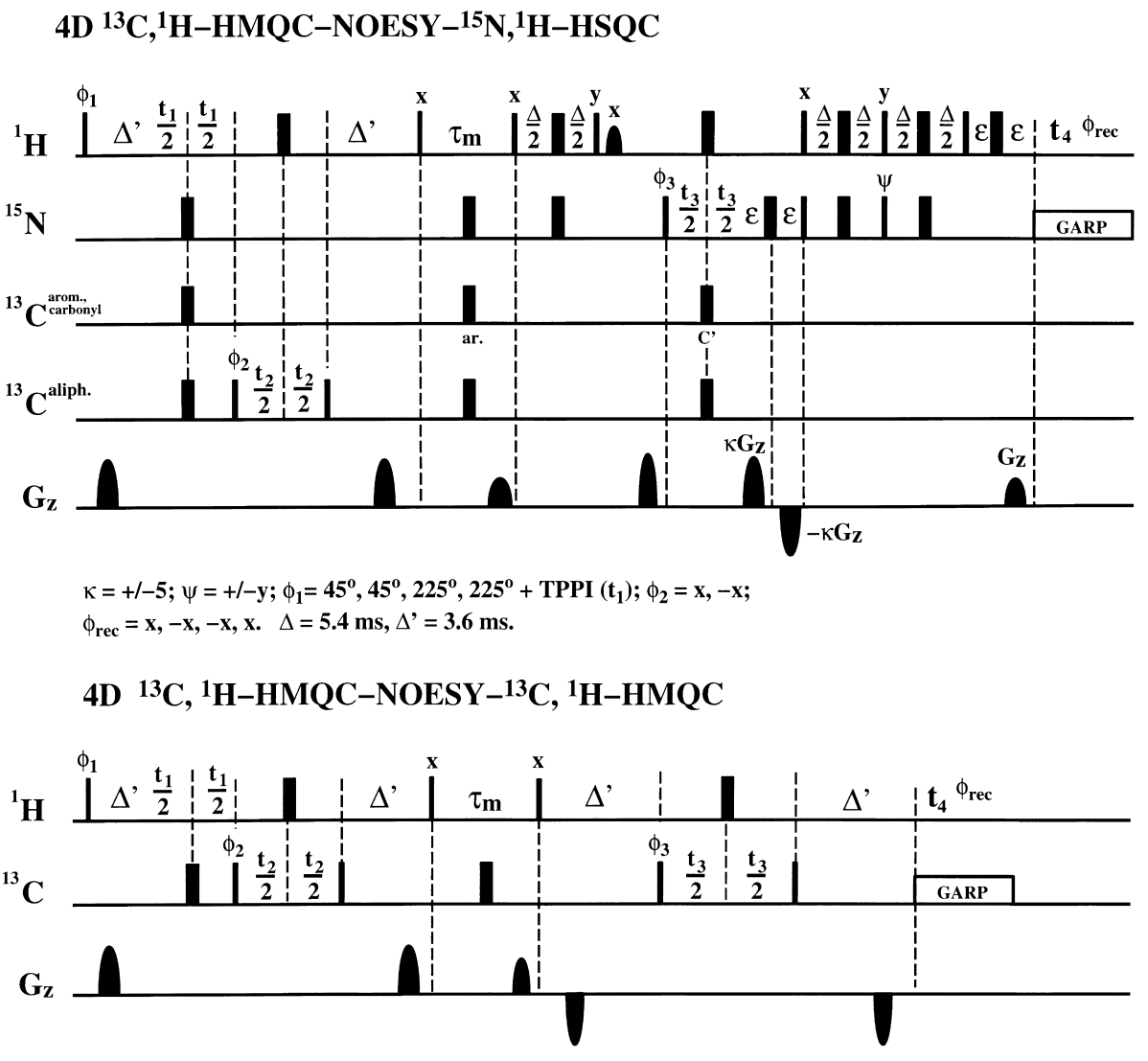

Fig. 37. (a) Sensitivity-enhanced 4D ^{13}C, ^{1}H-HMQC-NOESY-^{15}N, ^{1}H-HSQC experiment and b) 4D ^{13}C, ^{1}H-HMQC-NOESY-^{13}C, ^{1}H-HMQC experiment for the measurement of NOE cross peaks between side-chain protons in uniformly ^{13}C-labelled proteins.

they are useful in combination with the 3D NOESY experiments to unambiguously identify NOE cross peaks. This is especially important during the initial phase of the NOE analysis. In order to achieve sufficient resolution, extensive folding and a limited number of scans are used for each increment of the evolution periods. The length of the phase cycle in these experiments can be kept at a minimum and artifacts suppressed efficiently by the use of pulsed field gradients. The 4D ^{13}C- and ^{15}N-edited NOESY experiment shown in Fig. 37a corresponds to the 3D pulse sequence of Fig. 36a preceded by a ^{13}C, ^{1}H HMQC [219]. As a result of pulse imperfection and the rather short ^{13}C T_2 relaxation times the use of sensitivity enhancement is not recommended for the doubly ^{13}C-edited NOESY experiment. Therefore,

two HMQC experiments are used to evolve ^{13}C chemical shifts (Fig. 37b). A reduced dimensionality 3D $^{13}C/^{15}N$ edited NOESY experiment, that contains a linear combination of the chemical shifts observed in the corresponding 4D experiment, but at much higher digital resolution has also been proposed [220].

Other types of experiments, that yield symmetric cross peak information in heteronuclear edited NOESY experiments are simultaneous [152,221–223] 3D [224] or 4D [225] $^{13}C/^{15}N$ edited experiments. These experiments provide the information from two separate heteronuclear edited experiments in one spectrum. This has a potential sensitivity gain of $\sqrt{2}$. However, simultaneous heteronuclear coherence transfer ($^{1}H \leftrightarrow {}^{15}N$ and $^{1}H \leftrightarrow {}^{13}C$) leads to less than optimal transfer efficiencies: ^{13}C is the faster relaxing spin but has the larger ^{1}J coupling, while ^{15}N spins relax more slowly and have the smaller ^{1}J-coupling. Thus, if the INEPT delay is optimized for ^{13}C, the heteronuclear polarization transfer is not optimum for ^{15}N and vice versa. In addition, the protein has to be dissolved in 90% H_2O, which makes water suppression a more demanding task and the observation of ^{1}H resonances under the water resonance is not easily possible. Therefore, for larger proteins, the use of simultaneous $^{13}C/^{15}N$ edited NOESY experiments cannot be recommended [152].

For 100% $^{2}H,^{15}N$-labelled proteins dissolved in H_2O 4D $^{15}N,^{15}N$-edited experiments have been proposed to obtain H^N,H^N-NOEs, that allow the determination of secondary structure and potentially the global fold of the protein [226–228]. As the overall relaxation times are significantly longer in perdeuterated proteins and spin diffusion pathways into the side-chains are eliminated, the cut-off distance for the observation of NOEs between amide protons is increased. Therefore, potentially many more H^N, H^N distance restraints with increased upper bounds can be derived, which might allow one to obtain the overall fold of the protein. Another approach has recently been proposed where the structurally important NOEs of hydrophobic residues (which are usually located in the core of a protein) can be obtained in combination with deuteration. By incorporation of ^{1}H, ^{13}C, ^{15}N-{Ile, Leu, Val} into a perdeuterated ^{15}N-labelled protein [203,204], or selective ^{1}H-enrichment of methyl groups in an otherwise fully deuterated and uniformly ^{13}C, ^{15}N-labelled protein [205], NOEs for hydrophobic residues are observed in a perdeuterated protein background with much higher sensitivity compared to a fully protonated sample. In combination with the H^N, H^N-NOEs obtained from the experiments described before, an even better definition of the initial fold of a protein can be expected. However, the practical use of these approaches for the structure determination of larger proteins has still to be demonstrated.

A ^{13}C-edited ROESY-HMQC experiment has been proposed to obtain stereospecific assignments for C_β methylene protons in larger proteins [229]. As the ROE is positive for all molecular tumbling correlation times τ_C [230], indirect ROE contributions (''spin diffusion'' peaks), with one intermediate spin have opposite sign relative to direct ROE effects. Also, for even numbers of intermediate spins, positive and negative spin diffusion contributions almost cancel, so that the ROEs observed with relatively long mixing times closely represent the internuclear distances, even for larger proteins. For optimum sensitivity, the mixing time should be in the range of the spin-locked relaxation time $T_{1\rho}$. As ROE cross peaks have opposite signs compared to exchange peaks and NOE cross peaks in slow tumbling molecules, a ^{15}N-edited ROESY experiment can be used to identify ROE peaks between amide protons and H_2O molecules that are bound to a protein [231].

However, for larger proteins, spin-locked experiments, especially when combined with a heteronuclear correlation experiment, usually have poor signal-to-noise, as a result of the fast T_2 and $T_{1\rho}$ relaxation rates. As the relaxation rate of ^{13}C, ^{1}H two-spin-coherence is much slower for IS spin systems, than the corresponding relaxation rate of the individual ^{13}C or ^{1}H single quantum coherences [162], HMQC-type experiments are advantageous compared to HSQC-type heteronuclear correlation experiments (see Section 3.6). In order to avoid dephasing of the two-spin coherence caused by additional ^{1}H, ^{1}H J-couplings the multiple quantum coherence is spin-locked [232]. Using this technique, considerable sensitivity improvements have been observed in ^{1}H spin-locked ROESY-CT-HMQC experiments compared to ROESY-CT-HSQC experiments. A pulse sequence for the spin-locked 3D ROESY-CT-HMQC experiment is shown in Fig. 38.

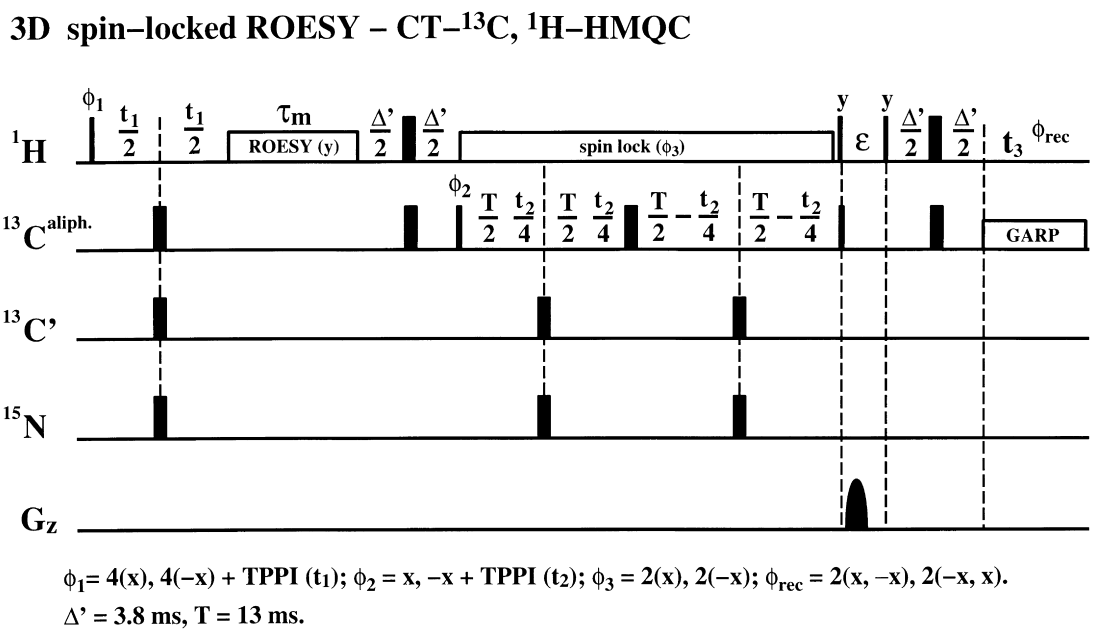

Fig. 38. Pulse sequence for a 3D spin-locked ROESY-CT-^{13}C,^{1}H-HMQC experiment.

6.2. Filtered experiments for complexes of labelled and unlabelled molecules

To understand the function of biological macromolecules, it is important to elucidate the molecular interactions between these molecules. For studying the structures of molecular complexes or oligomeric proteins, it is therefore necessary to be able to distinguish between intra- and intermolecular NOEs. This can be accomplished by heteronuclear filtered NOE experiments performed on a sample of the complex consisting of differentially labelled molecules. In the example of a binary complex consisting of a ^{13}C-,^{15}N-labelled molecule (e.g. protein A) and an unlabelled molecule (peptide B), four kinds of NOE cross peaks can be observed [20,21, 233,234]:

intramolecular

$A \leftrightarrow A$ ^{1}H-(^{13}C, ^{15}N) $\leftrightarrow$ ^{1}H-(^{13}C, ^{15}N)

$B \leftrightarrow B$ ^{1}H-(^{12}C, ^{14}N) $\leftrightarrow$ ^{1}H-(^{12}C, ^{14}N)

intermolecular :

$A \leftrightarrow B$ ^{1}H-(^{13}C, ^{15}N) $\leftrightarrow$ ^{1}H-(^{12}C, ^{14}N)

$B \leftrightarrow A$ ^{1}H-(^{12}C, ^{14}N) $\leftrightarrow$ ^{1}H-(^{13}C, ^{15}N)

The connectivity of protons to the heteronuclei ^{13}C and ^{15}N can therefore be used to separate intra- and intermolecular NOEs and the intramolecular NOEs of A and B. While suppression of ^{12}C-,^{14}N-bound protons is easily achieved by selecting for ^{13}C-,^{15}N-bound protons, complete suppression of ^{13}C-,^{15}N-bound protons is more challenging, because of the variable size of the ^{1}J couplings. Two implementations of filter building blocks to achieve the latter task have been described [162,235–242], that are designed to either select or suppress magnetization of heteronucleus-bound protons. In both pulse sequences of Fig. 39, the degree of suppression of the undesired terms is a product of two cosine terms, and the building blocks are therefore called ''*J* filters of second order''. Whereas the sequence in Fig. 39a achieves the suppression by scaling the transfer amplitude by a factor $\cos(\pi J\Delta')\cos(\pi J\Delta'')$,

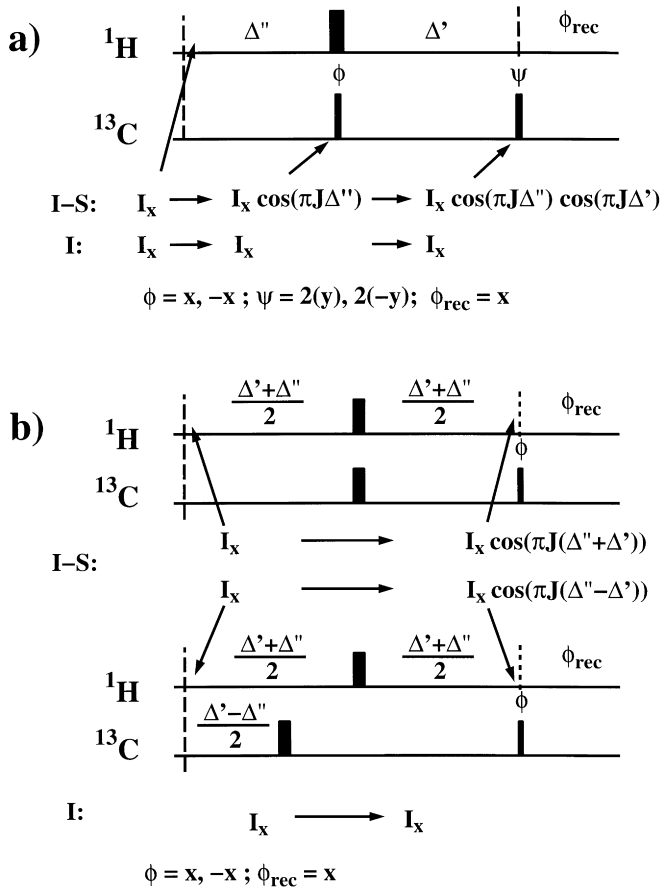

Fig. 39. Implementations of a ''second order *J* filter'' for the suppression of heteronucleus-bound protons. In both cases, the degree of suppression is given by: $\cos(\pi J\Delta')\cos(\pi J\Delta'')$. (a) Two 90°(S) pulses applied after evolution of the IS-coupling achieve suppression of the undesired signals in each scan, provided the heteronuclear antiphase coherence generated cannot be converted into observable coherence by the rest of the pulse sequence. (b) Addition of two scans with 180°(S) pulses at times $(\Delta' + \Delta'')/2$ and $(\Delta' - \Delta'')/2$ results in suppression of the S-bound protons. The filter function is identical to (a), but suppression is only achieved within two scans. For $\Delta' = \Delta''$, the sequence corresponds to a first order *J*-filter.

the sequence in Fig. 39b yields in two scans the sum of the transfer efficiencies: $\cos(\pi J(\Delta' + \Delta'')) + \cos(\pi J(\Delta' - \Delta''))$ which is equivalent to the initial transfer because of the equality:

$$\cos(\pi J\Delta')\cos(\pi J\Delta'') = \tfrac{1}{2}\{\cos(\pi J(\Delta' + \Delta'')) + \cos(\pi J(\Delta' - \Delta''))\} \quad (28)$$

The advantage of these filters, compared to ''first order *J* filters'' is that the suppression of *S*-bound *I* magnetization is efficient for a larger range of *J* values.

The sequence depicted in Fig. 39a achieves suppression of *S*-bound *I* magnetization in each scan, because the antiphase operator $2I_yS_z$ present after Δ' or Δ' is turned into heteronuclear zero- and double quanta by 90°(*S*) pulses, which are not transformed into observable magnetization if the pulse sequence is designed accordingly. Otherwise, a phase cycle on phases ϕ and ψ is needed. The sequence shown in Fig. 39b [243] also constitutes a second order *J* filter after addition of two scans, if the 180°(*S*) pulse is applied at time $(\Delta' + \Delta'')/2$ in the first and at time $(\Delta' - \Delta'')/2$ in the second scan (cf. Eq. (28)).

Alternatively, the 180°(*S*) pulse can be applied at

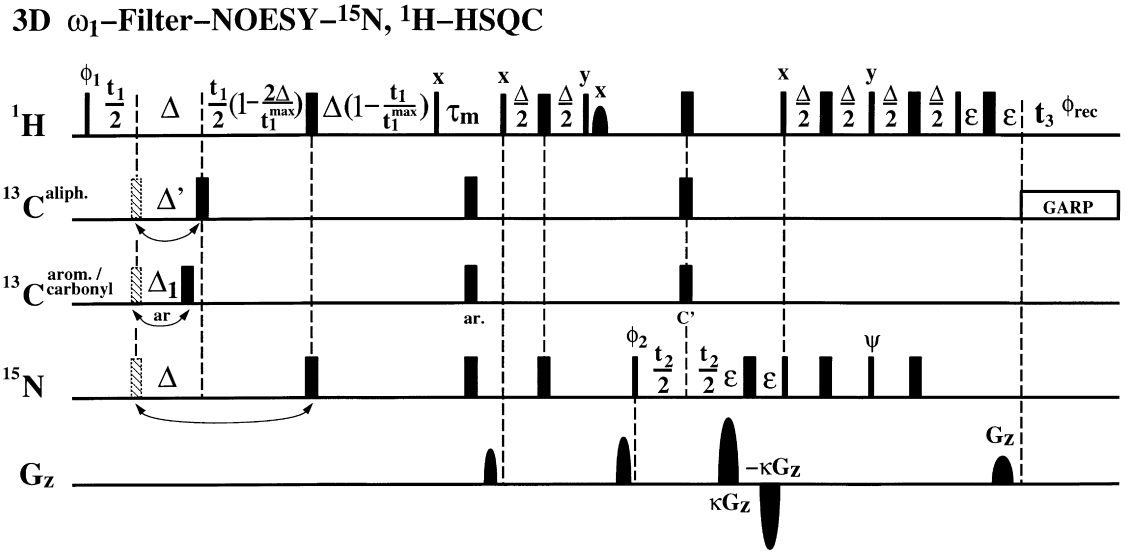

Fig. 40. Pulse sequence for a 3D ω_1-filtered NOESY-^{15}N,^{1}H-HSQC using first order J filters according to Fig. 39b.

the beginning and in the middle of a delay $1/J$ in every other transient (jumping 180°(S) pulse), so that evolution of heteronuclear coupling inverts the signal of S-bound I spins in every other transient. This corresponds to a 1st order J filter only, but has the advantage that separate spectra for I nuclei bound and not bound to S spins can be generated, if the two FIDs with different timing of the 180°(S) pulse are stored separately. This is illustrated with a 3D ω_1-filtered NOESY-^{15}N, ^{1}H-HSQC experiment in Fig. 40. The jumping 180°(S) pulses refocus J_{IS} during t_1. S is $^{13}C^{aliph}$, $^{13}C^{arom}$, and ^{15}N. The heteronuclear first order filters are implemented according to Fig. 39b, with the delays chosen to suppress aliphatic and aromatic protons and H^N protons. Transients are stored separately for the two positions of the jumping 180°(S) pulses of the filters, in order to separate the inter- and intramolecular NOEs. This can in principle be done independently for the aromatic ^{13}C, aliphatic ^{13}C and ^{15}N nuclei and would allow the correspondingly edited subspectra to be obtained. A semi-constant-time evolution is implemented for t_1 in order to utilize the filter delay 2Δ for chemical shift evolution.

If one is only interested in suppressing the ^{13}C and ^{15}N bound protons the pulse sequence in Fig. 41a can be used. Here first order filters are implemented for amide and aromatic protons, while a second order filter is used to suppress ^{13}C-bound aliphatic protons. The suppression is achieved in a single scan corresponding to Fig. 39a. The filter element is combined with efficient water suppression using a WATERGATE sequence with a 3-9-19 proton 180° pulse. Therefore, on a sample dissolved in water, the pulse sequence Fig. 41a will allow NOEs to be observed between a doubly labelled protein and an unlabelled peptide simultaneously with all the intra-peptide NOEs, since no filtering is applied in the ω_1 dimension. In order to observe NOEs only between the labelled protein and an unlabelled ligand heteronuclear editing has to be applied in the ω_1 dimension. For that purpose, the 3D ω_1-^{13}C-edited, ω_2-^{13}C, ^{15}N-filtered NOESY experiment shown in Fig. 41b is recommended.

Recent improvements of heteronuclear filter experiments consist of the use of frequency-swept adiabatic pulses to optimize ^{13}C-filtering. Owing to the wide range of $^{1}J_{C,H}$-couplings and the large spectral width of ^{13}C chemical shifts it is very difficult to suppress all ^{13}C-bound protons simultaneously in ^{13}C-filtered experiments. As an alternative to treating the different ^{13}C-chemical shift ranges (i.e. aliphatic,

a) 2D NOESY–ω_2–^{13}C,^{15}N–filter with watergate

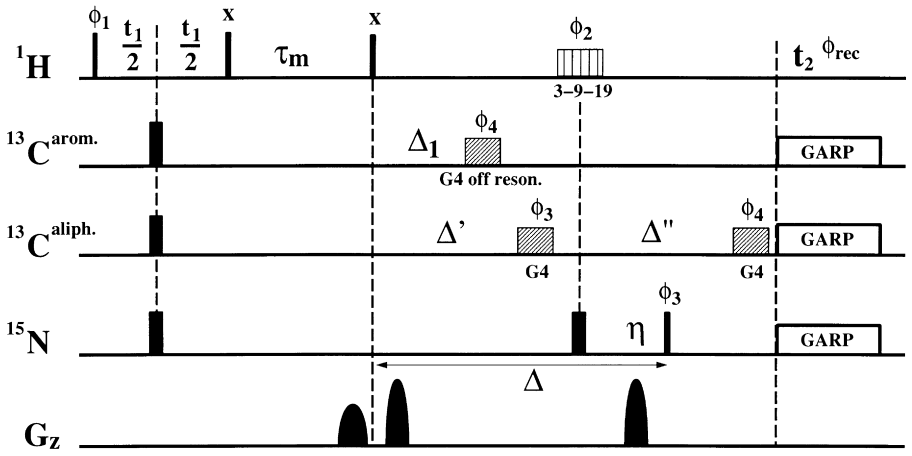

ϕ_1= 45°, 225° + TPPI (t_1); ϕ_2 = 2(x), 2(y); ϕ_3 = 4(x), 4(–x); ϕ_4 = 8(y), 8(–y);
ϕ_{rec} = x, 2(–x), x.
Δ = 5.4 ms; Δ' = 3.5 ms; Δ" = 4.0 ms, Δ_1 = 3.1 ms; τ_P (G4) = 400 μs.

b) 3D–ω_2–^{13}C–edited, ω_3–^{13}C,^{15}N–filtered NOESY with watergate

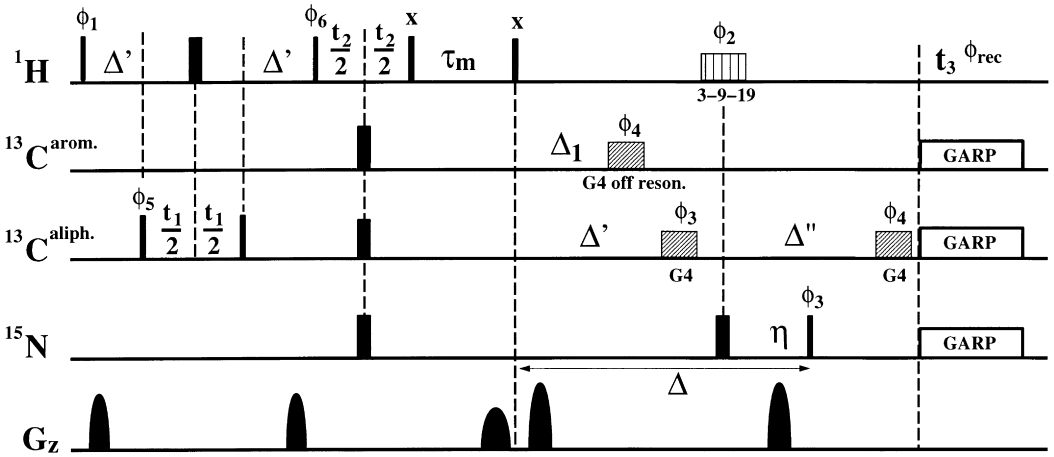

ϕ_1=x + TPPI (t_2); ϕ_2 = 2(x), 2(y); ϕ_3 = 4(x), 4(–x); ϕ_4 = 8(y), 8(–y);
ϕ_5 =x, –x + TPPI (t_1); ϕ_6 = x + TPPI (t_2); ϕ_{rec} = x, 2(–x), x.
Δ = 5.4 ms; Δ' = 3.5 ms; Δ" = 4.0 ms, Δ_1 = 3.1 ms; τ_P (G4) = 400 μs.

Fig. 41. (a) 2D ω_2-^{13}C,^{15}N-filtered WATERGATE NOESY. First and second order filters are combined with WATERGATE for solvent suppression. (b) 3D ω_2-^{13}C-edited, ω_3-^{13}C,^{15}N-filtered NOESY experiment to exclusively observe NOE cross peaks between e.g. a labelled protein and an unlabelled ligand.

aromatic) as separate frequency bands by application of band-selective pulses, the full ^{13}C chemical shift range can be covered by the use of adiabatic pulses. The frequency sweep in these adiabatic pulses can then be adjusted according to the approximate linearity of ^{13}C chemical shifts and the corresponding $^{1}J_{C,H}$-couplings to achieve greatly improved heteronuclear filters [113,114].

7. Conclusions

The intention of this review was to summarize and evaluate the numerous triple resonance pulse sequences that have been introduced since 1989 for the assignment of doubly (^{13}C, ^{15}N) or triply (^{13}C, ^{15}N, ^{2}H)-labelled proteins and the extraction of intra- and intermolecular distance restraints from NOESY experiments. Special attention has been given to the detailed discussion of optimized pulse sequences rather than to list all possible implementations without comment. A typical set of NMR experiments which are required for the structure determination of a protein or protein complex is given in Table 1 (Section 2). To facilitate the use of these NMR experiments pulse programs (in Bruker DRX format) are available via internet from http://www.NMR.EMBL-Heidelberg.de. Section 2 is dedicated to the comparison of different homo- and heteronuclear assignment strategies and explaining which experiments to use for a certain step during the assignment process. Section 3 is focused on the discussion of basic building blocks of triple resonance experiments and on the use of special techniques for optimization of solvent and artifact suppression, especially the combination of pulsed field gradients with water-flip-back. In Sections 4 and 5 experiments for assigning backbone and side-chain resonances are reviewed and the modifications of the pulse sequences that are required for application to ^{2}H-labelled samples in order to study proteins with molecular weights above 25 kD are discussed. Section 6 is concerned with three- and four-dimensional heteronuclear NOESY experiments which are critical for the extraction of NOE-based proton/proton distance restraints.

For the discussion of NMR experiments for the determination of *J*-couplings which are important for defining local conformations from backbone and side-chain dihedral angles, we refer to comprehensive reviews that have been published on these topics recently [208–211].

Although the experiments and strategies for the structure determination of larger proteins by heteronuclear multidimensional NMR spectroscopy are now fairly optimized, it is still necessary to further develop tools to automate the tedious assignment process. A number of programs have been introduced for the semi- or fully-automated assignment of protein backbone resonances [178–182]. More importantly, computational strategies have been designed to allow for automated assignments of NOESY cross peaks based on existing chemical shift assignments [244–246]. Although these protocols work well for smaller proteins ($<$100 residues) there is still need for improvements in their application to larger and more complex systems.

Finally, we could only briefly mention the new methodological developments based on residual dipolar couplings and cross-correlated relaxation effects that hold promise to provide additional, and truly long range restraints for the structure determination of biomolecules in solution. These exciting new developments indicate that biomolecular NMR spectroscopy is still at a stage where significant methodological improvements can be expected and promise to push the limits of biological systems capable of being studied by NMR even further.

Acknowledgements

This work was supported by the Fonds der Chemischen Industrie and the DFG and is mainly based on the results of two Ph.D. theses (M.S. and J.S.). We would like to thank numerous people for valuable discussions and contributions to this article: Dr. H. Schwalbe, M. Maurer, PD Dr. S. Glaser, Dr. T. Carlomagno, Dr. H. Försterling (University Frankfurt, Germany); Dr. E.T. Olejniczak, Dr. L. Yu, Dr. S.W. Fesik (Abbott Labs, USA), Dr. H. Kovacs (EMBL Heidelberg, Germany). We would also like to thank Dr. W. Bermel, Dr. R. Kerssebaum and Dr. T. Keller (Bruker, Germany) for valuable discussions and continuous support. Most of the pulse sequences and spectra shown were implemented and recorded at the EU-supported Large Scale Facility for Biomolecular NMR at the University of Frankfurt.

References

[1] C. Griesinger, O.W. Sørensen , R.R. Ernst, J. Magn. Reson. 73 (1987) 574.
[2] G.W. Vuister, R. Boelens, R. Kaptein, J. Magn. Reson. 80 (1988) 176.
[3] C. Griesinger, O.W. Sørensen, R.R. Ernst, J. Magn. Reson. 84 (1989) 14.
[4] L.E. Kay, G.M. Clore, A. Bax, A.M. Gronenborn, Science 249 (1990) 411.
[5] R.R. Ernst, Angew. Chem. 104 (1992) 817.
[6] L.P. McIntosh, R.H. Griffey, D.C. Muchmore, C.P. Nielson, A.G. Redfield, F.W. Dahlquist, Proc. Natl. Acad. Sci. 84 (1984) 1244.
[7] R.H. Griffey, R.E. Loomis, A.G. Redfield, L.P. McIntosh, T.G. Oas, F.W. Dahlquist, J. Am. Chem. Soc. 108 (1986) 6816.
[8] L.P. McIntosh, F.W. Dahlquist, A.G. Redfield, J. Biomol. Struct. Dyn. 5 (1987) 21.
[9] B.H. Oh, W.M. Westler, P. Derba, J.L. Markley, Science 240 (1988) 90 821.
[10] W.M. Westler, B.J. Stockman, J.L. Markley, Y. Hosoya, Y. Miyake, M. Kainosho, J. Am. Chem. Soc. 110 (1988) 6256.
[11] B.J. Stockman, M.D. Reilly, W.M. Westler, E.L. Ulrich, J.L. Markley, Biochemistry 28 (1989) 230.
[12] D.C. Muchmore, L.P. McIntosh, C.B. Russell, D.E. Anderson, F.W. Dahlquist, Methods Enzymol. 177 (1989) 44.
[13] R.A. Venters, T.L. Calderone, L.D. Spicer, C.A. Fierke, Biochemistry 30 (1991) 4491.
[14] A.P. Hansen, A.M. Petros, A.P. Mazar, T.M. Pederson, A. Rueter, S.W. Fesik, Biochemistry 31 (1992) 12713.
[15] T. Kigawa, Y. Muto, S. Yokoyama, J. Biomol. NMR 6 (1995) 129.
[16] J.W. Lustbader, S. Birken, S. Pollak, A. Pound, B.T. Chait, U.A. Mirza, S. Ramnarain, R.E. Canfield, J.M. Brown, J. Biomol. NMR 7 (1996) 295.
[17] R.H. Fogh, D. Schipper, R. Boelens, R. Kaptein, J. Biomol. NMR 4 (1994) 123.
[18] M.L. Remerowski, T. Domke, A. Groenewegen, H.A.M. Pepermans, C.W. Hilbers, F.J.M. van de Ven, J. Biomol. NMR 4 (1994) 257.
[19] G.M. Clore, A.M. Gronenborn, Science 252 (1991) 1390.
[20] C. Weber, G. Wider, B. von Freyberg, R. Traber, W. Braun, H. Widmer, K. Wüthrich, Biochemistry 30 (1991) 6563.
[21] S.W. Fesik, R.T.J. Gampe, H L. Eaton, G. Gemmecker, E.T. Olejniczak, P. Neri, T.F. Holzman, D.A. Egan, R. Edalji, R. Simmer, R. Helfrich, J. Hochlowski, M. Jackson, Biochemistry 30 (1991) 6574.
[22] M. Ikura, G.M. Clore, A.M. Gronenborn, G. Zhu, C.B. Klee, A. Bax, Science 256 (1992) 633.
[23] S.W. Fesik, E.R.P. Zuiderweg, J. Magn Reson. 78 (1988) 588.
[24] K. Wüthrich, NMR of Proteins and Nucleic Acids, Wiley-Interscience, New York, 1986.
[25] M. Ikura, L.E. Kay, A. Bax, Biochemistry 29 (1990) 4659.
[26] S. Grzesiek, J. Anglister, H. Ren, A. Bax, J. Am. Chem. Soc. 115 (1993) 4369.
[27] T. Yamazaki, W. Lee, M. Revington, D.L. Mattiello, F.W. Dahlquist, C.H. Arrowsmith, L.E. Kay, J. Am. Chem. Soc. 116 (1994) 6464.
[28] S.B. Shuker, P.J. Hajduk, R.P. Meadows, S.W. Fesik, Science 274 (1996) 1531.
[29] P.J. Hajduk, R.P. Meadows, S.W. Fesik, Science 278 (1997) 497.
[30] J.R. Tolman, J.M. Flanagan, M.A. Kennedy, J.H. Prestegard, Nature Struct. Biol. 4 (1997) 292.
[31] N. Tjandra, J.G. Omichinski, A.M. Gronenborn, G.M. Clore, A. Bax, Nature Struct. Biol. 4 (1997) 732.
[32] N. Tjandra, A. Bax, Science 278 (1997) 1111.
[33] B. Reif, M. Hennig, C. Griesinger, Science 276 (1997) 1230.
[34] K. Pervushin, R. Riek, G. Wider, K. Wüthrich, Proc. Natl. Acad. Sci. 94 (1997) 12366.
[35] D. Marion, P.C. Driscoll, L.E. Kay, P.T. Wingfield, A. Bax, A.M. Gronenborn, G. M. Clore, Biochemistry 28 (1989) 6150.
[36] S.S. Wijmenga, K. Hallenga, C.W. Hilbers, J. Magn. Reson. 84 (1989) 634.
[37] P.C. Driscoll, G.M. Clore, D. Marion, P.T. Wingfield, A.M. Gronenborn, Biochemistry 29 (1990) 3542.
[38] P.C. Driscoll, A.M. Gronenborn, P.T. Wingfield, G.M. Clore, Biochemistry 29 (1990) 4668.
[39] K. Shon, S.J. Opella, J. Magn. Reson. 82 (1989) 193.
[40] D. Marion, L.E. Kay, S.W. Sparks, D.A. Torchia, A. Bax, J. Am. Chem. Soc. 111 (1989) 1515.
[41] E.R.P. Zuiderweg, S.W. Fesik, Biochemistry 28 (1989) 2387.
[42] M. Ikura, L.E. Kay, R. Tschudin, A. Bax, J. Magn. Reson. 86 (1990) 204.
[43] E.R.P. Zuiderweg, L.P. McIntosh, F.W. Dahlquist, S. W. Fesik, J. Magn. Reson. 86 (1990) 210.
[44] S.J. Archer, M. Ikura, D.A. Torchia, A. Bax, J. Magn. Reson. 95 (1991) 636.
[45] L.E. Kay, M. Ikura, R. Tschudin, A. Bax, J. Magn. Reson. 89 (1990) 496.
[46] L.E. Kay, M. Ikura, G. Zhu, A. Bax, J. Magn. Reson. 91 (1991) 422.
[47] R. Powers, A.M. Gronenborn, G.M. Clore, A. Bax, J. Magn. Reson. 94 (1991) 209.
[48] S. Grzesiek, A. Bax, J. Magn. Reson. 96 (1992) 432.
[49] L.E. Kay, M. Wittekind, M.A. McCoy, M.S. Friedrichs, L. Müller, J. Magn. Reson. 98 (1992) 443.
[50] W. Boucher, E.D. Laue, S. Campbell-Burk, P.J. Domaille, J. Am. Chem. Soc. 114 (1992) 2262.
[51] W. Boucher, E.D. Laue, S.L. Campbell-Burk, P.J. Domaille, J. Biomol. NMR 2 (1992) 631.
[52] L.E. Kay, M. Ikura, A. Bax, J. Magn. Reson. 91 (1991) 84.
[53] R.T. Clubb, V. Thanabal, G. Wagner, J. Biomol. NMR 2 (1992) 203.
[54] R. Weisemann, H. Rüterjans, W. Bermel, J. Biomol. NMR 3 (1993) 113.
[55] R.T. Clubb, V. Thanabal, G. Wagner, J. Magn. Reson. 97 (1992) 213.
[56] J. Engelke, H. Rüterjans, J. Magn. Reson. B109 (1995) 318.
[57] S. Seip, J. Balbach, H. Kessler, J. Biomol. NMR 3 (1993) 233.

[58] S. Grzesiek, A. Bax, J. Am. Chem. Soc. 114 (1992) 6291.
[59] S. Grzesiek, A. Bax, J. Magn. Reson. 99 (1992) 201.
[60] M. Wittekind, L. Müller, J. Magn. Reson. B101 (1993) 201.
[61] S. Grzesiek, A. Bax, J. Biomol. NMR 3 (1993) 185.
[62] G.T. Montelione, B.A. Lyons, S.D. Emerson, M. Tashiro, J. Am. Chem. Soc. 114 (1992) 10974.
[63] S. Grzesiek, J. Anglister, A. Bax, J. Magn. Reson. B101 (1993) 114.
[64] B.A. Lyons, G.T. Montelione, J. Magn. Reson. B101 (1993) 206.
[65] T.M. Logan, E.T. Olejniczak, R.X. Xu, S.W. Fesik, J. Biomol. NMR 3 (1993) 225.
[66] J.M. Richardson, R.T. Clowes, W. Boucher, P.J. Domaille, C.H. Hardman, J. Keeler, E.D. Laue, J. Magn. Reson. B101 (1993) 223.
[67] R.T. Clowes, W. Boucher, C.H. Hardman, P.J. Domaille, E.D. Laue, J. Biomol. NMR 3 (1993) 349.
[68] A. Bax, G.M. Clore, P.C. Driscoll, A.M. Gronenborn, M. Ikura, L.E. Kay, J. Magn. Reson. 87 (1990) 620.
[69] M. Ikura, L.E. Kay, A. Bax, J. Biomol. NMR 1 (1991) 299.
[70] S.W. Fesik, H.L. Eaton, E.T. Olejniczak, E.R.P. Zuiderweg, L.P. McIntosh, F.W. Dahlquist, J. Am. Chem. Soc. 112 (1990) 886.
[71] A. Bax, G.M. Clore, A.M. Gronenborn, J. Magn. Reson. 88 (1990) 425.
[72] A. Majumdar, H. Wang, R.C. Morshauser, E.R.P. Zuiderweg, J. Biomol. NMR 3 (1993) 387.
[73] E.T. Olejniczak, R.X. Xu, S.W. Fesik, J. Biomol. NMR 2 (1992) 655.
[74] D.M. LeMaster, F.M. Richards, Biochemistry 27 (1988) 142.
[75] C.K. Brush, M.P. Stone, T.M. Harris, Biochemistry 27 (1988) 115.
[76] B.T. Farmer II, R.A. Venters, J. Am. Chem. Soc. 117 (1995) 4187.
[77] D. Nietlispach, R.T. Clowes, R.W. Broadhurst, Y. Ito, J. Keeler, M. Kelly, J. Asthurst, H. Oschkinat, P.J. Domaille, E.D. Laue, J. Am. Chem. Soc. 118 (1996) 407.
[78] T. Szyperski, G. Wider, J.H. Bushweller, K. Wüthrich, J. Biomol. NMR (1993) 3127–3132.
[79] T. Szyperski, G. Wider, J.H. Bushweller, K. Wüthrich, J. Am. Chem. Soc. 115 (1993) 9307.
[80] T. Szyperski, M.W. Pellecchia, J. Magn. Reson B105 (1994) 188.
[81] J.-P. Simorre, B. Brutscher, M.S. Caffrey, D. Marion, J. Biomol. NMR 4 (1994) 325.
[82] B. Brutscher, J.-P. Simorre, M.S. Caffrey, D. Marion, J. Magn. Reson. B105 (1994) 77.
[83] E.T. Olejniczak, S.W. Fesik, J. Am. Chem. Soc. 116 (1994) 2215.
[84] M. Wittekind, W.J. Metzler, L. Müller, J. Magn. Reson. B101 (1993) 214.
[85] K. Gehring, E. Guittet, J. Magn. Reson. B109 (1995) 206.
[86] B.T. Farmer II, T.B. Lavoie, L. Müller, W.J. Metzler, J. Magn. Reson. B107 (1995) 197.
[87] J.L. Sudmeier, E.L. Ash, U.L. Günther, X. Luo, P.A. Bullock, W.W. Bachovchin, J. Magn. Reson. B113 (1996) 236.
[88] T. Yamazaki, M. Yoshida, K. Nagayama, Biochemistry 32 (1993) 5656.
[89] H. Vis, R. Boelens, M. Mariani, R. Stroop, C.E. Vorgius, K.S. Wilson, R. Kaptein, Biochemistry 33 (1994) 14858.
[90] M. Pellecchia, H. Iwai, T. Szyperski, K. Wüthrich, J. Magn. Reson. 124 (1997) 274.
[91] V. Dötsch, R.E. Oswald, G. Wagner, J. Magn. Reson. B110 (1996) 107.
[92] L.P. McIntosh, E. Brun, L.E. Kay, J. Biomol. NMR 9 (1997) 306.
[93] T. Yamazaki, S.M. Pascal, A.U. Singer, J.D. Forman-Kay, L.E. Kay, J. Am. Chem. Soc. 117 (1995) 3556.
[94] N.S. Rao, P. Legault, D.R. Muhandiram, J. Greenblatt, J.L. Battiste, J.R. Williamson, L.E. Kay, J. Magn. Reson. B113 (1996) 272.
[95] B.T. Farmer II, R.A. Venters, J. Biomol. NMR 7 (1996) 59.
[96] M. Pellecchia, G. Wider, H. Iwai, K. Wüthrich, J. Biomol. NMR 10 (1997) 193.
[97] L. Szilagyi, O. Jardetzky, J. Magn. Reson. 83 (1989) 441.
[98] A. Pastore, V. Saudek, J. Magn. Reson. 90 (1990) 165.
[99] D.S. Wishart, B.D. Sykes, F.M. Richards, J. Mol. Biol. 222 (1991) 311.
[100] S. Spera, A. Bax, J. Am. Chem. Soc. 113 (1991) 5490.
[101] D.S. Wishart, B.D. Sykes, F.M. Richards, Biochemistry 31 (1992) 1647.
[102] D.S. Wishart, B.D. Sykes, J. Biomol. NMR 4 (1994) 171.
[103] J. Kuszeweski, J. Qin, A.M. Gronenborn, G.M. Clore, J. Magn. Reson. B106 (1995) 92.
[104] J. Kuszeweski, J. Qin, A.M. Gronenborn, G.M. Clore, J. Magn. Reson. B107 (1995) 293.
[105] P. Luginbühl, T. Szyperski, K. Wüthrich, J. Magn. Reson. B109 (1995) 229.
[106] R.R. Ernst, G. Bodenhausen, A. Wokaun, Principles of Nuclear Magnetic Resonance in One and Two Dimensions, Clarendon Press, Oxford, 1987.
[107] L. Emsley, G. Bodenhausen, Chem. Phys. Lett. 165 (1990) 469.
[108] H. Geen, R. Freeman, J. Magn. Reson. 93 (1991) 93.
[109] R. Freeman, Chem. Rev. 91 (1991) 1397.
[110] J. Baum, R. Tycko, A. Pines, Phys. Rev. A32 (1985) 3435.
[111] R. Fu, G. Bodenhausen, Chem. Phys. Lett. 245 (1995) 415.
[112] E. Kupce, R. Freeman, J. Magn. Reson. A117 (1995) 246.
[113] C. Zwahlen, P. Legault, S.J.F. Vincent, J. Greenblatt, R. Konrat, L.E. Kay, J. Am. Chem. Soc. 119 (1997) 6711.
[114] E. Kupce, R. Freeman, J. Magn. Reson. 127 (1997) 36.
[115] L. Emsley, G. Bodenhausen, Chem. Phys. Lett. 168 (1990) 297.
[116] M.A. McCoy, L. Müller, J. Magn. Reson. 99 (1992) 18.
[117] E.R.P. Zuiderweg, S.W. Fesik, J. Magn. Reson. 93 (1991) 653.
[118] M.A. McCoy, L. Müller, J. Am. Chem. Soc. 114 (1992) 2108.
[119] U. Eggenberger, P. Schmidt, M. Sattler, S.J. Glaser, C. Griesinger, J. Magn. Reson. 100 (1992) 604.
[120] M.A. McCoy, L. Müller, J. Magn. Reson. A101 (1993) 122.
[121] M.A. McCoy, L. Müller, J. Magn. Reson. 98 (1992) 674.
[122] F. Bloch, A. Siegert, Phys. Rev. 57 (1940) 522.
[123] N. F. Ramsey, Phys. Rev. 100 (1955) 1191.

[124] R.L. Vold, J.S. Waugh, M.P. Klein, D.E. Phelps, J. Chem. Phys. 48 (1968) 3831.
[125] R.E. Hurd, J. Magn. Reson. 87 (1990) 422.
[126] R.E. Hurd, B.K. John, J. Magn. Reson. 91 (1990) 648.
[127] G.W. Vuister, R. Boelens, R. Kaptein, R.E. Hurd, B.K. John, P.C.M. Van Zijl, J. Am. Chem. Soc. 113 (1991) 9688.
[128] A.L. Davis, J. Keeler, E.D. Laue, D. Moskau, J. Magn. Reson. 98 (1992) 207.
[129] J.R. Tolman, J. Chung, J.H. Prestegard, J. Magn. Reson. 98 (1992) 462.
[130] J. Boyd, N. Soffe, B.K. John, D. Plant, R.E. Hurd, J. Magn. Reson. 98 (1992) 660.
[131] J. Ruiz-Cabello, G.W. Vuister, C.T.W. Moonen, P. Van Geldern, J.S. Cohen, P.C.M. Van Zijl, J. Magn. Reson. 100 (1992) 282.
[132] A.L. Davis, R. Boelens, R. Kaptein, J. Biomol. NMR 2 (1992) 395.
[133] L.E. Kay, Prog. Biophys. Mol. Biol. 63 (1995) 277.
[134] L.E. Kay, Curr. Op. Struct. Biol. 5 (1996) 674.
[135] W.S. Warren, W. Richter, A.H. Andreotti, B.T. Farmer, Science 262 (1993) 2005.
[136] P.C.M. Van Zijl, S. Sukumar, M.O.N. Johnson, P. Webb, R.E. Hurd, J. Magn. Reson. A111 (1994) 203.
[137] D.L. Mattiello, W.S. Warren, L. Müller, B.T. Farmer II, J. Am. Chem. Soc. 118 (1996) 3253.
[138] A.A. Maudsley, A. Wokaun, R.R. Ernst, Chem. Phys. Lett. 55 (1978) 9.
[139] L. Mitschang, H. Ponstingl, D. Grindrod, H. Oschkinat, J. Chem. Phys. (1995) B102.
[140] J. Cavanagh, M. Rance, J. Magn. Reson. 88 (1990) 72.
[141] J. Cavanagh, A.G. Palmer III, P.E. Wright, M. Rance, J. Magn. Reson. 91 (1991) 429.
[142] A.G. Palmer III, J. Cavanagh, P.E. Wright, M. Rance, J. Magn. Reson. 93 (1991) 151.
[143] J. Cavanagh, M. Rance, Ann. Rep. NMR Spect. 27 (1993) 1.
[144] J. Schleucher, M. Sattler, C. Griesinger, Angew. Chem. 105 (1993) 1518.
[145] J. Schleucher, M. Sattler, C. Griesinger, Angew. Chem. Int. Ed. Engl. 32 (1993) 1489.
[146] J. Schleucher, M.G. Schwendinger, M. Sattler, P. Schmidt, S.J. Glaser, O.W. Sørensen, C. Griesinger, J. Biomol. NMR. 4 (1994) 301.
[147] M. Akke, P. Carr, A.G. Palmer III, J. Magn. Reson. B104 (1994) 298.
[148] L.E. Kay, P. Keifer, T. Saarinen, J. Am. Chem. Soc. 114 (1992) 10663.
[149] L.E. Kay, G.Y. Xu, T. Yamazaki, J. Magn. Reson. A109 (1994) 129.
[150] S.J. Glaser, T. Schulte-Herbrüggen, M. Sieveking, O. Schedletzky, N.C. Nielsen, O.W. Sørensen, C. Griesinger, Science 280 (1998) 421.
[151] M. Sattler, P. Schmidt, J. Schleucher, O. Schedletzky, S.J. Glaser, C. Griesinger, J. Magn. Reson. B108 (1995) 235.
[152] M. Sattler, M. Maurer, J. Schleucher, C. Griesinger, J. Biomol. NMR 5 (1995) 97.
[153] M. Sattler, M. Schwendinger, J. Schleucher, C. Griesinger, J. Biomol. NMR 6 (1995) 11.
[154] V.V.M. Krishnamurthy, J. Magn. Reson. B106 (1995) 170.
[155] S.S. Wijmenga, C.P.M. van Mierlo, E. Steensma, J. Biomol. NMR 8 (1996) 319.
[156] G. Lippens, C. Dhalliun, J.-M. Wieruszeski, J. Biomol. NMR 5 (1995) 327.
[157] J. Stonehouse, G.L. Shaw, J. Keeler, E.D. Laue, J. Magn. Reson. A107 (1994) 178.
[158] M. Piotto, V. Saudek, V. Sklenar, J. Biomol. NMR 2 (1992) 661.
[159] V. Sklenar, M. Piotto, R. Leppik, V. Saudek, J. Magn. Reson. A102 (1993) 241.
[160] A.G. Redfield, S.D. Kunz, E.K. Ralph, J. Magn. Reson. 19 (1975) 114.
[161] S. Grzesiek, A. Bax, J. Am. Chem. Soc. 115 (1993) 12593.
[162] R.H. Griffey, A.G. Redfield, Q. Rev. Biophys. 19 (1987) 51.
[163] S. Grzesiek, H. Kuboniwa, A.P. Hinck, A. Bax, J. Am. Chem. Soc. 117 (1995) 5312.
[164] Z. Shang, G.V.T. Swapna, C.B. Ríos, G.T. Montelione, J. Am. Chem. Soc. 119 (1997) 9274.
[165] R.M. Gschwind, G. Gemmecker, H. Kessler, J. Biomol. NMR (1998).
[166] J.P. Marino, J.L. Diener, P.B. Moore, C. Griesinger, J. Am. Chem. Soc. 119 (1997) 7361.
[167] M. McCoy, J. Magn. Reson. B107 (1995) 270.
[168] H. Matsuo, E. Kupce, H. Li, G. Wagner, J. Magn. Reson. B113 (1996) 91.
[169] C. Griesinger, H. Schwalbe, J. Schleucher, M. Sattler, In: W.R. Croasmun, R.M.K. Carlson (Eds.), Two-Dimensional NMR Spectroscopy, VCH Publishers Inc, New York, 1994 p. 457.
[170] A. Bax, M. Ikura, L.E. Kay, D.A. Torchia, R. Tschudin, J. Magn. Reson. 86 (1990) 304.
[171] T.J. Norwood, H. Boyd, H.E. Heritage, N. Soffe, I.D. Campbell, J. Magn. Reson. 87 (1990) 488.
[172] T.D. Spitzer, G.E. Martin, R.C. Crouch, J.P. Shockcor, B.T. Farmer II, J. Magn. Reson. 99 (1992) 433.
[173] J.C. Madsen, O.W. Sørensen, J. Magn. Reson. 100 (1992) 431.
[174] S.R. Van Doren, E.R.P. Zuiderweg, J. Magn. Reson. 104 (1994) 193.
[175] G. Zhu, A. Bax, J. Magn. Reson. 90 (1990) 405.
[176] T. Szyperski, D. Braun, C. Fernandez, C. Bartels, K. Wüthrich, J. Magn. Reson. B108 (1995) 197.
[177] J.C. Madsen, O.W. Sørensen, J. Magn. Reson. 100 (1992) 431.
[178] R.P. Meadows, E.T. Olejniczak, S.W. Fesik, J. Biomol. NMR 4 (1994) 79.
[179] D. Zimmerman, C. Kulikowski, L. Wang, B. Lyons, G. T. Montelione, J. Biomol. NMR 4 (1994) 241.
[180] M. S. Friedrichs, L. Müller, M. Wittekind, J. Biomol. NMR 4 (1994) 703.
[181] J.B. Olson Jr., J.L. Markley, J. Biomol. NMR 4 (1994) 385.
[182] D.E. Zimmerman, G.T. Montelione, Curr. Op. Struct. Biol. 5 (1995) 664.
[183] H.L. Eaton, S.W. Fesik, S.J. Glaser, G.P. Drobny, J. Magn. Reson. 90 (1990) 452.
[184] E.R.P. Zuiderweg, L. Zeng, B. Brutscher, R.C. Morshauer, J. Biomol. NMR 8 (1996) 147.
[185] T. Carlomagno, M. Maurer, M. Sattler, M.G. Schwendinger, S.J. Glaser, C. Griesinger, J. Biomol. NMR 8 (1996) 161.

[186] A. Majumdar, H. Wang, C. Morshauser, R.P. Zuiderweg, J. Biomol. NMR 3 (1993) 387.
[187] M.W.F. Fischer, L. Zeng, E.R.P. Zuiderweg, J. Am. Chem. Soc. 118 (1996) 12457.
[188] S.J. Archer, V.K. Vinson, T.D. Pollard, D.A. Torchia, Biochemistry 32 (1993) 6680.
[189] O. Zerbe, T. Szyperski, M. Ottiger, K. Wüthrich, J. Biomol. NMR 7 (1996) 99.
[190] F. F. Damberger, J.G. Pelton, C.J. Harrison, H.C.M. Nelson, D.E. Wemmer, Protein Sci. 3 (1994) 1806.
[191] T.M. Logan, M.M. Zhou, D.G. Nettesheim, R.P. Meadows, R.L. VanEtten, S.W. Fesik, Biochemistry 33 (1994) 11087.
[192] G.W. Vuister, S.J. Kim, C. Wu, A. Bax, J. Am. Chem. Soc. 116 (1994) 9206.
[193] T. Yamazaki, J.D. Forman-Kay, L.E. Kay, J. Am. Chem. Soc. 115 (1993) 11054.
[194] F. Löhr, H. Rüterjans, J. Magn. Reson. B112 (1996) 259.
[195] P. Plateau, M. Guéron, J. Am. Chem. Soc. 104 (1982) 7310.
[196] P.J. Hore, J. Magn. Reson. 55 (1983) 283.
[197] S. Grzesiek, A. Bax, J. Am. Chem. Soc. 117 (1995) 6527.
[198] F. Löhr, H. Rüterjans, J. Magn. Reson. 124 (1997) 255.
[199] G.D. Henry, B.D. Sykes, J. Biomol. NMR 5 (1995) 59.
[200] X. Shan, K.H. Gardner, D.R. Muhandiram, N.S. Rao, C.H. Arrowsmith, L.E. Kay, J. Am. Chem. Soc. 118 (1996) 6570.
[201] M. Sattler, S.W. Fesik, Structure 4 (1996) 1245.
[202] L.E. Kay, K.H. Gardner, Curr. Op. Struct. Biol. 7 (1997) 722.
[203] W.J. Metzler, M. Wittekind, V. Goldfarb, L. Müller, B.T. Farmer II, J. Am. Chem. Soc. 118 (1996) 6800.
[204] D. Nietlispach, R.T. Clowes, R.W. Broadhurst, Y. Ito, J. Keeler, M. Kelly, J. Ashurst, H. Oschkinat, P.J. Domaille, E.D. Laue, J. Am. Chem. Soc. 118 (1996) 407.
[205] M.K. Rosen, K.H. Gardner, R.C. Willis, W.E. Parris, T. Pawson, L.E. Kay, J. Mol. Biol. 263 (1996) 627.
[206] B.O. Smith, Y. Ito, A. Raine, S. Teichmann, L. Ben-tovim, D. Nietlispach, R.W. Broadhurst, T. Terada, M. Kelly, H. Oschkinat, T. Shibata, S. Yokoyama, E.D. Laue, J. Biomol. NMR 8 (1996) 360.
[207] K.H. Gardner, M.K. Rosen, L.E. Kay, Biochemistry 36 (1997) 1389.
[208] C. Biamonti, C.B. Rios, B.A. Lyons, G.T. Montelione, Adv. Biophysical Chemistry 4 (1994) 51.
[209] M. Eberstadt, G. Gemmecker, H. Kessler, Angew. Chem. Int. Ed. Engl. 34 (1995) 1671.
[210] H. Schwalbe, P. Schmidt, C. Griesinger, in: D.M. Grant, R.K. Harris (Eds.), Encyclopedia of Nuclear Magnetic Resonance, John Wiley, Chichester, 1995 p. 1473.
[211] C. Griesinger, M. Hennig, J.P. Marino, B. Reif, H. Schwalbe, in: L.J. Berliner, N.R. Krishna (Eds.), Biomolecular NMR, Plenum Press, New York, 1998.
[212] D.R. Muhandiram, N. Farrow, G.-Y. Xu, S.H. Smallcombe, L.E. Kay, J. Magn. Reson. B102 (1993) 317.
[213] T. Frenkiel, C. Bauer, M.D. Carr, B. Birdsall, J. Feeney, J. Magn. Reson. 90 (1990) 420.
[214] M. Ikura, A. Bax, M. Clore, A. Gronenborn, J. Am. Chem. Soc. 112 (1990) 9020.
[215] G.M. Clore, L.E. Kay, A. Bax, Biochemistry 30 (1991) 12.
[216] E.R.P. Zuiderweg, A.M. Petros, S.W. Fesik, E.T. Olejniczak, J. Am. Chem. Soc. 113 (1991) 370.
[217] G.W. Vuister, G.M. Clore, A.M. Gronenborn, R. Powers, D.S. Garrett, R. Tschudin, A. Bax, J. Magn. Reson. B101 (1993) 210.
[218] L.E. Kay, G.M. Clore, A. Bax, A.M. Gronenborn, Science 249 (1990) 411.
[219] D.R. Muhandiram, G.Y. Xu, L.E. Kay, J. Biomol. NMR 3 (1993) 463.
[220] B. Brutscher, N. Morelle, F. Cordier, D. Marion, J. Magn. Reson. B109 (1995) 238.
[221] O.W. Sørensen, J. Magn. Reson. 89 (1990) 210.
[222] B.T. Farmer II, J. Magn. Reson. 93 (1991) 635.
[223] R. Boelens, M. Burgering, R. H Fogh, R. Kaptein, J. Biomol. NMR 4 (1994) 201.
[224] S.M. Pascal, D.R. Muhandiram, T. Yamazaku, J.D. Forman-Kay, L.E. Kay, J. Magn. Reson. B103 (1994) 197.
[225] B.T. Farmer, L. Müller, J. Biomol. NMR 4 (1994) 673.
[226] R.A. Venters, W.J. Metzler, L.D. Spicer, L. Müller, B.T. Farmer II, J. Am. Chem. Soc. 117 (1995) 9592.
[227] S. Grzesiek, P. Wingfield, S. Stahl, J.D. Kaufman, A. Bax, J. Am. Chem. Soc. 117 (1995) 9594.
[228] T.K. Mal, S.J. Matthews, H. Kovacs, I.D. Campbell, J. Boyd J. Biomol. NMR (1998) 10.
[229] M.G. Clore, A. Bax, A. Gronenborn, J. Biomol. NMR 1 (1991) 13.
[230] A.A. Bothner-By, R.L. Stephens, J.T. Lee, C.D. Warren, R.W. Jeanloz, J. Am. Chem. Soc. 106 (1984) 811.
[231] G.M. Clore, A. Bax, P.T. Wingfield, A.M. Gronenborn, Biochemistry 29 (1990) 5671.
[232] S. Grzesiek, A. Bax, J. Biomol. NMR 6 (1995) 335.
[233] S.W. Fesik, R.T.J. Gampe, T.F. Holzman, D.A. Egan, R. Edalji, J.R. Luly, R. Simmer, R. Helfrich, V. Kishore, D.H. Rich, Science 250 (1990) 1406.
[234] M.K. Rosen, S.W. Michnick, M. Karplus, S.L. Schreiber, Biochemistry 30 (1991) 4774.
[235] E. Wörgötter, G. Wagner, K. Wüthrich, J. Am. Chem. Soc. 108 (1987) 6162.
[236] G. Otting, H. Senn, G. Wagner, K. Wüthrich, J. Magn. Reson. 70 (1986) 500.
[237] H. Senn, G. Otting, K. Wüthrich, J. Am. Chem. Soc. 109 (1987) 1090.
[238] S.W. Fesik, R.T.J. Gampe, T.W. Rockway, J. Magn. Reson. 74 (1987) 366.
[239] G. Otting, K. Wüthrich, J. Magn. Reson. 85 (1989) 586.
[240] G. Wider, C. Weber, K. Wüthrich, J. Am. Chem. Soc. 113 (1991) 4676.
[241] G. Gemmecker, E.T. Olejniczak, S.W. Fesik, J. Magn. Reson. 96 (1992) 199.
[242] M. Ikura, A. Bax, J. Am. Chem. Soc. 114 (1992) 2433.
[243] C. Griesinger, Entwicklung neuer NMR-Spektroskopischer Methoden, Konformationsanalyse zyklischer Peptide, Ph.D. thesis, Frankfurt, 1986.
[244] M. Nilges, J. Mol. Biol. 245 (1995) 645.
[245] C. Mumenthaler, W. Braun, J. Mol. Biol. 254 (1996) 465.
[246] M. Nilges, Curr. Op. Struct. Biol. 6 (1996) 617.